Distribution Agreement

In presenting this thesis or dissertation as a partial fulfillment of the requirements for an advanced degree from Emory University, I hereby grant to Emory University and its agents the non-exclusive license to archive, make accessible, and display my thesis or dissertation in whole or in part in all forms of media, now or hereafter known, including display on the world wide web. I understand that I may select some access restrictions as part of the online submission of this thesis or dissertation. I retain all ownership rights to the copyright of the thesis or dissertation. I also retain the right to use in future works (such as articles or books) all or part of this thesis or dissertation.

Signature:

_____ _____

Troy Justin O'Neal Date

The early involvement of CNS-draining lymphatics and host response to West Nile virus infection

By

Troy Justin O'Neal
Doctor of Philosophy

Graduate Division of Biological and Biomedical Science
Microbiology and Molecular Genetics

_____

Mehul Suthar, Ph.D.
Advisor

_____

Steven Bosinger, Ph.D.
Committee Member

_____

Arash Grakoui, Ph.D.
Committee Member

_____

Jacob Kohlmeier, Ph.D.
Committee Member

_____

Bernardo Mainou, Ph.D.
Committee Member

Accepted:

_____

Lisa A. Tedesco, Ph.D.
Dean of the James T. Laney School of Graduate Studies

_____

Date

The early involvement of CNS-draining lymphatics and host response to West Nile virus infection

By

Troy Justin O'Neal

B.Sc., Georgia Institute of Technology, 2011

M.Sc., University of Michigan-Ann Arbor, 2014

Advisor: Mehul S. Suthar, Ph.D.

An abstract of

A dissertation submitted to the Faculty of the James T. Laney School of Graduate Studies of Emory University in partial fulfillment of the requirements for the degree of Doctor of Philosophy

in Graduate Division of Biological and Biomedical Science

Microbiology and Molecular Genetics

2019

Abstract

The early involvement of CNS-draining lymphatics and host response to West Nile virus infection

By Troy Justin O'Neal

West Nile virus (WNV) is a mosquito-borne flavivirus of global importance, which can result in neuroinvasive infection leading to encephalitis, prolonged neurological dysfunction or death. The early induction of the host response and efficient $CD8^+$ T cell responses are both required for protection. We found that viral RNA and activated conventional dendritic cells (cDCs) accumulated in the meninges and CNS-draining lymph nodes (LNs) prior to neuroinvasion. Furthermore, WNV-specific $CD8^+$ T cells accumulated in the CNS-draining LNs and the spleen with similar kinetics. WNV-specific $CD8^+$ T cells from the spleen and brain exhibited dramatically different activation and inhibitory marker expression and cytokine production, whereas WNV-specific $CD8^+$ T cells from the meninges and CNS-draining LNs displayed unique intermediate phenotypes. Notably, meningeal and brain WNV-specific $CD8^+$ T cells produced both tumor necrosis factor (TNF)-α and interferon (IFN)-γ and had the highest fraction of cells expressing PD-1. CNS-localized WNV-specific $CD8^+$ T cells were more efficient at controlling viral infection of cortical neurons than peripheral WNV-specific $CD8^+$ T cells. These findings characterize the early involvement of CNS-draining lymphatics during WNV pathogenesis and indicate that anatomic localization influences $CD8^+$ T cell programming during WNV infection. The type I IFN (IFN-I) response promotes induction of innate antiviral defenses, restricting early viral replication. We developed WNV-inclusive single-cell RNA sequencing (scRNA-seq), an approach to examine transcriptional heterogeneity in IFN-stimulated gene (ISG) induction and viral RNA abundance across single cells. We observed that only a small fraction of cells within the bulk population produced high levels of IFN-β transcript. Genes associated with the IFN-I response exhibited both high unimodal and bimodal variation. The majority of ISGs negatively correlated with viral RNA abundance, often displaying a sharp decline in expression for cells with high levels of viral RNA. WNV-inclusive scRNA-seq represents a robust approach for parallel single-cell transcriptomics and WNV RNA detection, which can be implemented in other systems to identify novel therapeutic targets or extend the resolution of *in vivo* studies to single infected cells.

The early involvement of CNS-draining lymphatics and host response to West Nile virus infection

By

Troy Justin O'Neal

B.Sc., Georgia Institute of Technology, 2011

M.Sc., University of Michigan-Ann Arbor, 2014

Advisor: Mehul S. Suthar, Ph.D.

A dissertation submitted to the Faculty of the James T. Laney School of Graduate Studies of Emory University in partial fulfillment of the requirements for the degree of Doctor of Philosophy

in Graduate Division of Biological and Biomedical Science

Microbiology and Molecular Genetics

2019

Contents

INTRODUCTION

Flaviviruses

Flaviviruses, often transmitted by arthropod vectors, annually account for several hundred million infections worldwide (1-4). Flavivirus infections of humans are generally acute and self-limiting and in many cases asymptomatic, but can cause a spectrum of severe symptoms, including hemorrhagic fever, encephalitis, meningitis, congenital malformations, long-term neurological deficits and even fatality (1-6). The mosquito-borne dengue virus (DENV) is responsible for nearly 70 million infections annually alone and can result in dengue hemorrhagic fever following secondary infection with a different serotype (4, 7, 8). A recently licensed tetravalent DENV vaccine has shown limited efficacy and is not recommended for populations less than 9 and over 45 years of age (9, 10). Yellow fever virus (YFV) is a member of the flavivirus genus capable of causing acute-onset hepatitis and hemorrhagic fever (11-15). However, the live-attenuated vaccine YFV-17D combined with improved mosquito control has lowered the incidence of yellow fever in urban areas since the mid 20th century (12, 15). Neurotropic flaviviruses include West Nile virus (WNV), Zika virus (ZIKV), Japanese encephalitis virus (JEV), Powassan virus (POWV), and tick-borne encephalitis virus (TBEV). A licensed vaccine for JEV is available for clinical use, and investigational vaccine candidates exist for ZIKV and WNV although none have progressed beyond Phase II clinical trials (16-19). Altogether, the lack of effective prophylactic and therapeutic measures to prevent or treat flavivirus infection underscores the need to better understand pathogenesis and correlates of protective immunity.

WNV ecology and pathogenesis

WNV is a neurotropic flavivirus responsible for annual epidemics of virus-induced encephalitis worldwide (1-3, 5, 6). The virus cycles between birds and mosquitoes, causing incidental infection and disease in humans and other mammals (20). *Culex* and *Aedes* mosquito species serve as the principal transmission vectors, while a wide range of avian hosts function as the natural reservoir (3, 21, 22). Transmitting mosquitoes include both ornithophilic vectors, those that primarily feed on birds, and bridge vectors, opportunistic feeders that can infect incidental hosts (21, 22). Humans, as well as other mammals, are referred to as incidental hosts and not amplifying hosts, as they do not develop viremia at a sufficiently high level to infect feeding mosquitoes (21, 22). Whereas other arboviruses are more restricted in their vector and host range, the broad distribution of WNV worldwide can potentially be attributed to its capacity to be transmitted by numerous mosquito species and infect a variety of vertebrates, including but not limited to birds, humans, horses, alligators and killer whales (3, 20, 22, 23). Notably, WNV has been associated with mortality of avian hosts in the United States although similar observations have not been made in tropical regions, possibly due to differences in the range of indigenous avian species and exposure to other flaviviruses (24, 25). Furthermore, some evidence suggests that other vertebrates, such as squirrels, might be capable of serving as amplifying hosts, although birds remain the major natural reservoir (26).

Mosquitoes acquire WNV after feeding on viremic birds. While viremic titers are highly species-specific, many avian species will not surpass a peak viremia of $1x10^8$ 50% tissue culture infectious dose ($TCID_{50}$) per mL (22, 27). Following ingestion of a

viremic blood meal, the virus infects and replicates in midgut epithelial cells within 8 h (22, 28). The first barrier for WNV within the midgut is the peritrophic membrane, a filamentous matrix formed around the blood meal as early as 2-8 h post-feeding and reaching ~100 μm in thickness by 24 h (22, 29). This requires WNV to infect midgut epithelial cells within 8 h of feeding before the intact peritrophic membrane is fully formed (22, 30). Following replication in midgut epithelial cells, WNV traverses the basal lamina to disseminate into the haemolymph and ultimately seed the salivary glands (22). The basal lamina and salivary gland barriers represent additional impediments for invading pathogens and are thought to contribute to the mosquito vector range for different viruses (22). Once within the salivary gland, WNV replicates in salivary gland cells, thereby increasing the viral burden in this tissue to upwards of 10^7 plaque-forming unit (PFU) equivalents (22, 30). During feeding, the mosquito probes multiple times throughout the dermis depositing infectious saliva until it strikes a blood vessel (3, 22, 31). Over the course of a feeding, mosquitoes inoculate with a median dose of up to 10^6 PFU, depending on the species (31). Additionally, a small amount of WNV (~10^2 PFU) is dispensed directly into the bloodstream, which may result in early viremia and alter the kinetics of viral spread (31).

The virion membrane is derived from the host, and therefore differences in lipid composition and carbohydrate complexity between arthropod and vertebrate hosts are an important consideration (28, 32, 33). Viral glycoproteins on the envelope contain high-mannose glycans when derived from mosquito cells (33, 34). In fact, *in vitro* studies have demonstrated that mosquito cell-derived virus infects a higher percentage of bone marrow-derived dendritic cells than mammalian cell-derived virus, suggesting

that differences in glycosylation and lipid content may contribute to cell tropism (35). Furthermore, mosquito cell-derived and mammalian cell-derived virus display differential dissemination kinetics in the mouse model, suggesting that host glycosylation and lipid content on cellular membranes may influence early viral spread (36). The high-mannose glycans found on mosquito cell-derived virions might increase binding to extracellular matrix and cells at the primary inoculation site, whereas mammalian cell-derived virus might more readily spread through the lymphatics and blood to the draining lymph node and spleen (36). Furthermore, mice inoculated with WNV via mosquito feeding exhibited higher peak viremia and enhanced early viral spread as compared to subcutaneous footpad inoculation via needle (37). Extending these findings, the study also demonstrated that mosquito saliva factors, which counteract hemostasis and modulate the local immune response, are responsible for the observed enhancement of WNV infection (37).

WNV infection of humans often presents as a self-limiting febrile illness (38). In severe cases, however, infection can progress to West Nile neuroinvasive disease (WNND) characterized by encephalitis, meningitis, flaccid paralysis or even death (1, 2, 5, 6, 38). WNV-induced encephalitis has been reported at a higher frequency for elderly people and those that are immunosuppressed (38). Additionally, short-term and long-term neurological sequelae have been observed for patients recovering from WNND and often persist for months (38). WNV pathogenesis in humans remains incompletely defined, but the mouse model of WNV infection represents a robust system in which to study disease and neuropathogenesis. Using the mouse model, WNV pathogenesis has been described in three phases comprising early post-inoculation, visceral-organ

dissemination, and neuroinvasion (3, 39). Early induction of the host response in the periphery is critical for control of viral replication and priming of adaptive immunity (40-42). The neuroinvasive stage is characterized by central nervous system (CNS) invasion, neuronal infection, neuroinflammation, and neuronal cell death (3, 39). The major correlates of protections are type I interferon (IFN-I)-dependent antiviral defenses, which have been shown to restrict cellular tropism and protect against virus-induced pathology, and humoral and T cell-mediated responses, which are required for viral clearance and provide long-lived immunity (3, 39, 42-45).

The host response to WNV infection

The induction of innate antiviral defenses is critical for the control of WNV infection, both early in the periphery and following neuroinvasion (42, 46-48), and the antiviral programs that govern these cell-intrinsic measures have been broadly characterized by large-scale IFN-stimulated gene (ISG) screens and transcriptomic studies (49-54). Pattern recognition receptors, including toll-like receptors (TLRs) and retinoic acid-inducible gene I (RIG-I)-like receptors (RLRs), are critical to the induction of the innate immune response within cells (55, 56). During flavivirus infection, PRRs detect common viral structures in cytosolic and endosomal compartments, such as 5'-triphosphate ssRNA or dsRNA (55, 57). RLRs, RIG-I and MDA5 (myeloma differentiation-associated gene 5), bind to non-self RNA ligand and signal through the mitochondrial antiviral signaling (MAVS) adaptor protein to activate transcription factors and induce IFN-I regulatory factor (IRF)-mediated transcription of IFN-I and ISGs (3, 46, 48, 55, 56). IFN-I (IFN-α/β) and other pro-inflammatory cytokines restrict viral replication

through the induction of crucial antiviral programs (42, 56, 58, 59). Binding of IFN-β to its cognate receptor (IFNAR1/2 heterodimer) triggers activation of Janus kinases, Jak1 and Tyk2, resulting in phosphorylation of signal transducer and activator of transcription 1 (STAT1) and STAT2 (56, 60-64). The phosphorylated STAT1-STAT2 heterodimer along with IRF9 then assemble the ISG factor 3 (ISGF3) complex and translocate to the nucleus (56, 61). There, the ISGF3 complex promotes expression of genes containing IFN-stimulated response elements (ISRE), inducing an antiviral state (56, 65, 66). TLR3 and TLR7 recognize endosomal WNV RNA and signal through their respective adaptor proteins TRIF (TIR-domain-containing adapter-inducing interferon-β) and MyD88 (myeloid differentiation primary response 88) to initiate IFN-β transcription (67). Additionally, the cyclic GMP-AMP synthase (IFN-I)–stimulator of interferon genes (STING) pathway has been demonstrated to have a non-canonical role in restricting WNV infection (55, 68). The importance of IFN-I and RLR signaling has been demonstrated by numerous *in vivo* studies. MAVS-deficient mice display enhanced viral dissemination, expanded tissue tropism, early entry into the CNS, and rapid mortality (48). Similarly, mice with a deletion of IFN-I signaling exhibit uncontrolled viral replication and rapid mortality, supporting that IFN-I signaling is required for protection (40, 42, 46). Furthermore, cell-intrinsic roles for IFN-I and RLR signaling have been identified. Mice with a deletion of IFN-I signaling specifically in $CD11c^{+}$ cells display uncontrolled viral replication, expanded tissue tropism, and rapid mortality (47). Previously published findings with *Mavs*$^{-/-}$ → WT bone marrow chimeric mice revealed that MAVS expression in hematopoietic cell populations is critical for protection, control of WNV neuropathogenesis, and timely viral clearance from the CNS (69).

To counteract these innate antiviral defenses, flaviviruses have been shown to evade antiviral host factors and directly or indirectly antagonize IFN-I signaling and the JAK-STAT pathway (70-82). The non-polyadenylated single-strand RNA genome encodes three structural (C, prM and E) and seven nonstructural (NS1, NS2A, NS2B, NS3, NS4A, NS4B, and NS5) proteins, which are synthesized as a single polyprotein before cleavage by host and viral proteases (3). NS5 is critical to formation of the 5' cap structure, mediating the guanine N-7 and ribose 2′-O methylations (57). A single point mutation in WNV NS5 abrogates its 2′-O methyltransferase function, preventing WNV evasion of IFN-induced protein with tetratricopeptide repeats 1 (IFIT1)-mediated restriction of viral translation (78, 80). DENV and ZIKV NS5 bind STAT2 and facilitate proteasomal degradation (83-85). WNV and TBEV NS5 block Jak1 and Tyk2 activation by interacting with host prolidase to block IFNAR1 expression on the cell surface (74). WNV NS4A and NS4B facilitate ER membrane rearrangement and thereby ER stress, which is thought to interfere with JAK-STAT signaling (70, 75, 82). YFV NS5 can only bind STAT2 following IFN-I signaling which promotes the formation of the STAT1-STAT2 heterodimer (86). Interestingly, YFV NS5 does not facilitate STAT2 degradation as DENV or ZIKV NS5, but instead inhibits binding of the ISGF3 complex to ISRE-regulated genes thereby preventing ISG induction (86). Altogether, these findings highlight the crucial role of the IFN-I response in controlling viral replication.

Integrating single-cell approaches

Our understanding of the transcriptional programs that mediate virologic control has been largely informed by conventional bulk assays. However, recent single-cell studies

have begun to examine the transcriptional heterogeneity across infected cell populations (87-91). Studies with influenza virus, poliovirus, dengue virus (DENV) and Zika virus (ZIKV) have revealed heterogeneity in viral RNA levels across single cells (87-91). Several studies examining IFN-I induction at single-cell resolution indicate that only a small fraction of infected cells express *Ifnb1* mRNA through a wide range of assays, including single-cell quantitative PCR (qPCR), single-mRNA molecule in situ hybridization, fluorescently-tagged cells, and single-cell RNA sequencing (scRNA-seq) (88, 92-97). Stochasticity in signaling cascades that orchestrate transcription factor activation or variability at the level of *Ifnb1* expression, such as chromatin organization, could contribute to the absence of detectable *Ifnb1* mRNA in the majority of infected cells (93-100). Previous work with DENV found differences in IFN-I and pro-inflammatory cytokine production between DENV-infected and bystander human dendritic cells using high dimensional mass cytometry by time-of-flight (CyTOF) analysis (101). Additional studies have found that paracrine signaling of IFN-I is critical for amplification of innate antiviral defenses through the use of PRR agonists or nonproductive viral infection (53, 93-97). Finally, virus-inclusive scRNA-seq has been proposed as a discovery platform to identify novel proviral and antiviral candidate genes for host-targeted therapeutics (89). In the study, Zanini and colleagues identified novel host factors with potential antiviral activity against ZIKV or DENV (89). Population-level transcriptional analyses provide valuable insight into gene expression changes across multiple conditions, but by nature of the assay can mask patterns, such as bimodal variation, which can only be observed at single-cell resolution (92, 95, 96). Altogether, we have an in-depth understanding of the molecular mechanisms that coordinate the

induction of antiviral defenses following flavivirus infection, but the existing heterogeneity in these processes across single cells is still poorly understood.

Dendritic cells and WNV infection

Dendritic cells (DCs) are key targets of WNV infection and play an integral role throughout each phase of WNV pathogenesis through early control of viral replication, IFN-I and proinflammatory cytokine production, and priming of B cell and T cell responses (43, 46-48, 102, 103). DCs are divided into four distinct subsets: conventional type 1 DCs (cDC1s), conventional type 2 DCs (cDC2s), plasmacytoid DCs (pDCs), and monocyte-derived DCs (moDCs) (104-107). Conventional DCs (cDCs) initiate T cell responses through co-stimulatory signals and antigen presentation in MHC I (major histocompatibility complex class I) and MHC II and can direct T cell polarization through cytokine secretion (104-107). $IRF8^{+}XCR1^{+}$ cDC1s specifically excel at cross-presentation of exogenous antigen on MHC I and activation of $CD8^{+}$ T cells, whereas $IRF4^{+}CD172a^{+}$ cDC2s are generally proficient at antigen presentation on MHC II and preferentially stimulate $CD4^{+}$ T cells (104-109). Less efficient at antigen presentation, pDCs express TLR7 and TLR9 and are a key producer of IFN-I in response to viral RNA (104-107). Lastly, inflammatory moDCs differentiate from monocytes and are phenotypically similar to $CD11b^{+}$ DCs (106, 107). Previous studies have implicated DCs, a key target cell of WNV, in mediating protective immune responses to WNV infection (43, 46-48, 102, 103). MAVS-deficient bone marrow-derived DCs and macrophages (MΦs) exhibit increased viral burden and are unable to produce IFN-I following WNV infection (48). As mentioned previously, deletion of IFN-I signaling in $CD11c^{+}$ cells

results in uncontrolled viral replication, supporting that DC-intrinsic IFN-I signaling is critical for survival (47). Previously published findings indicate that Batf3-deficient mice, which lack cDC1s, fail to generate optimal WNV-specific effector $CD8^+$ T cell responses (103, 110). Furthermore, recent data demonstrated that infected and bystander $CD8\alpha^+CD11c^+$ DCs, but only infected $CD11b^+CD11c^-$ myeloid cells, present the immunodominant WNV NS4B peptide epitope in complex with MHC I, supporting that cDC1s are key to priming WNV-specific $CD8^+$ T cell responses (111). WNV infection of human monocyte-derived DCs results in dampened proinflammatory cytokine production and T cell co-stimulatory capacity, suggesting that contributions from both infected and bystander DC populations may be critical for priming effective T cell responses (112). Altogether, these published findings demonstrate the importance of DCs in mediating early virologic control and promoting protective immunity.

$CD8^+$ T cell-mediated immunity during WNV infection

Naïve $CD8^+$ T cells circulate through secondary lymphoid tissues where they can be activated by T cell receptor (TCR) stimulation from DCs presenting their cognate antigen in complex with MHC (113-117). DC-mediated priming of T cells requires three distinct signals: TCR engagement by peptide-MHC complex, co-stimulation of CD28 by CD80/86, and inflammatory cytokines (113-120). Following activation, antigen-specific $CD8^+$ T cells undergo rapid expansion resulting in a large pool of effector $CD8^+$ T cells potentially subject to alternative cell fates, including central memory, effector memory, and resident memory (113-116, 121-124). Activated T cells downregulate CD62L and CCR7 and upregulate S1P1R (sphingosine-1-phosphate receptor 1) to egress through

efferent lymphatics (114, 116, 117, 125, 126). Upregulation of LFA-1 (lymphocyte function-associated antigen-1), which binds ICAM-1 (intercellular adhesion molecule-1), is important for adhesion to the vascular endothelium, extended contact with APCs, and binding to target cells for cytotoxic killing (118, 123, 127, 128). Increased expression of integrin α4β1 (also known as very late antigen-4, VLA-4), which binds VCAM-1 (vascular cell adhesion protein-1), plays a key role in T cell migration to numerous tissue sites during inflammation, including the skin, lung and CNS (115, 116, 122, 124, 129, 130). Additionally, integrin α4β7 is a well-established marker of gut homing (114, 116, 130, 131). Integrin αeβ7 (αe also referred to as CD103) and CD69 have been implicated in the maintenance of some resident memory T (T_{RM}) cell populations in non-lymphoid tissues. Findings with influenza have demonstrated that the establishment of T_{RM} cell populations in the lungs requires local recognition of cognate antigen (132). Upon rechallenge or secondary infection, T_{RM} cells are well-positioned at key sites of infection to respond rapidly (114, 116, 123, 124). Even recent work in tumor immunity has highlighted that T_{RM} cells can promote early maturation of cross-presenting dermal DCs which then migrate to secondary lymphoid tissues to quickly amplify the $CD8^+$ T cell response (133). Recently, antiviral $CD8^+$ T cells have been shown to persist in the CNS following resolution of primary WNV infection (134). IFN-γ production from persisting antiviral $CD8^+$ T cells promotes microglia-mediated elimination of presynaptic termini resulting in spatial memory deficits (134). Therefore, the potential consequences of T_{RM} establishment in the CNS following neurotropic viral infection remain an important area of future research.

WNV-specific $CD8^+$ T cell responses are essential for protection and required for

viral clearance from the CNS (44, 135). The deletion of CD8α or MHC I in mice results in higher viral burden, enhanced pathology in the CNS, and increased mortality (44). $CD8^+$ T cells control WNV replication through numerous well-established mechanisms, including expression of death receptors (e.g. FasL, TRAIL) (136, 137), secretion of cytotoxic molecules (e.g. granzyme B, perforin) (113, 138, 139), and production of antiviral cytokines (e.g. TNF-α and IFN-γ) (138, 140, 141). Previous work with LCMV has demonstrated differences in phenotype, function, and cellular fate between splenic red pulp and white pulp antigen-specific $CD8^+$ T cells, supporting that anatomic localization and environmental cues can influence antiviral $CD8^+$ T cell responses during infection (142). Similarly, WNV-specific $CD8^+$ T cells from red pulp have been shown to display a more effector-like phenotype than $CD8^+$ T cells from the white pulp (143). Following migration to the CNS, CXCL10 production by infected cerebellar neurons recruits CXCR3-expressing WNV-specific $CD8^+$ T cells to coordinate viral clearance, highlighting the region specificity of chemokine-mediated neuroinflammation (144, 145). In IL-1R1-deficient mice, $CD11c^+$ DCs have been implicated in providing a critical reactivation signal to CNS-infiltrating WNV-specific $CD8^+$ T cells, which mediate protective immunity; however, the exact mechanism and location of these interactions have yet to be elucidated (102). Furthermore, CSF1R antagonism results in loss of CNS-localized APCs, including microglia, and limited reactivation of CNS-infiltrating $CD8^+$ T cells (146). These findings establish that WNV-specific $CD8^+$ T cells are recruited to the CNS and mediate viral clearance following critical interactions with CNS-localized APCs. Altogether, we have a broad understanding of WNV pathogenesis and immunity; however, the role of meningeal immunity and early involvement of CNS-

draining lymphatics is currently a notable gap in knowledge.

Meningeal immunity and neuroinflammation

Neuroinflammation during neurotropic virus infection is required for protection (147-153). Neurotropic viruses can enter the central nervous system (CNS) via direct infection of brain microvascular endothelial cells, axonal retrograde transport in peripheral neurons, infiltration of infected peripheral immune cells, or disruption of the blood-brain barrier (BBB), blood-meningeal barrier or blood-cerebrospinal fluid (CSF) barrier (151, 152). Importantly, neurotropic viruses may induce pathology without directly infecting the CNS parenchyma. For example, viral antigen and inflammation are observed in the meninges of neonates following ZIKV infection but not the parenchyma (154-156). CNS invasion by neurotropic viruses can trigger the release of inflammatory mediators and infiltration of peripheral immune cells into the CNS, potentially contributing to pathology and neurological dysfunction (134, 149-151, 153, 157-159). Neuroinflammation is a hallmark of viral infections of the CNS and, in this context, is often required for protection through the control of viral replication and coordinated clearance (149, 151). However, chronic inflammatory responses, in addition to acute neuronal death, can lead to prolonged neurological deficits, such as impaired cognition or motor function (134, 160-162). Here, the immune response must strike a tactful balance to rapidly eliminate virus from the CNS, while mitigating the long-term consequences of chronic inflammatory processes. As an example of these checks and balances, the vasodilation effects of inflammatory mediators such as TNF-α and IL-1β can be counteracted by IFN-I and Interferon-λ (IFN-λ), which indirectly restrict WNV neuroinvasion through signaling in CNS vascular

endothelial cells thereby tightening the blood-brain barrier (BBB) (55, 163). More importantly, T_{RM} establishment in the CNS could contribute to immunopathology after viral clearance and should be a central focus of future studies.

Over the last decade, advances in the field of CNS immunity have begun to redefine our understanding of the CNS as an immunologically specialized compartment, highlighting the integral involvement of the meninges as a central feature of the neuro-immune axis (147, 149, 164-167). The meninges are a protective layer of tissues that envelops the CNS, comprised of the dura mater, arachnoid mater, and pia mater (147, 164-167). An emerging body of evidence implicates the meninges as a fundamental interface between the CNS and periphery, containing a diversity of immune cells such as dendritic cells (DCs), T cells, B cells, neutrophils, innate lymphoid cells (ILCs), mast cells, and border-associated MΦs (147, 167-170). The dura mater is the dense outermost layer, which is highly vascularized and innervated (166, 171-173). Comparable to peripheral tissues, the dura mater contains lymphatic vessels, which were recently ‘rediscovered’ and well-characterized (165, 171, 174), and fenestrated vasculature to allow diffusion of large molecules from the blood. The arachnoid mater consists of a thin cell layer joined together by tight junctions and serves as a critical initial barrier to safeguard the CNS parenchyma by preventing the free exchange of molecules from the dura mater into the CSF within the subarachnoid space (166, 173). Nonfenestrated blood vessels consisting of endothelial cells bound by tight junctions span the subarachnoid space (166). Representing the final barrier that surrounds the CNS parenchyma, the pia mater and underlying glia limitans restrict access of molecules to the parenchyma (166, 173).

Lymphatic vessels found within the dura mater express Lyve1 and CD31, two classical markers of peripheral lymphatics, and drain to the superficial and deep cervical lymph nodes (scLNs and dcLNs, respectively) (164, 165, 171, 174). Immune surveillance is mediated by antigen-presenting cells (APCs), such as DCs and border-associated MΦ that populate the meninges, choroid plexus, and perivascular spaces, which sample the environment and presumably communicate with peripheral immune cell populations within the meningeal space or following drainage to the dcLN or scLN (147, 175, 176). At steady state, microglia are the only immune cell population residing within the parenchyma; however, neuroinflammation dramatically alters the immune landscape as peripheral inflammatory leukocytes infiltrate the parenchyma to mediate control of viral spread (135, 144, 145, 147, 149, 167, 177-179). Previous studies using models of traumatic CNS injury, experimental autoimmune encephalitis (EAE), and neurodegenerative diseases have demonstrated that meningeal immunity plays a pivotal role in the course of disease (147, 164, 167, 178, 180, 181). In the EAE model of multiple sclerosis (MS), auto-reactive $CD4^+$ T cells become reactivated within the meninges following interactions with local APCs likely presenting myelin antigen, resulting in CNS damage (182, 183). During coronavirus infection, stromal cells within the meninges secrete CCL19 and CCL21 to recruit and reactivate antiviral $CCR7^+$ $CD8^+$ T cells, which are required for protection (184). In the lymphocytic choriomeningitis virus (LCMV) model, peripheral $CD8^+$ T cells and myelomonocytic cells are recruited to the meninges, where resident cells such as DCs and MΦ are infected, resulting in vascular pathology, detrimental edema and brain stem herniation (178, 181). During WNV infection, previous findings have highlighted that in the absence of the CXCL10-CXCR3

signaling axis $CD8^+$ T cells remain in the meningeal vasculature adjacent to the cerebellum rather than infiltrating the parenchyma and mediating viral clearance (144, 145). Furthermore, the meninges have been speculated to be the site wherein CNS-localized DC or MΦ populations provide a crucial reactivation signal to infiltrating WNV-specific $CD8^+$ T cells which is necessary for efficient viral clearance in the CNS (102, 146). Despite these significant contributions to the field, the role of meningeal immunity has yet to be fully elucidated in the context of neurotropic flavivirus infection.

West Nile virus-inclusive single-cell RNA sequencing reveals heterogeneity in the type I interferon response within single cells

Justin T. O'Neal[a,b], Amit A. Upadhyay[b,d], Amber Wolabaugh[b,d], Nirav B. Patel[c], Steven E. Bosinger[b,c,d], Mehul S. Suthar[a,b]

[a]Department of Pediatrics, Division of Infectious Disease, Emory University School of Medicine, Atlanta, Georgia, USA

[b]Emory Vaccine Center, Yerkes National Primate Research Center, Atlanta, Georgia, USA

[c]Yerkes Genomics Core, Yerkes National Primate Research Center, Atlanta, Georgia, USA

[d]Department of Pathology and Lab Medicine, Emory University School of Medicine, Atlanta, Georgia, USA

This chapter was originally published in the Journal of Virology. Copyright © American Society for Microbiology, J Virol. 2019;93(6). doi: 10.1128/JVI.01778-18. PubMed PMID: 30626670; PMCID: PMC6401468.

ABSTRACT

West Nile virus (WNV) is a neurotropic mosquito-borne flavivirus of global importance. Neuroinvasive WNV infection results in encephalitis and can lead to prolonged neurological impairment or death. Type I interferon (IFN-I) is crucial for promoting antiviral defenses through the induction of antiviral effectors, which function to restrict viral replication and spread. However, our understanding of the antiviral response to WNV infection is mostly derived from analysis of bulk cell populations. It is becoming increasingly apparent that substantial heterogeneity in cellular processes exists among individual cells, even within a seemingly homogenous cell population. Here, we present WNV-inclusive single-cell RNA sequencing (scRNA-seq), an approach to examine the transcriptional variation and viral RNA burden across single cells. We observed that only a few cells within the bulk population displayed robust transcription of IFN-β mRNA, and this did not appear to depend on viral RNA abundance within the same cell. Furthermore, we observed considerable transcriptional heterogeneity in the IFN-I response, with genes displaying high unimodal and bimodal expression patterns. Broadly, IFN-stimulated genes negatively correlated with viral RNA abundance, corresponding with a precipitous decline in expression in cells with high viral RNA levels. Altogether, we demonstrated the feasibility and utility of WNV-inclusive scRNA-seq as a high-throughput technique for single-cell transcriptomics and WNV RNA detection. This approach can be implemented in other models to provide insights into the cellular features of protective immunity and identify novel therapeutic targets.

IMPORTANCE

West Nile virus (WNV) is a clinically relevant pathogen responsible for recurrent epidemics of neuroinvasive disease. Type I interferon is essential for promoting an antiviral response against WNV infection; however, it is unclear how heterogeneity in the antiviral response at the single-cell level impacts virologic control. Specifically, conventional approaches lack the ability to distinguish differences across cells with varying viral abundance. The significance of our research is to demonstrate a new technique for studying WNV infection at the single-cell level. We discovered extensive variation in antiviral gene expression and viral abundance across cells. This protocol can be applied to primary cells or *in vivo* models to better understand the underlying cellular heterogeneity following WNV infection for the development of targeted therapeutic strategies.

INTRODUCTION

Mosquito-borne flaviviruses represent a significant public health burden, annually accounting for millions of infections worldwide that, in certain cases, can culminate in severe systemic or neuropathological outcomes (1-3, 153). West Nile virus (WNV), a member of the *Flaviviridae* family, causes yearly epidemics of encephalitis and virus-induced myelitis on a global scale with nearly 50,000 reported cases of WNV disease and over 21,000 cases of neuroinvasive disease from 1999 to 2016 in the United States alone (1-3, 153). Currently, there are no licensed vaccines or approved targeted therapeutics to prevent or treat WNV-infected patients, underscoring the need to better understand the cellular response to WNV infection (1-3, 153).

Type I IFN (IFN-α/β or IFN-I) is the first line of defense against viral infection and coordinates the early antiviral programs to restrict viral replication, as well as shape the adaptive immune response (46-48, 56, 74, 102, 144, 185-187). Loss of IFN-I signaling in WNV-infected mice results in uncontrolled viral replication and rapid mortality, demonstrating that the IFN-I response is required for protective immunity (42, 46-48). Pattern recognition receptors, including toll-like receptors (TLRs) and retinoic acid-inducible gene I (RIG-I)-like receptors (RLRs), detect broad viral signatures, such as 5'-triphosphate ssRNA or dsRNA, in the cytosolic and endosomal compartments (46-48, 56). For flavivirus infection, RLRs are critical for inducing IFN-I and binding to cytosolic viral RNA signals through adaptor proteins, such as mitochondrial antiviral signaling protein (MAVS), to activate transcription factors and induce interferon regulatory factor (IRF)-mediated transcription of IFN-β (*Ifnb1*) and a subset of IFN-stimulated genes (ISGs) (46-48, 56, 58, 59, 93-95, 97, 188). Signaling in both an autocrine and paracrine

manner, secreted IFN-β binds the IFN-I receptor (IFNAR1/2 heterodimer) to activate Janus kinases, Jak1 and Tyk2, which phosphorylate signal transducer and activator of transcription 1 (STAT1) and STAT2 (46, 53, 56, 58, 59, 74, 83, 85, 95-97, 186, 189). Phosphorylated STAT1 and STAT2 form a heterodimer and recruit IRF9 to form the ISG factor 3 (ISGF3) complex. The ISGF3 complex then translocates to the nucleus and induces IFN-stimulated response element (ISRE)-regulated genes, thereby reshaping the cellular landscape to an antiviral state (46, 53, 56, 58, 59, 78, 83, 85, 95-97, 185, 186, 189).

The induction of IFN-I and ISGs within a bulk population of infected cells has been well characterized. However, mean values obtained via conventional bulk assays mask transcriptional differences between infected and bystander cells and obscure any heterogeneity present within the infected population. Recently, single-cell studies have examined the heterogeneity across virally infected cells. Findings with influenza virus, poliovirus, dengue virus (DENV) and Zika virus (ZIKV) have revealed extensive variation in viral RNA abundance within single cells (87, 89, 91). Using high dimensional mass cytometry by time-of-flight (CyTOF) analysis, others have described differences in IFN-I and pro-inflammatory cytokine production in infected and bystander human dendritic cells following DENV infection (101). Studies examining IFN-I induction at the single-cell level have used fluorescently-tagged cells, single-mRNA molecule *in situ* hybridization, single-cell quantitative PCR (qPCR), and single-cell RNA sequencing (scRNA-seq) (88, 92-97). Previous studies have found that only a small fraction of infected cells express *Ifnb1* mRNA (88, 94-97). This is thought to be attributable to stochasticity in signaling components and downstream signaling cascades leading to

transcription factor activation or variability in the processes of *Ifnb1* expression, perhaps at the level of chromatin organization (88, 93-95, 97-100). Using PRR agonists or nonproductive viral infection, others have demonstrated that IFN-I-dependent paracrine signaling is pivotal in amplifying the host antiviral response (53, 93-97). Lastly, single-cell transcriptomic studies have also been used to globally investigate virus-host interactions and identify novel candidate genes for host-targeted therapeutics (89). Knockdown screens or knockout studies can only probe a subset of nonessential host genes, limiting their scope (49-52, 54, 190). However, virus-inclusive scRNA-seq is a powerful platform for the discovery of novel proviral and antiviral candidate genes in an unbiased manner as recently highlighted by Zanini and colleagues with DENV and ZIKV (89).

Altogether, these studies have shed considerable light on the transcriptional differences present in single cells, and specifically with *Ifnb1* expression and viral RNA abundance. However, we still lack a thorough understanding of the cellular heterogeneity in the IFN-I response following WNV infection. Population-level transcriptional analyses are valuable and widely used approaches, but in certain cases can belie gene expression patterns, such as bimodal variation, which can only be observed at single-cell resolution (92, 95, 96). To better understand the underlying transcriptional differences across cells with varying viral abundance, we developed WNV-inclusive scRNA-seq, a modified SMART-Seq protocol that incorporates a virus-specific primer for parallel recovery of host messenger RNA (mRNA) and viral RNA from single cells. We found that only a small fraction of cells exhibited robust *Ifnb1* expression, and this did not significantly correlate with high viral RNA. We observed

considerable transcriptional heterogeneity in ISG expression and viral RNA abundance across cells. ISGs exhibited both unimodal and bimodal variation and were negatively correlated with intracellular viral RNA, displaying a steep decline in gene expression with increasing viral abundance. Combining single-cell mRNA sequencing with quantification of non-polyadenylated viral RNA, we present WNV-inclusive scRNA-seq as a high-throughput technique for single-cell transcriptome analysis of WNV-infected cells.

RESULTS

Population-level analysis of WNV infection in murine fibroblast L929 cells. We first modeled WNV infection kinetics in murine fibroblast L929 cells, an IFN-competent cell line extensively used to study IFN-I-dependent signaling (97, 191). Cells were infected at a multiplicity of infection (MOI) of 0.1, 1 or 10, as determined on BHK-21 cells, and intracellular viral envelope (E) protein immunostaining was performed at 6, 12, 24 and 48 hr post-infection. Infected cells were labeled with WNV E16 antibody (Ab), which recognizes a domain III (DIII) neutralizing epitope within the E protein (192). For all three MOIs, nearly 100% of cells stained positive for intracellular viral E protein by 48 hr post-infection (Fig. 1A). At an MOI of 10, intracellular viral E protein was detected in nearly 100% of cells as early as 24 hr post-infection, suggesting that the majority of these cells were likely infected during primary virus adsorption (Fig. 1A). For cells infected at an MOI of 1, intracellular viral E protein was detected in approximately 60% of cells at 24 hr post-infection (Fig. 1A).

To diminish asynchronous second-round infection, cells were infected with WNV (MOI of 1) and incubated in the presence of WNV E16 neutralizing Ab (192). Inoculation with UV-inactivated WNV served as a non-replicating input control for internalized viral RNA, and no expression of viral E protein was detected (Fig. 1B, 1C). Notably, limiting *in vitro* spread resulted in a 5.5-fold decrease in the percentage of viral E protein-positive cells (10.6%) at 24 hr post-infection, corresponding with a comparable 5.2-fold reduction in viral RNA levels (Fig. 1B, 1C). Collectively, these two conditions, WNV and WNV (+Ab), provide a cell population with a range of viral abundance and another of

predominantly bystander cells with which to survey the IFN-I response at the population and single-cell level in all subsequent analyses.

Before pursuing a single-cell approach, we next sought to evaluate transcriptional changes following WNV infection at the population level by bulk RNA-seq. As expected, numerous genes associated with the innate immune response and antiviral defense response were up-regulated following infection (Fig. 1D, 1E). Furthermore, the majority of these genes were expressed at similar levels independent of reduced asynchronous second-round infection (Fig. 1D, 1E). ISGs and PRR genes exhibited a more consistent level of mean gene expression across these two conditions (Fig. 1E). Conversely, IFN-I and cytokine genes displayed the most variability in expression between genes within their respective categories (Fig. 1E). Most notably, *Ifna2* and *Ifna5* displayed around two-fold higher levels of expression when allowing for *in vitro* spread, although *Ifna2* dropped outside of the pre-selected significance cutoff ($p < 0.01$; Fig. 1E, 1F). This population-level analysis provides a contextual fundamental framework from which to build as we examine the transcriptional differences observed across single cells. Leveraging single-cell sequencing techniques complemented with viral RNA detection, we next extended the resolution of our analysis to single cells to better understand the underlying transcriptional heterogeneity present following WNV infection.

WNV-inclusive scRNA-seq captures mRNA and viral RNA from single cells. WNV-inclusive scRNA-seq is adapted from the well-established Smart-seq2 protocol (193) and the commercially available SMART-Seq v4 Ultra Low Input RNA Kit (Takara) used

for scRNA-seq. The SMART-Seq v4 protocol from Picelli and colleagues is modified to include a virus-specific primer (WNV SC primer) during the reverse transcription (RT) step. For scRNA-seq analysis, L929 cells are inoculated with virus for 1 hr at an MOI of 1 and then incubated in the presence or absence of WNV E16 neutralizing Ab (192) for 24 hr (Fig. 2A). Viable single cells are sorted by conventional flow cytometry into 96-well plates containing 10 µL lysis buffer per well (Fig. 2B). In the RT reaction, 3' SMART-Seq CDS Primer II A (30-nucleotide poly-dT sequence with a 5' 25-nucleotide ISPCR universal anchor sequence and WNV SC primer (21-nucleotide sequence complementary to positive-strand viral RNA with a 5' 25-nucleotide ISPCR universal anchor sequence are added to capture host transcripts and viral RNA, respectively (Fig. 2C). Following template switching, PCR Primer II A served as the primer for parallel downstream amplification of both host and viral complementary DNA (cDNA) (Fig. 2C). Samples underwent Nextera tagmentation and were sequenced on an Illumina HiSeq at a depth of approximately 1 million reads per cell (96, 194). Altogether, we successfully captured and profiled a total of 127 cells across three conditions: Mock, WNV, and WNV (+Ab). The outlined approach delivers exceptional coverage and sequencing depth allowing for accurate quantification of host transcripts and non-polyadenylated viral RNA.

Viral RNA was successfully recovered from single cells following WNV infection, and the majority of WNV reads were aligned with the targeted region of the WNV genome (Fig. 2D). To ensure that the addition of WNV SC primer did not adversely affect the recovery of host mRNAs, the concentration of WNV SC primer was carefully titrated and cDNA quality was evaluated on an Agilent 2100 Bioanalyzer (Supplementary Fig. 1). Furthermore, we examined the levels of housekeeping genes

(*Gapdh*, *Rpl5*, *Arf1* and *Pgk1*) across cells in all three conditions: Mock, WNV, and WNV (+Ab). Unsurprisingly, expression of housekeeping genes was not significantly different between mock and infected conditions, demonstrating that the amplification of viral RNA does not impair the recovery of host mRNA (Fig. 2E).

Heterogeneity in viral RNA abundance and ISG induction at single-cell resolution. At the single-cell level, we observed large differences in viral RNA abundance in the presence and absence of limited *in vitro* spread (Fig. 2D). In the absence of neutralizing antibody, we detected a wide range of intracellular viral RNA levels, with the majority of cells having greater than 2^{10} viral RNA counts per million transcripts (Fig. 2D). Interestingly, only 24% of cells had greater than 2^{10} viral RNA counts per million transcripts when limiting asynchronous secondary infection (Fig. 2D). Furthermore, the heterogeneity of viral RNA abundance in the presence of neutralizing antibody suggests that there is variability in WNV replication during the primary round of infection (Fig. 2D). Notably, the percentage of single cells positive for viral RNA (Fig. 2D) is significantly higher than the percentage predicted by flow cytometry-based viral E protein immunostaining for both infection conditions (Fig. 1B).

When examining transcriptional dynamics across single cells, we noticed some interesting trends. Only a small fraction of WNV-infected cells produced greater than 2^5 *Ifnb1* counts per million transcripts (Fig. 3A). Intriguingly, we observed a similar expression signature for *Ifna4* and *Ifna2* despite high levels of *Irf7*, a transcription factor that drives IFN-α production (195-197), in the majority of cells (Fig. 3A). Furthermore, we identified three chemokine genes (*Ccl5*, *Ccl4* and *Cxcl11*) that displayed comparable

cellular distributions to IFN-I genes. Other pro-inflammatory cytokine genes, *Cxcl10*, *Tnf*, *Il6* and *Il23a*, exhibited cellular heterogeneity but still maintained a portion of cells with no detectable transcript. Genes *Ddx58* and *Dhx58*, which respectively encode the RLRs RIG-I and LGP2 (Laboratory of Genetics and Physiology 2), were highly expressed with most cells containing greater than 2^5 counts per million transcripts (Fig. 3B). Interestingly, *Tlr3* and *Ifih1*, another important RLR gene that encodes MDA5 (melanoma differentiation-associated gene 5), displayed greater variation in expression across cells, including a fraction with no detectable transcript (Fig. 3B). Components of the ISGF3 complex (*Irf9*, *Stat1* and *Stat2*) are critical for IFN-I signaling and are induced to greater than 2^5 counts per million transcripts in the majority of cells (Fig. 3B). Next, we sought to examine the expression patterns for a panel of experimentally validated WNV-targeting antiviral effector genes (*Rsad2*, *Tnfsf10*, *Ifi44l*, *Oas1b*, *Oas3*, *Ifitm3*, *Eif2ak2* and *Mov10*) and two well-established ISGs (*Ifit3* and *Mx1*) (50, 53, 137, 198-205). Antiviral effector genes feature both unimodal (*Tnfsf10*, *Ifi44l*, *Ifitm3*, *Eif2ak2*, *Mov10* and *Mx1*) and bimodal (*Rsad2*, *Oas1b*, *Oas3* and *Ifit3*) variation across single cells (Fig. 4). Notably, several genes (*Ddx58*, *Tlr3*, *Stat1*, *Tnfsf10*, *Eif2ak2*, *Ifit3* and *Mx1*) revealed significantly different transcriptional signatures across cells with and without limited *in vitro* spread (Fig. 3B, 4). Strikingly, most cells have no detectable reads for *Tnfsf10* and *Mx1* when allowing for *in vitro* spread; however, in the presence of neutralizing Ab, the inverse is true (Fig. 4).

Correlation between host gene expression and viral RNA abundance for single cells. Building upon our ability to assess viral RNA abundance in single cells, we

calculated Spearman's correlation coefficients for host gene expression and viral RNA burden across all WNV cells, which spanned a range of viral RNA levels. To comprehensively identify pathways that might be linked to viral RNA abundance, we performed gene ontology (GO) enrichment analysis using the online bioinformatics tool DAVID (206, 207), wherein we independently evaluated all positively correlated ($\rho > 0.35$) and negatively correlated ($\rho < -0.35$) genes of significance ($p < 0.001$). The top pathways extracted from the GO enrichment analysis for negatively correlated genes were the antiviral defense response, cellular response to IFN-β, response to virus, negative regulation of viral replication, innate immune response and antigen processing and presentation via MHC I (class I major histocompatibility complex molecule) (Fig. 5A). For the positively correlated gene set, the top pathways included transcriptional regulation, amino acid transport, ribosomal RNA (rRNA) processing, regulation of protein ubiquitination and ER stress response, providing a broad description of viral RNA-correlated genes (Fig. 5A). Next using curated gene lists from published large-scale ISG screen and single-cell transcriptomic studies (53, 208, 209), we examined the distribution of correlation coefficients for ISGs and cell cycle-associated genes subdivided by phase (G1/S, S, G2/M, M and M/G1). Predictably, the majority of genes do not correlate with viral RNA abundance, and the distribution of coefficients skews heavily towards zero (Fig. 5B). When assessing viral RNA correlations for cell cycle-associated genes, most genes were not significantly positively or negatively correlated, although minor shifts were observed for S, M and M/G1 phase genes (Fig. 5B). Interestingly, 124 out of 294 ISGs were negatively correlated with viral RNA corresponding with a dramatic shift in the coefficient distribution (Fig. 5B). As predicted

by the GO enrichment analysis, numerous genes associated with the ER stress response (*Gadd45a*, *Ppp1r15a*, *Selenos*, *Ddit3*, *Atf4* and others) were strongly positively correlated with viral abundance (Fig. 5B). A subset of correlated ISGs and a panel of non-correlated cytokine genes are represented in a correlation matrix (Fig. 5C). Negatively correlated ISGs strongly clustered together with high correlation coefficients approaching 1 (Fig. 5C). Conversely, ISGs positively correlated with viral RNA only weakly correlated with other positively correlated ISGs (Fig. 5C). Many cells expressing high levels of IFN-I and pro-inflammatory cytokines also featured elevated viral abundance, but not to the extent of reaching a significant positive correlation (Fig. 5C). Scatter plots were generated for a subset of viral RNA-correlated genes and collated in order of increasing correlation coefficients (Fig. 6). Trends associated with negatively correlated ISGs mostly featured a precipitous decline in gene expression as viral RNA levels in single cells exceeded around 2^{15} counts per million transcripts (Fig. 6). Alternatively, positively correlated genes often were characterized by slopes near or less than 1 (Fig. 6). For WNV-validated antiviral effector genes (*Rsad2*, *Tnfsf10*, *Ifi44l*, *Oas1b*, *Oas3*, *Ifitm3*, *Eif2ak2* and *Mov10*), all genes are negatively correlated with viral RNA as expected (Fig. 6). Interestingly, *Tnfsf10*, *Ifi44l* and *Mx1* present unique correlation trends with viral RNA in that the cells with the highest viral abundance have no detectable transcripts for these genes (Fig. 6).

DISCUSSION

Standard scRNA-seq protocols with oligo-dT-based priming have been used to examine transcriptional dynamics during viral infection, but the unique genomic structure of flaviviruses, and other non-polyadenylated viruses that are clinically important pathogens, represents a distinct hurdle for such studies (91). We have independently developed and demonstrated the feasibility of WNV-inclusive scRNA-seq as an attractive approach for the quantification of host transcripts and viral RNA within single cells. This protocol, in combination with previously published work by Zanini and colleagues (89), establishes virus-inclusive scRNA-seq as a viable and tractable system for other non-polyadenylated RNA viruses.

WNV-inclusive scRNA-seq revealed extensive transcriptional heterogeneity in viral RNA abundance and the IFN-I response across single cells (Fig. 2D, 3, 4). The majority of WNV reads mapped to the targeted region of the WNV genome (Fig. 2D). However, minimal non-random background was observed in Mock cells with a median value of 45 WNV CPM for Mock cells, as compared to 37246 WNV CPM for WNV cells. This background may result from index hopping (210) and could be accounted for in subsequent iterations by using unique indexes. In support of published findings (88, 94-97), we found that few cells produce IFN-β transcript following viral infection (Fig. 3A). However, we observed a strong induction of numerous ISGs (*Irf7*, *Ddx58*, *Dhx58*, *Irf9*, *Stat1* and *Stat2*) with high unimodal expression signatures (Fig. 3), highlighting the well-established importance of IFN-I-dependent paracrine signaling (53, 93-97). Interestingly, we saw a bifurcation in ISG correlations with viral RNA, wherein 124 out of 294 ISGs were negatively correlated with intracellular viral abundance (Fig. 5B). Furthermore, a

considerable fraction of ISGs featured a precipitous downward trend in expression with increasing viral RNA, dissimilar to the gradual upward trend exhibited by positively correlated genes (Fig. 6). Collectively, these findings are reflective of the dynamic balance and interplay between host and viral factors within a single cell. This represents the first single-cell transcriptomics study of flavivirus infection to examine the correlation of ISGs with intracellular viral RNA. To extend this arm of our analysis, we examined WNV-targeting antiviral effector genes that have been previously validated through short hairpin RNA (shRNA) and small interfering RNA (siRNA) knockdown screens, cell-based overexpression assays and *in vivo* knockout models (50, 53, 137, 198-205). These validated antiviral effector genes exhibited both unimodal (*Tnfsf10*, *Ifi44l*, *Ifitm3*, *Eif2ak2* and *Mov10*) and bimodal (*Rsad2*, *Oas1b* and *Oas3*) expression patterns and all negatively correlated with viral RNA (Fig. 4, 6), demonstrating the technical capacity of WNV-inclusive scRNA-seq to probe virus-host interactions and identify novel antiviral candidate genes.

The discovery that bimodal variation in IFN-stimulated genes (ISGs) correlates with viral RNA abundance (Fig. 4, 6) bears notable relevance to previous work examining WNV antagonism of IFN-I signaling. WNV, among other flaviviruses, directly or indirectly antagonizes IFN-I signaling and the JAK-STAT pathway to counter cellular antiviral defenses (71-73, 76, 77). The WNV nonstructural protein NS5 blocks Jak1 and Tyk2 activation by interacting with prolidase to inhibit surface expression of IFNAR1 (71, 74). Additionally, WNV recruits plasma membrane-derived cholesterol to replication sites in the ER, and NS4A and NS4B contribute to membrane rearrangement and associated ER stress, which is thought to interfere with JAK-STAT signaling (70, 71, 75,

82). Bimodal ISG expression patterns correlated with viral abundance (Fig. 4, 6) may result from viral antagonism in primary infected cells allowing for higher replication. This is supported by the almost uniformly high expression observed for ISGs when limiting *in vitro* spread (Fig. 4), a cell population with a predominantly low-level of WNV replication (Fig. 2D). Alternatively, bimodality may arise from preexisting cell-intrinsic differences, such as the level of critical signaling components, specifically at the initial stage of infection.

WNV-inclusive scRNA-seq provides a single-cell transcriptomics protocol to probe cellular heterogeneity in the host response and quantify viral RNA. The outlined approach can potentially serve as a valuable tool for *in vivo* studies to examine cell-intrinsic responses to viral infection, extending the resolution to infected single cells. Such studies can also leverage the added ability with this approach to screen for infected cells by qPCR and cherry-pick cDNA for sequencing to mitigate the cost. Our study demonstrates the feasibility and utility of WNV-inclusive scRNA-seq as a high-throughput technique for single-cell transcriptomics and viral RNA detection, which can be used to provide insights into the cellular features of protective immunity.

MATERIALS AND METHODS

Cells and viruses. Murine fibroblast L929 cells were obtained from ATCC and grown at 37°C with 5% CO_2 in DMEM (Corning) supplemented with 10% heat-inactivated FBS, 2mM L-glutamine (Corning), 25 mM HEPES buffer (Corning), 1mM sodium pyruvate (Corning), MEM nonessential amino acids (Corning) and antibiotics/antimycotics (Corning). WNV isolate Texas 2002-HC (WNV-TX) has been previously described (3, 143, 211), and its titer was determined by standard plaque assay on BHK-21 cells. Working stocks were generated by passaging WNV-TX twice on Vero cells (ATCC CCL81) and used for *in vitro* experiments. WNV was incubated directly under ultraviolet (UV) light for 1 hr to generate UV-inactivated WNV, which was confirmed by plaque assay before use.

Infection and antibody treatment. L929 cells were plated to 70-80% confluent and infected with WNV-TX at different MOIs (0.1, 1 or 10). Following a 1 hr virus adsorption period at 37°C, cells were washed once with complete DMEM (cDMEM) and subsequently incubated for 6-48 hr with cDMEM or cDMEM supplemented with WNV E16 neutralizing antibody (5 μg/mL), a gift from Michael Diamond (Washington University, St. Louis, Missouri) (192). Cells were trypsinized for flow staining or lysed for RNA at 6, 12, 24 or 48 hr post-infection. Antibody titration in supplemental media was performed at multiple MOIs (0.1, 1 or 10) for 48 hr post-infection to determine the optimal concentration to considerably reduce *in vitro* spread before use.

Flow cytometry. Conditions were run in biological triplicate samples. Cells were treated with 0.125% trypsin in PBS for 5 min at 37°C. All centrifugation steps were performed at 1250 rotations per minute for 5 min at 4°C. Cells were pelleted, resuspended in FACS buffer (1x PBS, 1% FBS, 1 mM EDTA), and blocked for 10 min on ice with anti-mouse Fc Shield (TONBO Biosciences) at 0.5 µL per sample in FACS buffer. Subsequently, samples were stained for 20 min on ice with Ghost 780 viability dye (TONBO Biosciences) at 0.1 µL per sample in PBS. Samples were washed and resuspended in FACS buffer. For WNV E protein staining, samples were fixed following viability staining with 1x Transcription Factor Fix/Perm (diluted in Transcription Factor Fix/Perm Diluent; TONBO Biosciences) for 20 min on ice and washed twice with 1x Flow Cytometry Perm Buffer (diluted in ddH_2O; TONBO Biosciences). WNV E16 antibody was conjugated to Allophycocyanin (APC) using the Lightning-Link APC Antibody Labeling Kit (Novus Biologicals). Samples were stained with APC-conjugated WNV E16 antibody at 0.25 µg per sample in Flow Cytometry Perm Buffer for 30 min on ice. Samples were washed, resuspended in FACS buffer, and run on a BD LSR II flow cytometer.

Single-cell sorting. Cells were stained with Ghost 780 viability dye (TONBO Biosciences) as stated above and filtered through a 35 µm strainer into a 5 mL FACS tube. Single viable cells were sorted into skirted 96-well PCR plates containing 10 µL RLT buffer (Qiagen) with beta-mercaptoethanol (1:100) per well using a BSL-3 level BD Aria II flow cytometer.

Quantitative RT-PCR (qPCR). Time-matched mock and WNV-infected L929 cells (1×10^5 cells per condition; in triplicate) were lysed in RNA Lysis Buffer. Total RNA was isolated from cells using the Quick-RNA MiniPrep Kit (Zymo Research). Purified RNA was reverse transcribed using random primers with the High-Capacity cDNA Reverse Transcription Kit (Applied Biosystems). WNV RNA levels were quantified by qPCR using PrimeTime Gene Expression Master Mix (Integrated DNA Technologies), WNV-specific primers and probe set, and TaqMan gene expression assay (ThermoFisher) for the host gene *Gapdh* (Mm99999915_g1). WNV-specific primer and probe sequences (Forward primer: 5' – TCAGCGATCTCTCCACCAAAG – 3'; Reverse primer: 5' – GGGTCAGCACGTTTGTCATTG – 3'; and Probe: 5' – 6FAM-TGCCCGACC-ATGGGAGAAGCTC-MGB – 3') were adapted from Lanciotti and colleagues (211) and correspond to WNV isolate Texas 2002-HC (GenBank accession number: DQ176637.1). C_T values were normalized to the reference gene *Gapdh* and represented as fold change over time-matched mock values using the formula $2^{-\Delta\Delta CT}$. All primers and probes were purchased from Integrated DNA Technologies (IDT). qPCR was performed in 384-well plates and run on an Applied Biosystems 7900 HT Real-Time PCR System.

Bulk mRNA sequencing (RNA-seq). L929 cells were infected with WNV (MOI of 1) and incubated in the absence or presence (+Ab) of WNV E16 neutralizing Ab. In biological triplicate (n = 3), 50,000 viable cells were sorted into 100 µL RLT buffer (Qiagen) with beta-mercaptoethanol (1:100) at 24 hr post-infection for each condition: time-matched mock, WNV and WNV (+Ab). mRNA sequencing libraries were prepared at Yerkes Genomics Core (http://www.yerkes.emory.edu/nhp_genomics_core/), and the

quality of the libraries was verified using DNA-1000 Kits (Agilent Bioanalyzer) and quantified using the Qubit 2.0 Fluorometer (LifeTechnologies). Libraries were clustered and sequenced on an Illumina HiSeq (100 bp single-end reads). Sequencing reads were mapped to the GENCODE mouse reference genome (GRCm38.p5 Release M16). Reads were normalized and differential expression analysis performed using DESeq2 (212). Normalized reads were expressed as fold change over time-matched mock values.

Single-cell RNA sequencing (scRNA-seq). SMART-Seq v4 Ultra Low Input RNA Kit (Takara) was used for cDNA preparation. The protocol was modified to include a WNV-specific viral primer during the RT step. WNV SC primer (5’ – AAGCAGTGGTATCAACGCAGAGTACGGGTCAGCACGTTTGTCATTG – 3’) targets the positive-sense envelope protein (E) gene (211) and contains the 5' 25-nucleotide ISPCR universal anchor sequence (underlined) from the Smart-seq2 protocol published by Picelli and colleagues (193) for downstream amplification alongside 3’ SMART-Seq CDS Primer II A-primed transcripts. Similar to 3’ SMART-Seq CDS Primer II A, 1 µL of WNV SC primer (12 µM) was added to the RT reaction for all samples. Other WNV-specific primer sequences and concentrations were evaluated. The scRNA-seq protocol was optimized to ensure high sensitivity for WNV RNA detection and to mitigate the formation of primer dimers or template-switching oligo (TSO) concatemers observed at high concentrations or with other primer sequences. During template switching, the RT product is extended with a sequence complementary to the TSO due to the addition of 2-5 untemplated nucleotides and the capacity of the RT enzyme to switch templates just

as described in Smart-seq2 (193). PCR is performed using PCR Primer II A (the ISPCR universal anchor sequence) for concurrent amplification of both host and viral cDNA. Following PCR amplification, cDNA quantification is performed for each sample, and cDNA quality assessment is accomplished using an Agilent 2100 Bioanalyzer. For library preparation, amplified cDNA is fragmented and appended with dual-indexed barcodes using Illumina Nextera XT DNA Library Prep kits. Sequencing was performed using 101-bp single-end reads at Yerkes Genomics Core (http://www.yerkes.emory.edu/nhp_genomics_core/) as previously described (213) on an Illumina HiSeq 3000 at a depth of ~1,000,000 reads per cell. In total, 127 cells were successfully captured and profiled for single-cell transcriptomic analysis: 25 Mock cells, 68 WNV cells, and 34 WNV (+Ab) cells.

Bioinformatics pipeline. Libraries were sequenced on an Illumina HiSeq 3000 generating 101-bp single-end reads. FastQC (214) was used to check the quality of fastq files. The primary assembly of GENCODE mouse reference genome (GRCm38.p5 Release M16) (215) and the complete genome of WNV isolate Texas 2002-HC (GenBank accession number: DQ176637.1) from ViPR (216) were used for mapping reads. The genome index was built by combining both the genomes, and alignments were carried out for the combined genomes. STAR v2.5.2b (217) was used with default parameters to map reads and obtain reads per gene counts (–quantMode Gene Counts). The counts obtained with STAR were used for downstream analysis in R. The counts were used to create a SingleCellExperiment v1.0.0 (218) object. The scater v1.6.3 (219) library was used for the quality control of cells. Genes that were not

expressed in any cell were filtered out. The isOutlier function from scran was used to remove cells that had a library size and a number of detected genes greater than 3 median absolute deviations lower than the median values or those with the percentage of mitochondrial genes that were 3 median absolute deviations higher than the median value (220). The cell cycle phase was predicted using the cyclone function in scran package v1.6.3 (218, 220). The normalized expression values were obtained using the calculateCPM function in the scater library.

Statistical analysis and software. Prism 6 (GraphPad), ggplot2 R package, ggridges R package, corrplot R package and Hmisc R package were used for statistical analyses and graphical presentation of data. Spearman's rank correlation coefficients (ρ) and associated *p* values were computed for each gene pairing using the rcorr function in Hmisc R package. Two-way ANOVA with Tukey's multiple comparison correction was used to evaluate significant differences between conditions for the percentage of WNV E-positive cells and relative viral RNA. Wilcoxon rank-sum test with continuity correction was performed to assess significant differences between single-cell distributions for host mRNA and viral RNA counts per million transcripts (CPM).

FIGURE LEGENDS

Figure 1. Population-level analysis of WNV infection in L929 cells.

(A) L929 cells were infected with WNV at an MOI of 0.1, 1, or 10 and incubated for 6, 12, 24, or 48 hr (n = 3). (B) Intracellular viral E protein staining was performed by flow cytometry using the WNV E16 antibody. (B-C) L929 cells were inoculated with UV-inactivated WNV (UV) or WNV at an MOI of 1 and incubated for 12 or 24 hr in the presence (+Ab) or absence of the WNV E16 neutralizing antibody (5 μg/mL) to reduce *in vitro* spread (n = 3). (C) Viral RNA quantification was measured by qPCR, and C_T values were normalized to the reference gene *Gapdh* and represented as fold change over time-matched mock values. (A-C) Two-way ANOVA with multiple comparison correction was used to test for significance (*$p < 0.05$). (D-F) Cells were infected as in (B) and examined by bulk RNA-seq analysis at 24 hr post-infection (n = 3). (D-E) Heat map showing mean gene expression values normalized and represented as fold change over time-matched mock values. Expression fold change values correspond to the color gradient on the bottom. (D) Gene cluster description can be found on the left. (E) Expression fold change displayed for a panel of select genes. (F) Scatter plot for comparison of up-regulated and down-regulated genes in WNV and WNV (+Ab) conditions. Cutoff values were as follows: 1.5 fold change and $p < 0.01$.

Figure 2. WNV-inclusive single-cell RNA sequencing.

(A) L929 cells were infected with WNV (MOI of 1) and incubated in the presence of the WNV E16 neutralizing Ab (5 μg/mL) to limit *in vitro* spread. (B) Single cells were sorted into 96-well PCR plates containing 10 μL lysis buffer per well. (C) During reverse

transcription (RT), 3' SMART-Seq CDS Primer II A (30-nucleotide poly-dT sequence with a 5' 25-nucleotide ISPCR universal anchor sequence) and a WNV-specific viral primer (21-nucleotide sequence complementary to positive-strand viral RNA with a 5' 25-nucleotide ISPCR universal anchor sequence) are added to capture host transcripts and viral RNA, respectively. When the reverse transcriptase reaches the 5' end of both host mRNA and viral RNA, its terminal transferase activity adds 2-5 untemplated nucleotides that serve as an anchor for the template-switching oligo (TSO), which allows extension of the RT product with sequence complementary to the universal anchor sequence. PCR Primer II A binds this sequence for concurrent amplification of both host and viral cDNA. In the final library preparation step, transposase 5 (Tn5)-based Nextera tagmentation adds sequencing indexes. Illumina sequencing is performed using 101-bp single-end reads, thereby quantifying host mRNA and viral RNA from single cells. (B-C) In total, 127 cells were successfully captured and profiled: 25 Mock cells, 68 WNV cells, and 34 WNV (+Ab) cells. (D) Coverage and alignment of WNV reads are shown with reference to the WNV genome and WNV SC primer (viral primer) location, and y-axes are in log10 scale. The cells representing the median value for WNV and Mock conditions are shown. Violin plot showing expression as counts per million transcripts (CPM) in log2 scale for WNV RNA in all three conditions described in 2A. Wilcoxon rank-sum test with continuity correction was performed to test significance (**$p < 10^{-9}$). (E) Violin plots showing expression as CPM in log2 scale for housekeeping genes. Wilcoxon rank-sum test with continuity correction was performed to test significance (ns = not significant; *$p < 10^{-3}$; **$p < 10^{-6}$).

Figure 3. Cellular heterogeneity in IFN-stimulated gene induction following WNV infection.

Violin plots showing single-cell distributions for host gene expression as counts per million transcripts (CPM) in log2 scale. Genes are grouped by categories: (A) IFN-I production and other cytokines; and (B) PRR and IFN-I signaling. Conditions are described in Fig. 2A. Wilcoxon rank-sum test with continuity correction was performed to test significance (ns = not significant; *$p < 10^{-3}$; **$p < 10^{-6}$).

Figure 4. Unimodal and bimodal variation in antiviral effector gene expression at single-cell following WNV infection.

Violin plots showing single-cell distributions for antiviral effector gene expression as counts per million transcripts (CPM) in log2 scale. Conditions are described in Fig. 2A. Wilcoxon rank-sum test with continuity correction was performed to test significance (ns = not significant; *$p < 10^{-3}$; **$p < 10^{-6}$).

Figure 5. ISGs negatively correlate with WNV RNA abundance.

(A) Gene ontology (GO) enrichment analysis for genes significantly ($p < 0.001$) positively correlated ($\rho > 0.35$) and negatively correlated ($\rho < -0.35$) with viral RNA. Enrichment scores (ES) calculated for each pathway by the formula: $-\log_{10}(p\text{-value})$. Dotted line indicates significance cutoff ($p = 0.05$; ES = 1.3). (B) Density plots of host gene expression correlated viral RNA across all WNV cells. Spearman's correlation coefficients (ρ) calculated for each host gene by viral RNA. Gene set labels (left) and totals (right) are shown. Cell cycle-associated genes are additionally subdivided by

phase. Select genes were marked and labeled. Dotted lines indicate correlation coefficients (ρ) equal to -0.35 and 0.35. (C) Correlation matrix for 57 of 124 negatively correlated ISGs, all positively correlated ISGs, 9 non-correlated cytokine genes and WNV RNA. Correlation coefficients (ρ) calculated for each gene pairing are indicated by the color gradient at the bottom. White boxes represent comparisons for which the correlation did not meet the significance cutoff ($p < 0.001$).

Figure 6. Sharp downward trends for ISGs negatively correlated with viral RNA.

Scatter plots showing expression as counts per million transcripts (CPM) in log2 scale of positively and negatively correlated host genes by WNV RNA. Each cell is represented by a single dot with minimal transparency so areas of high density are easily discernable. Correlation coefficients (ρ) are indicated for each gene and correspond to the color gradient at the top. Scatter plots have been collated from the lowest to the highest correlation coefficient. All genes shown here meet the following criteria: $|\rho| > 0.4$ and $p < 0.0005$.

Figure 1

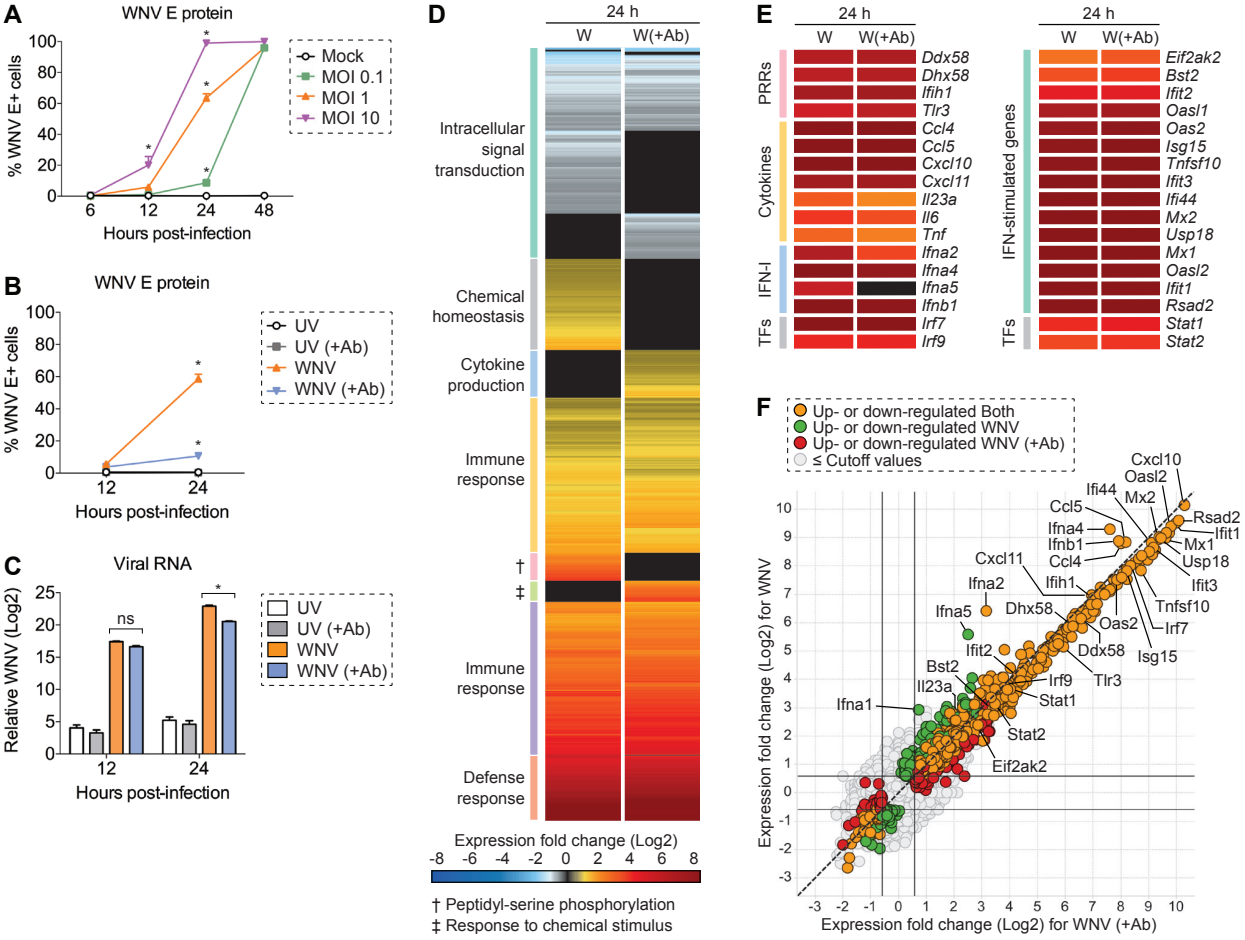
A
WNV E protein
% WNV E+ cells
Hours post-infection
Mock
MOI 0.1
MOI 1
MOI 10
B
WNV E protein
% WNV E+ cells
Hours post-infection
UV
UV (+Ab)
WNV
WNV (+Ab)
C
Viral RNA
Relative WNV (Log2)
ns
Hours post-infection
UV
UV (+Ab)
WNV
WNV (+Ab)
D
24 h
W
W(+Ab)
Intracellular signal transduction
Chemical homeostasis
Cytokine production
Immune response
†
‡
Immune response
Defense response
Expression fold change (Log2)
† Peptidyl-serine phosphorylation
‡ Response to chemical stimulus
E
24 h
W
W(+Ab)
PRRs
Cytokines
IFN-I
TFs
Ddx58
Dhx58
Ifih1
Tlr3
Ccl4
Ccl5
Cxcl10
Cxcl11
Il23a
Il6
Tnf
Ifna2
Ifna4
Ifna5
Ifnb1
Irf7
Irf9
IFN-stimulated genes
TFs
Eif2ak2
Bst2
Ifit2
Oasl1
Oas2
Isg15
Tnfsf10
Ifit3
Ifi44
Mx2
Usp18
Mx1
Oasl2
Ifit1
Rsad2
Stat1
Stat2
F
Up- or down-regulated Both
Up- or down-regulated WNV
Up- or down-regulated WNV (+Ab)
≤ Cutoff values
Expression fold change (Log2) for WNV
Expression fold change (Log2) for WNV (+Ab)
Cxcl10
Oasl2
Ifi44
Mx2
Ccl5
Ifna4
Ifnb1
Rsad2
Ifit1
Mx1
Usp18
Cxcl11
Ccl4
Ifih1
Ifit3
Ifna2
Ifna5
Dhx58
Tnfsf10
Oas2
Irf7
Ifit2
Ddx58
Isg15
Bst2
Il23a
Irf9
Tlr3
Ifna1
Stat1
Stat2
Eif2ak2

Figure 2

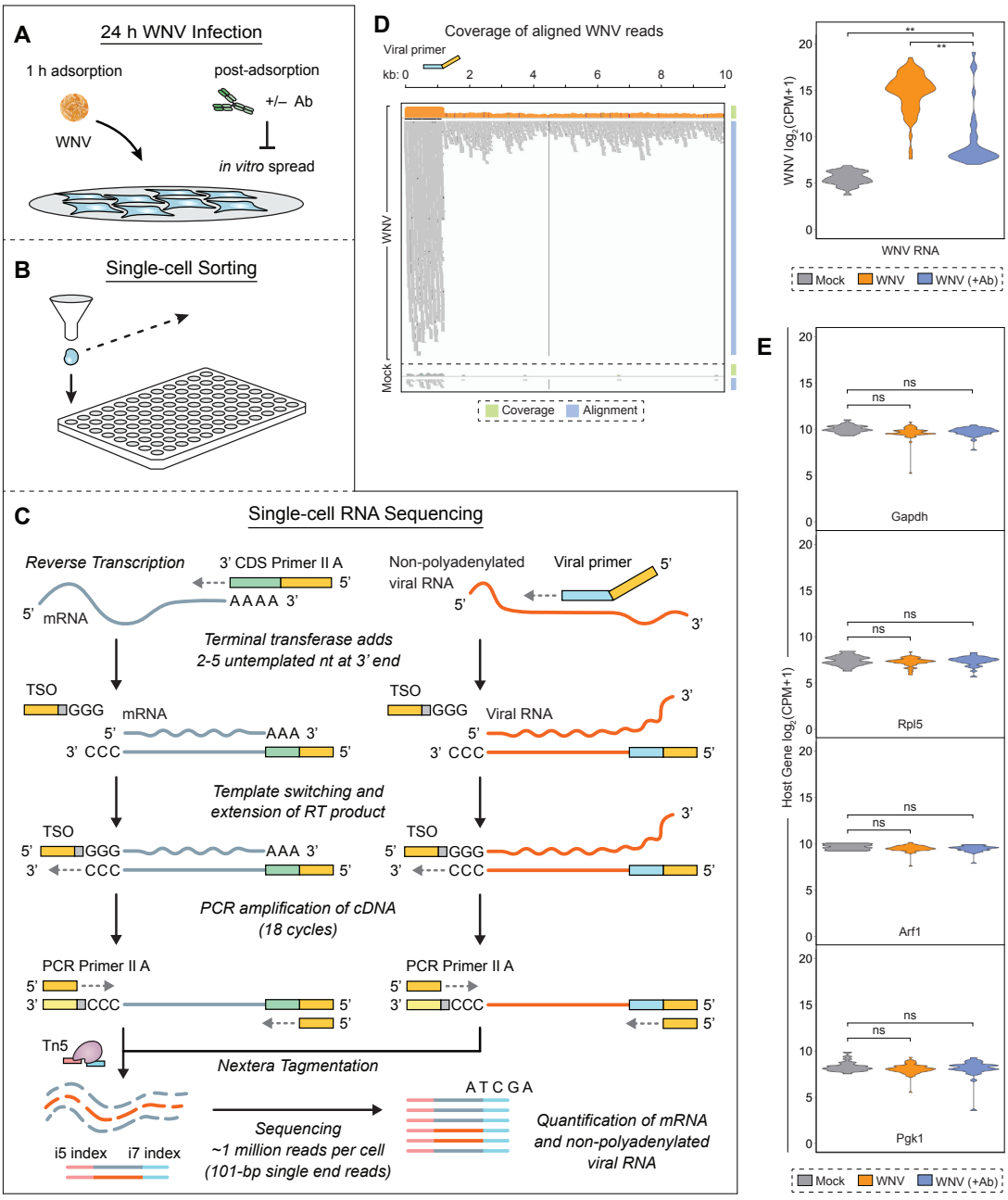
A
24 h WNV Infection
1 h adsorption
post-adsorption
+/– Ab
WNV
in vitro spread
B
Single-cell Sorting
C
Single-cell RNA Sequencing
Reverse Transcription
3' CDS Primer II A
5'
AAAA 3'
mRNA
Non-polyadenylated viral RNA
Viral primer
Terminal transferase adds 2-5 untemplated nt at 3' end
TSO
GGG
CCC
Template switching and extension of RT product
PCR amplification of cDNA (18 cycles)
PCR Primer II A
Tn5
Nextera Tagmentation
i5 index
i7 index
Sequencing
~1 million reads per cell
(101-bp single end reads)
A T C G A
Quantification of mRNA and non-polyadenylated viral RNA
D
Coverage of aligned WNV reads
Viral primer
kb: 0
2
4
6
8
10
WNV
Mock
Coverage
Alignment
E
WNV log2(CPM+1)
WNV RNA
Mock
WNV
WNV (+Ab)
Host Gene log2(CPM+1)
Gapdh
Rpl5
Arf1
Pgk1
ns
**

Figure 3

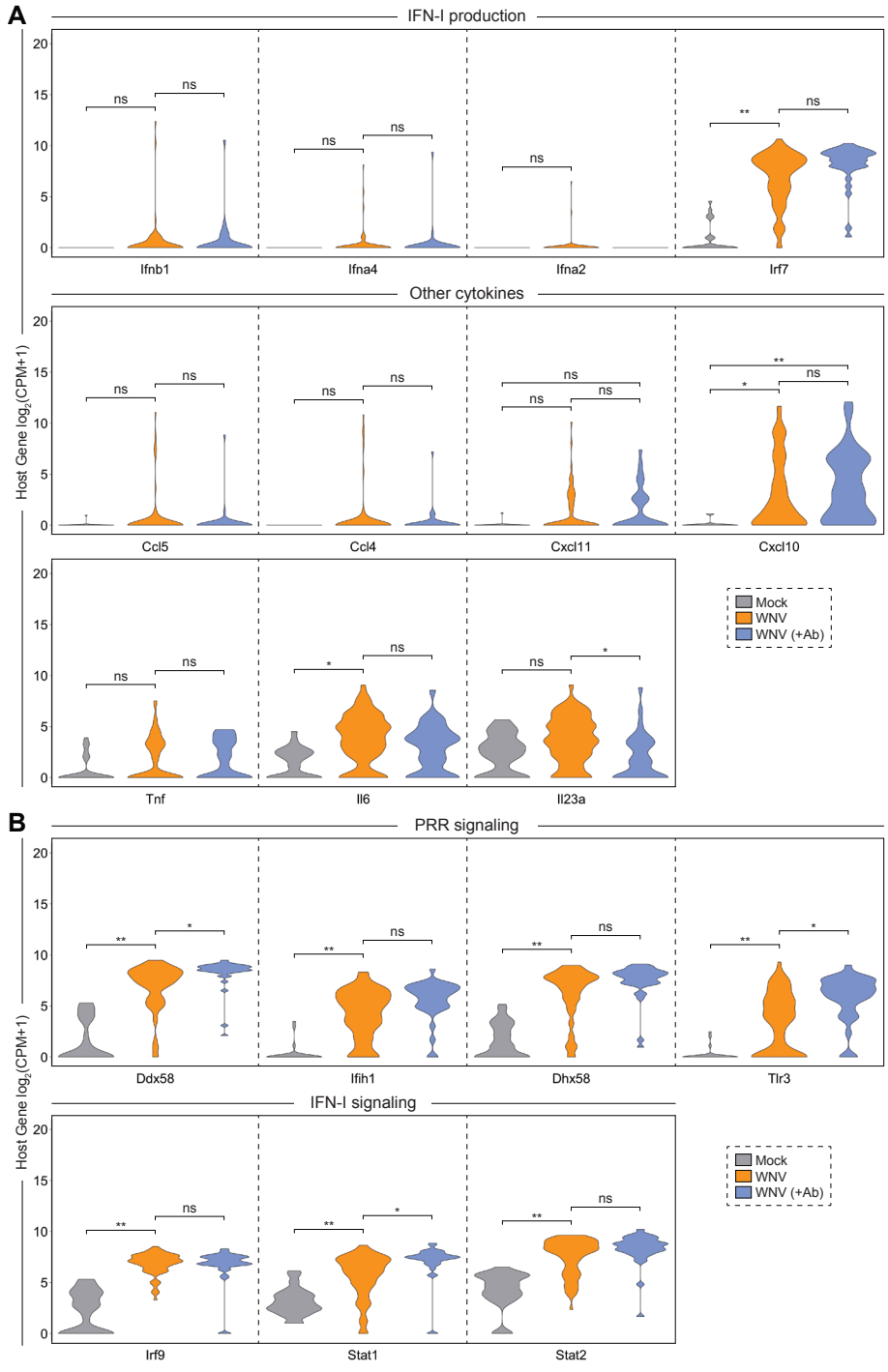
A
IFN-I production
Other cytokines
Host Gene log2(CPM+1)
Ifnb1
Ifna4
Ifna2
Irf7
Ccl5
Ccl4
Cxcl11
Cxcl10
Tnf
Il6
Il23a
Mock
WNV
WNV (+Ab)
B
PRR signaling
IFN-I signaling
Ddx58
Ifih1
Dhx58
Tlr3
Irf9
Stat1
Stat2
ns

Figure 4

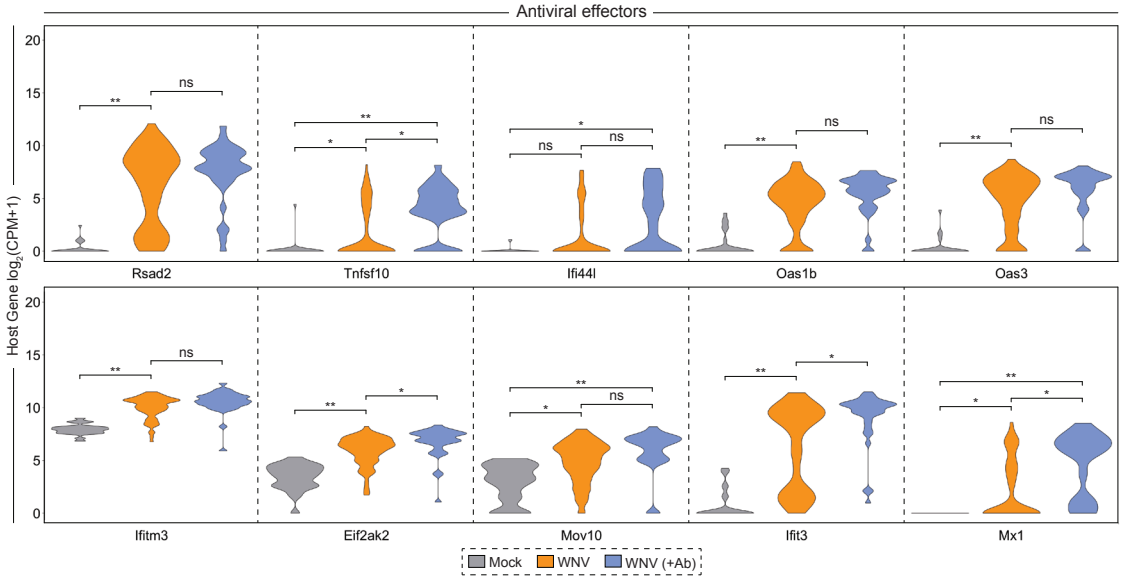
Antiviral effectors
Host Gene log2(CPM+1)
Rsad2
Tnfsf10
Ifi44l
Oas1b
Oas3
Ifitm3
Eif2ak2
Mov10
Ifit3
Mx1
Mock
WNV
WNV (+Ab)

Figure 5

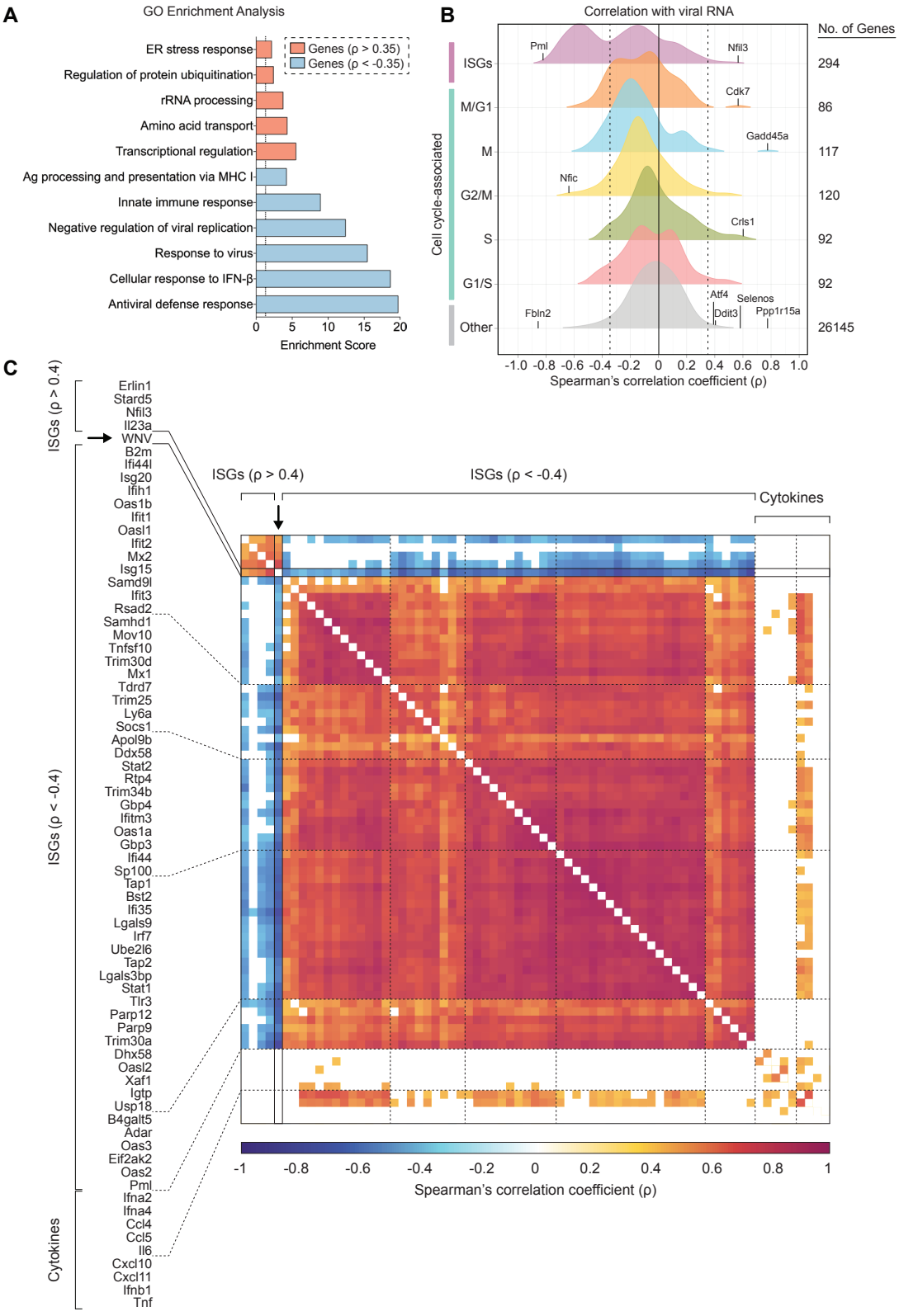
A
GO Enrichment Analysis
ER stress response
Regulation of protein ubiquitination
rRNA processing
Amino acid transport
Transcriptional regulation
Ag processing and presentation via MHC I
Innate immune response
Negative regulation of viral replication
Response to virus
Cellular response to IFN-β
Antiviral defense response
Genes (ρ > 0.35)
Genes (ρ < -0.35)
0 5 10 15 20
Enrichment Score
B
Correlation with viral RNA
No. of Genes
Cell cycle-associated
ISGs
M/G1
M
G2/M
S
G1/S
Other
294
86
117
120
92
92
26145
Pml
Nfil3
Cdk7
Gadd45a
Nfic
Crls1
Atf4
Selenos
Ddit3
Ppp1r15a
Fbln2
-1.0 -0.8 -0.6 -0.4 -0.2 0 0.2 0.4 0.6 0.8 1.0
Spearman's correlation coefficient (ρ)
C
ISGs (ρ > 0.4)
ISGs (ρ < -0.4)
Cytokines
Erlin1
Stard5
Nfil3
Il23a
WNV
B2m
Ifi44l
Isg20
Ifih1
Oas1b
Ifit1
Oasl1
Ifit2
Mx2
Isg15
Samd9l
Ifit3
Rsad2
Samhd1
Mov10
Tnfsf10
Trim30d
Mx1
Tdrd7
Trim25
Ly6a
Socs1
Apol9b
Ddx58
Stat2
Rtp4
Trim34b
Gbp4
Ifitm3
Oas1a
Gbp3
Ifi44
Sp100
Tap1
Bst2
Ifi35
Lgals9
Irf7
Ube2l6
Tap2
Lgals3bp
Stat1
Tlr3
Parp12
Parp9
Trim30a
Dhx58
Oasl2
Xaf1
Igtp
Usp18
B4galt5
Adar
Oas3
Eif2ak2
Oas2
Pml
Ifna2
Ifna4
Ccl4
Ccl5
Il6
Cxcl10
Cxcl11
Ifnb1
Tnf
-1 -0.8 -0.6 -0.4 -0.2 0 0.2 0.4 0.6 0.8 1
Spearman's correlation coefficient (ρ)

Figure 6

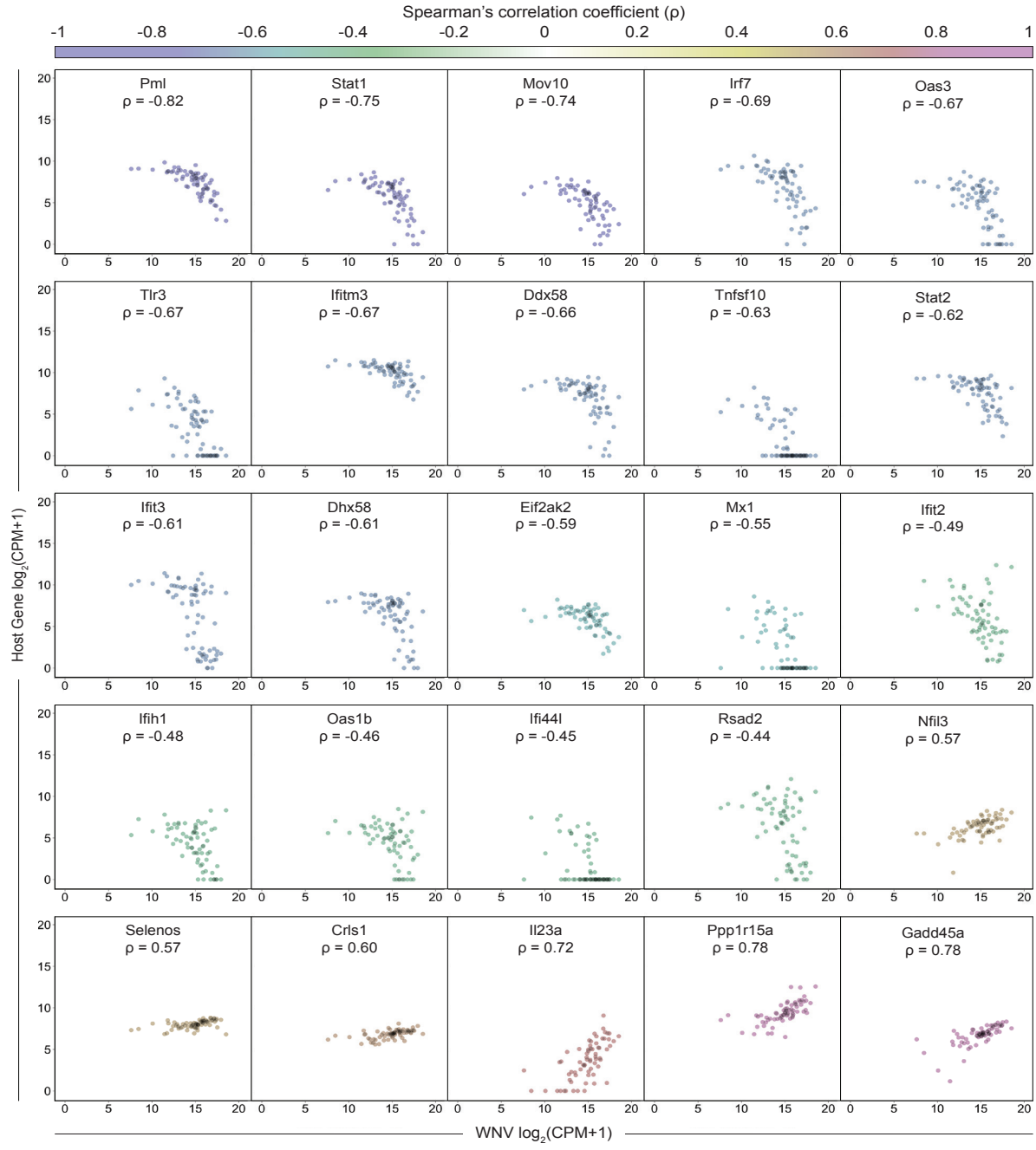
Spearman's correlation coefficient (ρ)
-1
-0.8
-0.6
-0.4
-0.2
0
0.2
0.4
0.6
0.8
1
Pml
ρ = -0.82
Stat1
ρ = -0.75
Mov10
ρ = -0.74
Irf7
ρ = -0.69
Oas3
ρ = -0.67
Tlr3
ρ = -0.67
Ifitm3
ρ = -0.67
Ddx58
ρ = -0.66
Tnfsf10
ρ = -0.63
Stat2
ρ = -0.62
Ifit3
ρ = -0.61
Dhx58
ρ = -0.61
Eif2ak2
ρ = -0.59
Mx1
ρ = -0.55
Ifit2
ρ = -0.49
Ifih1
ρ = -0.48
Oas1b
ρ = -0.46
Ifi44l
ρ = -0.45
Rsad2
ρ = -0.44
Nfil3
ρ = 0.57
Selenos
ρ = 0.57
Crls1
ρ = 0.60
Il23a
ρ = 0.72
Ppp1r15a
ρ = 0.78
Gadd45a
ρ = 0.78
Host Gene log2(CPM+1)
WNV log2(CPM+1)

Acknowledgments

We thank the Emory Vaccine Center Flow Core, specifically Kiran Gill and Barbara Cervasi, for assistance with cell sorting and the Yerkes Genomics Core for library preparation and sequencing.

Funding Information

This work was funded in part by National Institutes of Health grants U19AI083019 (M.S.S), (M.S.S), 5U19AI106772 (M.S.S), R21AI113485 (M.S.S.), ORIP/OD P51OD011132 (M.S.S), Emory University Department of Pediatrics Junior Faculty Focused Award (M.S.S), Children's Healthcare of Atlanta, Emory Vaccine Center, and The Georgia Research Alliance (M.S.S). The funders had no role in study design, data collection and analysis, decision to publish, or preparation of the manuscript.

Central nervous system-draining lymphatics and $CD8^+$ T cell control during West Nile virus infection

Justin T. O'Neal[a,b,1], Abigail Vanderheiden[a,b,1], Devon Eddins[a,b], Renan Aguilar-Valenzuela[a,b], Arash Grakoui[b], Mehul S. Suthar[a,b]

[a]Department of Pediatrics, Division of Infectious Disease, Emory University School of Medicine, Atlanta, Georgia, USA

[b]Emory Vaccine Center, Yerkes National Primate Research Center, Atlanta, Georgia, USA

[1]Co-first authors

ABSTRACT

Neuroinvasive West Nile virus (WNV) infection requires efficient $CD8^+$ T cell responses for virologic control. We found that the meninges and central nervous system (CNS)-draining lymph nodes (LNs) have detectable viral RNA early on during pathogenesis and CNS-localized WNV-specific $CD8^+$ T cells were phenotypically and functionally distinct from peripheral WNV-specific $CD8^+$ T cells. Viral RNA and conventional dendritic cell (DC) activation were observed in both peripheral and CNS-draining lymphoid tissues prior to early replication in the brain. The temporal dynamics of WNV-specific $CD8^+$ T cell accumulation in CNS-draining LNs resembled that of the spleen. WNV-specific $CD8^+$ T cells from the spleen and brain displayed dramatically different cytokine profiles and expression of activation and inhibitory markers, whereas WNV-specific $CD8^+$ T cells from meninges and CNS-draining LNs exhibited unique intermediate phenotypes. Brain WNV-specific $CD8^+$ T cells were more efficient at controlling viral infection in neuronal co-culture than splenic WNV-specific $CD8^+$ T cells. These findings highlight the early involvement of CNS-draining lymphatics during WNV pathogenesis and demonstrate that anatomic localization influences $CD8^+$ T cells both phenotypically and functionally.

INTRODUCTION

West Nile virus (WNV) is a neurotropic mosquito-borne flavivirus of global importance (1-3, 5, 6). Neuroinvasive WNV infection results in encephalitis and can lead to prolonged neurological impairment or death (1, 2, 5, 6). Induction of the host response mediates early virologic control in the periphery and promotes priming of adaptive immunity (40-42). Following early replication and dissemination to secondary lymphoid tissues, the neuroinvasive stage is characterized by brain parenchymal invasion, neuronal infection, neuroinflammation, and neuronal cell death (3, 39). Meningeal immunity has been demonstrated to play a pivotal role in central nervous system (CNS) defense against pathogen invasion (178, 181, 184). Antigen-presenting cells (APCs), such as dendritic cells (DCs) and border-associated macrophages (MΦs), within the meninges (dura, arachnoid and pia mater), choroid plexus, and perivascular spaces serve in an immune surveillance capacity to protect the CNS from invading pathogens (147, 175, 176). Immune cells traffick through meningeal lymphatic vessels, which drain to the superficial and deep cervical lymph nodes (scLNs and dcLNs, respectively) and support interactions between peripheral and CNS-localized immune cell populations (164, 165, 171, 174). Conventional DCs (cDCs) excel at initiating T cell responses by presenting antigen in MHC I (major histocompatibility complex class I) and MHC II and directing T cell polarization through cytokine secretion, whereas plasmacytoid DCs (pDCs), which are less efficient at antigen presentation, produce extensive amounts of type I interferon (IFN-I) in response to viral RNA and DNA (104-107). DCs, a key target cell of WNV infection, limit early viral replication and dissemination in the periphery through the production of IFN-I and pro-inflammatory cytokines and priming of both

humoral and cell-mediated responses (43, 46-48, 102, 103). Previous studies indicate that Batf3$^{-/-}$ mice, which lack cDC1s, fail to generate optimal WNV-specific effector CD8^{+} T cell responses (103, 110). Furthermore, infected and bystander CD8α^{+} CD11c^{+} DCs, but only infected CD11b^{+} CD11c^{-} myeloid cells, have been shown to present the immune-dominant WNV NS4B peptide epitope in complex with MHC I during WNV infection, supporting that DCs are critical for priming protective CD8^{+} T cell responses (111). Altogether, we have a broad understanding of the kinetics of viral spread in major tissue compartments and the integral role of DCs in virologic control; however, an in-depth examination of viral kinetics and immune cell dynamics within CNS-draining lymphatics is notably lacking.

CD8^{+} T cells are essential for control of WNV infection (44, 135). Mice lacking CD8α or MHC I exhibit increased mortality, higher viral burden in the CNS and periphery, and exaggerated pathology in the brain compared to wild-type mice (44). CD8^{+} T cells control WNV replication through the expression of death receptors, secretion of cytotoxic molecules, and production of antiviral cytokines such as TNF-α and IFN-γ (113, 136-141). Previous studies have demonstrated that CD8^{+} T cells require CXCR3 to migrate from meningeal vasculature adjacent to the cerebellum into the parenchyma and control WNV replication within this region of the CNS (144, 145). CNS-infiltrating antiviral CD8^{+} T cells require a reactivation signal from CNS-localized DC or MΦ populations during WNV infection, and the meninges have been speculated to be the site of these crucial interactions (102, 146). In the lymphocytic choriomeningitis virus (LCMV) model, splenic antigen-specific CD8^{+} T cells from white pulp and red pulp exhibited phenotypic and functional differences, supporting that

anatomic localization can influence antiviral T cell responses via environmental cues (142). During coronavirus infection, $CD8^+$ T cells were shown to require a re-activation signal for effective viral clearance after recruitment by CCL19 and CCL21-producing stroma cells in the meninges (184). In the experimental autoimmune encephalitis (EAE) model, CNS-infiltrating auto-reactive $CD4^+$ T cells have been shown to contribute to CNS damage following reactivation within the meninges upon stimulation from local APCs presumably presenting myelin antigen (182, 183). Altogether, these findings establish the importance of generating protective $CD8^+$ T cell responses and a potential role for meningeal immunity in promoting CNS defense during WNV infection.

In this study, we sought to define early viral kinetics and immune cell dynamics in peripheral lymphoid tissues and CNS-draining lymphatics, including the CNS-draining lymph nodes (LNs) and meninges. We found that WNV RNA and activated cDCs accumulate in the CNS-draining lymphatics prior to the peak viral burden in the CNS. Furthermore, accumulation of WNV-specific $CD8^+$ T cells in the CNS-draining LNs resembled that of the spleen, whereas meningeal T cell totals increased at later time points concurrent with brain T cell populations. Splenic and brain WNV-specific $CD8^+$ T cells exhibited disparate phenotypic profiles, while T cells from CNS-draining LNs and meninges displayed unique intermediate signatures. Substantial transcriptional differences were observed for splenic and CNS-localized WNV-specific $CD8^+$ T cells, further supporting that CNS-localized WNV-specific $CD8^+$ T cells were in a strong effector state as compared to splenic populations. Most notably, CNS-localized antigen-specific $CD8^+$ T cells were more efficient at controlling WNV infection of cortical neurons than splenic antigen-specific $CD8^+$ T cells, demonstrating that anatomic localization

influences the phenotypic signature and functional capacity of WNV-specific $CD8^+$ T cells. Our findings represent the first comprehensive analysis of early viral kinetics and immune cell dynamics between peripheral and CNS-draining lymphoid tissues, meninges and brain during neuroinvasive flavivirus infection.

RESULTS

Early viral spread in peripheral lymphoid tissues and initial DC response dynamics in skin draining lymph nodes. To assess early viral kinetics in peripheral lymphoid tissues, we performed qPCR on the spleen and immediate skin-draining LNs, namely the ipsilateral popliteal LN (popLN) and ipsilateral inguinal LN (ingLN), as well as distal draining LNs such as the contralateral popLN and the axillary LN (axilLN). Immediate skin-draining LNs (ipsilateral popLN and ingLN) showed peak viral burden around 1 day post-infection (p.i.) corresponding with previously published findings (31, 36, 37), whereas distal LNs such as the contralateral popLN and axilLN displayed the highest levels of viral RNA around 2 days p.i. (Fig. 1A). Viral RNA is detected in the serum at 10^3 copies per mL as early as 1 day p.i. and peaks at 4 days p.i. which coincides with early viral kinetics in the spleen (Fig. 1A). The spleen had detectable viral RNA as early as 1 day p.i. but did not peak until 4 days p.i. as well (Fig. 1A). When looking at ISG expression as a marker of the early innate immune response, we see a 5- to 8-fold increase in IFIT1 and RSAD2, two classically described IFN-I-stimulated genes (ISGs) (56, 59, 78, 203), by 1 day p.i. in the ipsilateral popLN, ingN and spleen (Fig. 1B). Interestingly, we do not see a marked increase in IFIT1 and RSAD2 expression in the axillary LN at 1 day p.i. (Fig. 1B), but these ISGs are upregulated by 2 days p.i. which is likely attributable to it having the lowest level of viral RNA at 1 day p.i. (Fig. 1A).

Dendritic cells are a key target cell of WNV infection, and therefore we next wanted to examine differential activation of dendritic cell subsets in the ipsilateral popLN and spleen compartments during the early post-inoculation phase of WNV

pathogenesis. In the ipsilateral popLN, cDC1s and pDCs exhibit elevated expression of the activation markers MHC I and CD86 with peak levels at 1 day p.i., while activation marker expression on cDC2s does not appear to increase over the first 3 days p.i. (Fig. 2). Interestingly, however, all three DC subsets display a steady increase in MHC I and CD86 expression through the first 1 to 3 days p.i. in the spleen (Fig. 2). In total, these results highlight the kinetics WNV dissemination in peripheral lymphoid tissues and indicate that DC subsets are differentially activated in the immediate skin-draining LN at 1 day p.i.

Viral RNA detection and activated cDC accumulation in CNS-draining lymphatics precede parenchymal invasion. To evaluate viral kinetics and the inflammatory response within CNS-draining lymphatics during WNV infection, we performed qPCR for viral RNA and ISG expression on CNS-draining LNs, brain and meninges. Viral RNA was detectable in CNS-draining LNs by 4 days p.i. (Fig. 3A). Additionally, viral RNA was detectable in the meninges as early as 4 days p.i. preceding the initial spike in viral replication in the brain which occurred between 4 and 6 days p.i. (Fig. 3A). Notably, CNS-draining LNs and meninges did not show a decline in viral RNA burden by 6 days p.i. unlike other peripheral compartments (Fig. 3A).

Given that viral RNA is detectable in the CNS-draining lymphatics early on in pathogenesis, we next wanted to assess shifts in antigen-presenting cell populations within these compartments. Correlating with viral RNA kinetics, we observed accumulation of cDCs, moDCs and inflammatory monocytes in the CNS-draining LNs at 4 days p.i. (Fig. 3B). For CNS-draining LNs, APC totals remained at levels higher than

mock through 6 to 8 days p.i. (Fig. 3B). These same myeloid cell populations did not significantly increase in the meninges through 8 days p.i. and began accumulating in the brain at 8 days p.i. (Fig. 3B). Corresponding with viral RNA levels, we observed that multiple APC populations, including cDCs, express higher levels of the activation markers MHC-I and CD86 at 4 days p.i. in CNS-draining LNs and meninges (Fig. 4). Altogether, these results demonstrate early detection of viral RNA and accumulation of activated APCs and in the CNS-draining LNs, which support early initiation of the inflammatory response in these compartments.

WNV-specific CD8$^+$ T cells exhibit differential accumulation in peripheral and CNS compartments. To further examine shifts in the cellular composition of CNS-draining LNs and meninges, we assessed the accumulation of antigen-specific CD8$^+$ T cells during WNV infection. WNV-specific CD8$^+$ T cells expand in the spleen at 5 and 7 days p.i. with the NS4B Tet$^+$ population contributing to around 2% of total CD8$^+$ T cells at 7 days p.i. (Fig. 5A). Notably, WNV-specific CD8$^+$ T cells increase in CNS-draining LNs and meninges by 7 days p.i. (Fig. 5B). By 10 days p.i., however, WNV-specific CD8$^+$ T cells have contracted in the CNS-draining LNs, potentially entering circulation, whereas both populations remain high in the meninges (Fig. 5B). Within the brain, WNV-specific CD8$^+$ T cell populations increase by 7 days p.i. with variability across mice; however, by 10 days p.i. all mice have consistently high totals for WNV-specific CD8$^+$ T cells (Fig. 5B). Notably, WNV-specific NS4B Tet$^+$ CD8$^+$ T cells accounted for roughly 30% of the total CD8$^+$ T cell population in the meninges and approximately 45% of total CD8$^+$ T cells in the brain at 10 days p.i. (Fig. 5B). In total, these data indicate that the

accumulation of WNV-specific $CD8^+$ T cell in CNS-draining LNs more closely resembles the temporal dynamics observed in the spleen rather than CNS tissues, supporting an early involvement of CNS-draining lymphatics during WNV pathogenesis.

Phenotypic differences between WNV specific $CD8^+$ T cells based on anatomic localization. Antigen-specific $CD8^+$ T cells are essential for controlling WNV in both the periphery and CNS, and the early involvement of CNS-draining lymphatics prompted us to explore whether phenotypic differences existed between T cell populations from peripheral lymphoid tissues, CNS-draining lymphoid tissues, meninges and brain. Therefore, we performed phenotypic analysis and cytokine profiling to determine if there were differences in the $CD8^+$ T cell responses across distinct anatomic compartments. These analyses could not be performed on bulk $CD8^+$ T cell populations as the results would be skewed by the differences between tissues in antigen-specific T cell frequencies (Fig. 5). Therefore, to normalize the WNV-specific $CD8^+$ T cell frequencies, we adoptively transferred naïve $CD8^+$ T cells from W4B T cell receptor (TCR)-transgenic mice, which have $CD8^+$ T cells that inherently recognize the immunodominant epitope in the WNV NS4B protein, to wild-type mice of a different congenic background (143) (Fig. 6A). We then utilized congenic markers to select for the transferred cells, of which >98% were WNV-specific (Fig. 6B).

We first compared the expression of various surface markers associated with $CD8^+$ T cell activation and effector function between peripheral and CNS compartments at 7 days p.i. (Fig. 6). Bulk NS4B Tet^- $CD8^+$ T cells, which serve as a negative control, displayed a low expression of CD44, a canonical marker of $CD8^+$ T cell activation (Fig.

6C). Conversely, WNV-specific W4B cells from spleen, scLN, dcLN, meninges and brain all upregulated CD44 expression (Fig. 6C). Interestingly, there were varying levels of CD44 expression among activated W4B cells across tissues (Fig. 6C). Cells isolated from the spleen and the meninges had the lowest MFIs, while cells isolated from the scLN, dcLN and brain had markedly higher MFIs (Fig. 6C). Notably, CD44 is an adhesion molecule that aids in the extravasation of $CD8^+$ T cells into tissues, in addition to promoting their movement within tissues. Therefore, these differences might reflect the degree of tissue residency of W4B cells across the various compartments. We can distinguish between $CD8^+$ T cells within the tissue, and those in the vasculature using intravital labeling of CD8 (143). When we compare the percentage of cells in the vasculature across tissues, we find lower CD44 expression on W4B cells for tissues where the majority of W4B cells are within the vasculature (data not shown). While CD44 is upregulated across these compartments, higher CD44 expression appears to correspond with higher frequencies of tissue-resident W4B cells.

Analysis of KLRG1 expression, another marker upregulated on $CD8^+$ T cells during the effector phase, showed that cells from the spleen (28%) and meninges (27%) had the highest frequency of KLRG1+ W4B cells (Fig. 6D). In contrast, W4B cells from the CNS-draining LNs and brain had a significantly lower frequency of KLRG1+ cells (Fig. 6D). This might suggest that W4B cells isolated from the spleen and meninges are most likely to be in the effector phase; however, when we examined inducible markers of activation, we did not see the same pattern. ICOS is an activation-induced co-stimulatory marker, and its expression was highest in the scLN, meninges and brain, suggesting that W4B cells in the brain, meninges, and scLN are receiving the most co-

stimulatory signals at 7 days p.i. (Fig. 6D). Analysis of PD-1, a co-inhibitory marker, found that the meninges (18%) and brain (10%) had the highest percentage of PD-1 expressing W4B cells, whereas the spleen (2.5%) and CNS-draining LNs (less than 5%) were significantly lower (Fig. 6D). PD-1 is upregulated after TCR activation, but its expression is also maintained when cells are receiving inhibitory signals. Therefore, PD-1 upregulation could reflect either recent stimulation with cognate antigen or the presence of immunoregulatory signals in the CNS (221-223). In total, these results demonstrate that $CD8^+$ T cells isolated from peripheral and CNS compartments have distinct phenotypes during WNV infection. W4B cells isolated from the CNS-draining LNs displayed extremely similar activation phenotypes, while the meninges and brain shared some but not all phenotypic markers.

To investigate differences in the cytokine production capacity of W4B cells across anatomic locations, we performed an *ex vivo* stimulation. Cells were stimulated with the cognate antigen NS4B peptide, and cytokines were accumulated within the cell via treatment with GolgiStop. As expected, unstimulated splenic W4B cells did not produce cytokines, and all stimulated W4B cells displayed detectable levels of cytokine production (Fig. 7), demonstrating that W4B cells are activated and able to respond to WNV at 7 days p.i. for all surveyed tissues. While all W4B cells responded to stimulation, we observed dramatically different cytokine profiles between peripheral and CNS tissues. Only 5-20% of W4B cells from peripheral compartments (spleen, scLN, and dcLN) produce either IFN-γ or TNF-α or both. Conversely, over 60% of meningeal W4B cells and over 85% of brain W4B cells exhibit IFN-γ or TNF-α production following *ex vivo* stimulation (Fig. 7). In addition to differences in total production, the cytokine

profiles were distinct between peripheral and CNS W4B cells. W4B cells from the periphery are predominantly producing TNF-α, and secreting little to no IFN-γ (Fig. 7). In contrast, brain and meningeal W4B cells are predominantly a TNF-α and IFN-γ double-positive population (Fig. 7). Of the single-producing populations in the CNS, W4B cells are more likely to be secreting IFN-γ than TNF-α (Fig. 7). These data show that W4B cells isolated from brain and meningeal compartments have a high-producing, polyfunctional cytokine signature, whereas peripheral W4B cells which have a low-producing, TNF-α-dominated signature.

Altogether, WNV-specific $CD8^+$ T cells are activated across the spleen, CNS-draining LNs, meninges and brain at day 7 p.i. with several notable differences between tissues. Brain and meningeal W4B cells expressed significantly higher levels of activation-induced receptors (ICOS and PD-1) as compared to the spleen and were around 5 times more likely to produce cytokines than W4B cells isolated from peripheral compartments (spleen, dcLN, scLN), in addition to displaying a distinct cytokine profile. In total, these findings demonstrate that there are substantial phenotypic differences for WNV-specific $CD8^+$ T cells across peripheral lymphoid tissues, CNS-draining lymphoid tissues, meninges and brain.

WNV-specific $CD8^+$ T cells from peripheral and CNS compartments are transcriptionally distinct. To further explore the differences between WNV-specific $CD8^+$ T cells in peripheral and CNS compartments at the transcriptional level, we performed RNA-seq analysis. We compared between splenic W4B cells and brain W4B cells as representative tissues for peripheral and CNS compartments, respectively. To

analyze transcriptional differences between peripheral and CNS-localized WNV-specific $CD8^+$ T cells, we utilized the same transgenic adoptive transfer system described above. W4B cells were transferred into naïve C57BL/6J mice (50,000 cells per mouse), and W4B cells were sorted from the spleen and brain at 7 days p.i. for RNA-seq (Fig. 8A).

Differential gene expression analysis found that, while there was overlapping gene expression between the two anatomic locations (1746 genes), 934 genes were uniquely expressed in splenic W4B cells and 736 genes in brain W4B cells (Fig. 8B). Many downregulated genes as compared to naïve were shared by W4B cells from both compartments (Fig. 8C). Notably, 422 of the uniquely expressed genes for W4B cells were upregulated, suggesting that upon entry to the CNS W4B cells are undergoing dramatic transcriptional changes as compared to splenic W4B cells from both naïve and infected mice. When examining $CD8^+$ T cell effector genes, Ifng and Fasl displayed higher levels of expression for brain W4B cells than splenic W4B cells (Fig. 8D). Additionally, we also observed a modest upregulation of the cytotoxic molecules granzyme B (Gzmb) and perforin (Prf1) (Fig. 8D). This increased expression suggests that brain W4B cells might be more effective at controlling WNV infection than splenic W4B cells. When probing genes for activation receptors, we found that several activation receptors (Il2ra, Cd69, Klrk1) were moderately to greatly enriched in brain W4B cells as compared to splenic W4B cells (Fig. 8D). Il2ra expression is a marker of cells in the effector phase, and IL-2R signaling will promote the production of cytokines and cytotoxic molecules (224), further supporting that brain W4B cells are more highly activated and display enhanced effector gene expression as compared to splenic W4B

cells. Given these differences, we next examined genes associated with T cell differentiation, specifically those that promote memory cell formation (Id3, Eomes, Stat3) and those that define the terminal effector phase (Tbx21 (T-bet), Prdm1 (Blimp1), Id2, Stat4). While 7 days p.i. is early for memory cell formation during WNV infection, memory precursor cells should express low levels of the effector phase transcripts and have begun to upregulate some of the memory-defining transcription factors (115, 116). Terminal effector cells will have the opposite phenotype with high levels of effector transcripts and downregulation of memory lineage transcripts (113, 117). Brain W4B cells did exhibit increased expression of some terminal effector markers compared to splenic W4B cells (Fig. 8D). Prdm1 and Id2 were both enriched in brain W4B cells as compared to splenic W4B cells, whereas Tbx21 and Stat4 expression were more similar between the two anatomic locations (Fig. 8D). Overall, both groups had relatively similar expression levels for memory lineage transcripts; however, brain W4B cells exhibited a notable downregulation for Id3 (Fig. 8D). Overall, W4B cells in both the spleen and brain seem to be firmly in the effector phase as expected, although brain W4B cells appear to be more terminally differentiated than splenic cells. Because we previously observed a higher frequency of PD-1 expression for brain and meningeal W4B cells (Fig. 6D), we next examined whether other inhibitory receptors were differentially expressed in brain and splenic W4B cells. Strikingly, multiple inhibitory receptors (Ctla4, Lag3, Tigit, Pdcd1 (PD-1), Il10ra, Cd244) displayed increased expression on brain W4B cells, whereas Havcr2 (Tim3) was similar (Fig. 8D). High expression of inhibitory receptors is often associated with an exhausted cell phenotype found in chronic infections (223, 225). However, during an acute infection such as WNV, this is potentially indicative that cells

are in a highly immunoregulatory environment and receiving suppressive signals (221, 222). To further highlight differences between naïve splenic, 7 days p.i. splenic and 7 days p.i. brain W4B cells, we also displayed in normalized read count values for a subset of genes. Interestingly, we observed that brain and splenic W4B cells from infected mice exhibited significantly higher levels of Tbx21 and Prf1 than naïve W4B cells, whereas for Ifng, FasL, Gzmb, Id3, Prdm1, and Pdcd1 the brain W4B cell levels were significantly different from either naïve or days p.i. splenic W4B cells (Fig. 8E). Altogether taken in context with the phenotypic and transcriptomic profiles, brain W4B cells appear to be highly activated effector-phase cells and inhibitory marker expression could be a result of the CNS microenvironment modulating the response to dampen excessive pro-inflammatory or cytotoxic activity. Overall, transcriptional analysis of brain and splenic W4B cells revealed that WNV-specific $CD8^+$ T cells localized to the CNS feature a highly antiviral profile, express high levels of both activating and inhibitory receptors, and appear to be more terminally differentiated than peripheral WNV-specific $CD8^+$ T cells.

CNS $CD8^+$ T cells are more efficient at controlling virus than peripheral $CD8^+$ T cells. We next hypothesized that brain W4B cells, which exhibit a polyfunctional antiviral phenotype, control WNV more efficiently than splenic W4B cells when co-cultured with cortical neurons. WNV can directly infect neurons and replicate to extremely high levels in the brain (up to 10^8 pfu/g tissue) (137, 139). Therefore, we optimized a cortical neuron co-culture model (137, 139) to determine if the observed phenotypic differences between peripheral and CNS WNV-specific $CD8^+$ T cells

translated to a functional difference. Conditions of the co-culture model were carefully optimized to determine the best timepoint of infection, MOI of infection, and CD8:cortical neuron ratio. Cortical neuron cultures were derived from WT embryonic mice and then infected with WNV. After virus adsorption, infected cortical neurons were co-incubated with WNV-specific $CD8^+$ T cells sorted from either the brain or spleen of mice at 7 days p.i. Cortical neurons and $CD8^+$ T cells were co-cultured for 24 hr at which point viral titers were assessed by focus-forming assay, allowing us to directly compare the capacity of $CD8^+$ T cells from distinct anatomic compartments to control WNV replication (Fig. 9A). Notably, the addition of W4B cells from either anatomic compartment resulted in a decrease in viral burden as compared to untreated neurons, supporting previously published findings that $CD8^+$ T cells help control WNV replication in neurons (137, 139). Interestingly, WNV-specific $CD8^+$ T cells from the brain were able to decrease viral burden by 2-fold as compared splenic WNV-specific $CD8^+$ T cells, demonstrating that CNS-derived WNV-specific $CD8^+$ T cells control WNV infection in cortical neurons more efficiently than splenic WNV-specific $CD8^+$ T cells (Fig. 9B).

DISCUSSION

Here, we demonstrate that the meninges and CNS-draining LNs have high levels of viral RNA at 4 days p.i. prior to brain parenchymal invasion and more closely resemble the post-viremic replication kinetics observed in the spleen than in the brain. These findings support the notion that these compartments are seeded with WNV much earlier than previously appreciated and suggest that WNV might be reaching CNS-border regions during the early viremic stage even prior to peak replication in the spleen and seeding the scLNs and dcLNs before brain parenchymal invasion. When examining immune cell dynamics within these tissue compartments, we observed accumulation of activated APC populations in the CNS-draining LNs at 4 days p.i. followed by an increase in WNV-specific $CD8^+$ T cells by 7 days p.i. which corresponded with viral RNA. However, despite viral RNA being detectable as early as 4 days p.i. similar to the CNS-draining LNs, the meninges more closely resembled the brain in many respects with APCs and WNV-specific $CD8^+$ T cells accumulating at 8 days p.i. and 10 days p.i., respectively. These findings represent the first characterization of viral RNA kinetics and immune cell dynamics within the CNS-draining lymphatics during WNV infection and altogether support an early involvement of CNS-draining lymphatics in WNV pathogenesis.

Phenotypic profiling of $CD8^+$ T cells across peripheral and CNS tissues identified profound differences based on anatomic location and tissue architecture. For W4B cells, expression of CD44, an activation-induced receptor associated with $CD8^+$ T cell movement, was inversely correlated with the level of vascularization of the residing tissue. However, other activation or inhibitory markers, such as PD-1, were differentially

expressed based on the division of periphery and CNS. W4B cells isolated from the spleen and brain have the most exaggerated differences, while those from the meninges and CNS-draining LNs might be best described as having an intermediate phenotype. Some phenotypic differences, such as the increased ICOS expression on W4B cells from CNS-draining LNs as compared to the spleen, might be due to recent migration from the CNS or differences in antigen load at those later points. Importantly, meningeal $CD8^+$ T cell populations may or may not have been subject to environmental cues within the brain parenchyma. Therefore, it is unclear whether the intermediate phenotype observed for meningeal WNV-specific $CD8^+$ T cells results from unique meningeal environmental cues or heterogeneity in exposure across the $CD8^+$ T cell population.

Thorough phenotypic and transcriptional profiling of WNV-specific $CD8^+$ T cells supports that $CD8^+$ T cells adopt a unique and highly antiviral terminal effector phenotype upon entry to the CNS. At 7 days p.i., W4B cells isolated from both the spleen and the brain expressed an activated effector T cell signature; however, brain W4B cells exhibited consistently higher levels of activation markers by both flow cytometry and RNA-seq analysis. Additionally, brain W4B cells had particularly enriched Il2ra expression, suggesting that cells are potentially continuing to receive effector phase-promoting signals. Notably, IL-2 signaling can promote the formation of SLECs in a Prdm1/Tbx21 dependent-manner (226), and indeed we see that Prdm1 expression is highly upregulated in brain W4B cells. Furthermore, Prdm1 drives a terminal effector transcriptional program and promotes the cytotoxic functions of the $CD8^+$ T cells (226). It is worth noting that the increase in effector cells could also be a reflection of viral load

as WNV replication in the spleen is declining at 7 days p.i. but approaching peak viral burden in the brain. Altogether, these findings suggest that brain WNV-specific $CD8^+$ T cells are more likely to be in a highly activated short-lived effector phase than cells from the spleen at 7 days p.i. and expressing high levels of both activating and inhibitory receptors.

Corresponding to the aforementioned effector phenotype, we observed that brain and meningeal W4B cells exhibit a polyfunctional antiviral signature, producing both IFN-γ and TNF-α, whereas W4B cells from the spleen, scLN, and dcLN have a 5-fold lower frequency of producing these cytokines. Brain and meningeal W4B cells favored the production of IFN-γ over TNF-α upon encounter with their cognate antigen, unlike peripheral W4B cells which preferentially produced TNF-α. Of note, IFN-γ can directly impact neuronal function and has been shown to promote non-cytolytic clearance of Sindbis virus from infected neurons (227), implying that brain W4B cells may secrete IFN-γ during WNV infection as an efficient way to clear virus while limiting cytotoxicity. However, a recent finding has shown that IFN-γ production from antiviral $CD8^+$ T cells persisting in the CNS parenchyma promotes microglia-mediated synaptic elimination (134). Therefore, the IFN-γ-dominated signature of the brain W4B cells might be necessary for virologic control in , but could cause unintended consequences during recovery.

A major finding to emerge from our analysis of splenic and brain W4B cells was that CNS localization was associated with enhanced expression of inhibitory receptors. Engagement of these receptors serves to dampen the effector functions of $CD8^+$ T cells by inhibiting the secretion and production of cytokines and cytotoxic molecules. As

discussed above, IFN-γ production has been associated with detrimental cognitive sequelae in the post-infectious CNS (134), and therefore the upregulation of inhibitory receptors on brain and meningeal W4B cells may be indicative of immunoregulation within these compartments to mitigate inflammation and limit neuronal damage inflicted by W4B cells. Following acute encephalitis from murine cytomegalovirus (MCMV) infection, the PD1:PD-L1 axis has been shown to contribute to the establishment of resident memory T (T_{RM}) cell populations within the CNS (222). A similar observation also has been made following murine polyomavirus (MuPyV) infection (221). In combination with previously published data that W4B cells express elevated levels of CD103 and CD69, this may suggest the establishment of T_{RM} cells in the CNS following WNV infection. Additionally, Il10ra, the IL-10 receptor gene, is highly upregulated on brain W4B cells. T regulatory (T_{reg}) cells are the primary producers of IL-10, and previous studies have demonstrated that increased T_{reg} cell numbers during WNV neuroinvasive disease is protective in both humans and mice (228). While the impacts of T_{reg} cells on $CD8^+$ T cell function in the CNS has not been directly assessed during WNV infection, this suggests a link between induction of a regulatory environment and protection from immunopathology for future study.

The $CD8^+$ T cell:cortical neuron co-culture system represents a unique model (137, 139), and here we describe the first functional demonstration that CNS-localized WNV-specific $CD8^+$ T cells control WNV infection of cortical neurons more efficiently than splenic WNV-specific $CD8^+$ T cells. The difference in functional capacity corresponded with phenotypic and transcriptional signatures, which revealed a highly activated and terminal effector phenotype for CNS-localized W4B cells. Importantly, a

notable limitation of the co-culture system is that it cannot perfectly recapitulate the microenvironment of the brain, including tissue architecture and multicellular interactions with CNS-resident cells, such as microglia, or other infiltrating peripheral leukocytes. The system, however, could be modified in the future to include other cell types such as microglia or T_{reg} cells to further interrogate the mechanisms immunoregulation during neuronal infection *ex vivo*.

In this study, we defined the early involvement of CNS-draining lymphatics during WNV pathogenesis and examine phenotypic and functional differences in WNV-specific $CD8^+$ T cells across peripheral and CNS compartments. Accumulation of viral RNA and activated cDCs in CNS-draining LNs occur prior to parenchymal invasion, and WNV-specific $CD8^+$ T cell accumulation parallels that of the spleen. Comprehensive phenotypic profiling of WNV-specific $CD8^+$ T cells in peripheral and CNS-draining lymphoid tissues, meninges and brain revealed that brain WNV-specific $CD8^+$ T cells are phenotypically distinct from splenic WNV-specific $CD8^+$ T cells with those from meninges and CNS-draining LNs displaying unique intermediate phenotypes. An emerging body of evidence implicates $CD8^+$ T cells and cytokines in memory formation and learning or other neurological sequelae following injury or infection. Future therapeutic interventions may require consideration of the unique programming of $CD8^+$ T cells in the CNS during neuroinvasive viral infection, as well as the consequences of persisting antiviral $CD8^+$ T cells in the CNS. Furthermore, future investigation of the specific cues within the CNS microenvironment, including those in the brain parenchyma and meninges, that prompt these phenotypic shifts could provide valuable insight into the underlying mechanisms of protection within the CNS.

MATERIALS AND METHODS

Viruses and animals. WNV isolate Texas 2002-HC (WNV-TX) has been previously described (211). Viral titers were measured by plaque assay on BHK-21 cells. C57BL/6J and Prtprc mice were obtained commerically from Jackson Laboratories or bred in-house at the Yerkes National Primate Research Center rodent facility at Emory University. W4B transgenic mice were originally obtained from the Bevan laboratory and bred in-house. For viral infections, adult male and female mice (8-12 weeks old) were inoculated subcutaneously in the rear footpad with 100 plaque-forming units (PFU) of WNV-TX (10 µL). Infected mice were monitored and weighed daily. All experiments adhered to the guidelines approved by the Emory University Institutional Animal Care and Committee.

Focus-forming assays. Focus-forming assays (FFAs) were performed on Vero cells with supernatants from WNV-infected cortical neuron cultures. Vero cells were cultured in DMEM (VWR, #45000-304) supplemented with 5% FBS, antibiotic/antimycotic, sodium pyruvate (VWR, #45000-710), HEPES (VWR, # 45000-690), L-glutamine (VWR, # 25005CI), and nonessential amino acids (VWR, #45000-700). Supernatants were serially diluted 10-fold in 1% FBS-DMEM. Vero cells were infected with 50 µL of diluted supernatant for 1 hr at 37°C followed by the addition of a methylcellulose overlay (2% methylcellulose (Sigma, #M0512), 2% FBS, OptiMem). Cells were then incubated for 48 hr at 37°C. Cells were fixed (2% PFA-PBS), permeabilized (0.1% saponin, 0.1% BSA, PBS), washed with PBS, and then incubated with an anti-WNV E16 primary antibody overnight at 4°C. Wells were incubated with HRP conjugated anti-human IgG (Thermo,

#62-842-0) for 2 hr at room temperature, and spots were visualized using True Blue Peroxidase Substrate (KPL, #507802) and read using an ELISPOT reader.

Quantitative PCR (qPCR). Mice were deeply anesthetized using an isoflurane vaporizer, and blood was collected via cheek bleed from each mouse in a BD Microtainer serum separator tube (SST) (VWR, #VT365967) to isolate serum. Mice were transcardially perfused with sterile DPBS. All tissues were collected in Omni Bead Ruptor Tubes (VWR, #10032-358) pre-filled with TRI Reagent (Zymo, #R2050-1-200). Tissues were homogenized using the Omni Beach Ruptor 24 (5.15 ms, 15 seconds) then centrifuged to remove tissue debris. RNA was extracted using the Direct-Zol 96 RNA Kit (Zymo, #R2056), and converted to cDNA using the High-capacity Reverse Transcriptase cDNA Kit (Thermo, #4368813). WNV RNA levels were quantified by qPCR as previously described (229) on an Applied Biosystems QuantStudio 5. Host gene expression for IFIT1 and RSAD2 were quantified on the same instrument using PowerUp SYBR Green Master Mix (Thermo, A25777) and previously published primer sets (Tian, 2013 #532).

Immunophenotyping by flow cytometry. Mice were anesthetized and intravital labelling was performed by injecting mice with CD45:PE or CD8:APC via the retro-orbital route. After 5 minutes, mice were euthanized via isoflurane overdose. Splenocytes were obtained by mechanical homogenization and filtration through a 70 µM filter (VWR, #10199-657). Brains were mechanically homogenized, digested for 15 min at room temperature in Liberase (Sigma, #540102000, 50 µg) buffer. The tissue

was pushed through a filter and pelleted. To remove myelin debris, the cells were resuspended in a 30% Percoll in PBS solution and spun at 2000 rpm for 20 min. Meninges were incubated in dissociation media (0.5 mg/mL DNaseI (Sigma, #DN25-100MG), 8 mg/mL Collagenase D (Sigma, #11088866001) , RPMI) for 40 min at 37°C on a shaker, then processed to a single-cell suspension and filtered. Lymph nodes were digested for 20 minutes at 37°C on a shaker in dissociation media (0.1 mg/mL DNase I, 20 µg/mL Liberase, RPMI). Tissue was passed through a filter to create a single-cell suspension. If cytokines were measured, samples were stimulated *ex vivo* with NS4B peptide (1 µg/mL) and GolgiStop (BD, #52-2092KZ) for 5 hr (143). For all samples, cells were resuspended in anti-CD16/32 antibody (Biolegend, #101302) for 20 min at room temperature, followed by surface staining for 30 min at 4°C. Cells were washed in FACS buffer, then fixed with BD Facs/Lyse buffer (#349202) for 10 min. For intracellular stains, cells were permeabilized with FoxP3 Fix/Perm buffer for 30 min at 4°C (Tonbo, #1020-L050), then stained with intracellular antibodies (30 min, 4°C). Cells were resuspended in 200 µL of FACS Buffer supplemented with Precision Count Beads (Biolegend, #424902) for acquisition. Data were collected using an LSRII instrument and analyzed using FlowJo software.

Adoptive transfer experiments. Spleens from naïve W4B mice were homogenized, treated with red blood cell lysis buffer (Lonza, #10-548E), and processed to a single-cell suspension. $CD8^+$ T cells were isolated using the Mojo Sort $CD8^+$ T cell Negative Selection Kit (Biolegend, #480035). $CD8^+$ T cells isolated from W4B mice were >95%

NS4B tetramer (230)-positive. W4B cells were resuspended in DMEM and 5,000 or 50,000 W4B cells were transferred to each recipient via retro-orbital route.

Bulk mRNA sequencing (RNA-seq). Brains and spleens from infected mice were processed to single-cell suspension as described above. Cells were stained with CD45.2(PE-Cy7), CD45.1(Bv450), CD8(AF700), CD3(PerCpCy5.5), and Live/Dead (BV510). Transferred W4B cells were sorted using congenic markers (n = 4), 10,000 viable cells were sorted into 100 µl RLT buffer (Qiagen) with β2-mercaptoethanol (1:100). mRNA sequencing libraries were prepared, quality assessed, and sequenced at Yerkes Genomics Core (http://www.yerkes.emory.edu/nhp_genomics_core/), and reads were mapped to the GENCODE mouse reference genome (GRCm38.p5, release M16) all as previously described (229). Reads were normalized and differential expression analysis performed using DESeq2 (212). Normalized reads were expressed as fold change over mock values.

Culture of cortical neurons. Embryos were harvested from pregnant dams at day 13-15 of gestation. Cortical hemispheres were isolated from the brain, and meningeal tissue was removed. The cortices were homogenized, digested in a 1% Trypsin-DNaseL solution (15 min, RT), and processed to a single-cell suspension. Cells were plated in DMEM supplemented with 5% Hi-Horse Serum (Thermo, #26050070), 5% FBS, antibiotics, non-essential amino acids, and HEPES. The next day media was changed to B27 (Thermo, #A3582801) supplemented Neurobasal Media (Thermo,

#21103049). Neurons were monitored for axonal outgrowth and were determined ready for experimental use 4-5 days post plating.

Antibodies. The following antibodies were used in this paper for flow cytometry. $CD8^+$ T cell panel: anti-CD8:AF700 (Clone 53.67), anti-CD8:APC (2.43), anti-CD3:PerCpCy5.5 (145-2C11), anti-CD45.2:PE-Cy7 (104), Ghost Dye Violet 510, anti-KLRG1:BV605 (2F1), anti-CD44:APC-Cy7 (IM7), anti-ICOS:BUV395 (C398.4A), anti-CD127:FITC (A7R34), anti-IFNγ:PE-Dazzle (XMG1.2), anti-TNFα: BV711 (MP6-XT22), anti-GrazymeB:BV450 (NGZB), anti-PD1:BV650 (J43). Myeloid cell panels: CD11c:BV650 (N418), CD26:PE-Cy7 (H194-112), I-A/I-E (MHC II):AF700 (M5/114.15.2), XCR1:PE (ZET), CD172a (SIRPα):BV510 (P84), Siglec H:AF647 (551), H2kb (MHC I):PacBlue (AF6-88.5), CD86:BV605 (GL-1), CD64:PerCP-Cy5.5 (X54-5/7.1), CD3:FITC (145-2C11), NK1.1:FITC (PK136), B220:FITC (RA3-6B2), CD45.2:PE-Dazzle594 (104), F4/80:FITC (BM8), Siglec H:BV421 (440c), CD45:PE (30-F11), XCR1:AF647 (ZET), CD45.2:BV605 (104), Ly6C:BV510 (HK1.4), CD11c:BUV737 (HL3), CD11b:BUV395 (M1/70), CD86:PE-Dazzle594 (GL-1), Ly6C:APC-Cy7 (HK1.4).

Statistical analysis and software. Statistical analyses and graphical presentation of data was performed using Prism 8 (GraphPad) software. One-way ANOVA with Tukey's multiple comparison correction and the multiple t tests were used to evaluate significant differences depending on the experiment.

FIGURE LEGENDS

Figure 1. Early viral dissemination and ISG expression in peripheral lymphoid tissues. (A) Schematic of lymphoid and CNS tissues examined in this study. Mice were infected with WNV via subcutaneous footpad inoculation. Meningeal lymphatic vessels drain to the scLN and dcLN, and the meninges and CNS-draining LNs represent previously understudied compartments. (B) Mice were infected with WNV (100 PFU) by subcutaneous footpad inoculation, and tissues collected at the indicated time points (n = 4). Relative WNV RNA was measured by qPCR where C_T values were normalized to the reference gene *Gapdh* and represented as fold change over time-matched mock values. Viral RNA copies were interpolated from the standard curve using sample C_T values and represented as WNV copies per mL serum. (C) Relative IFIT1 and Relative RSAD2 were quantified in a similar method as described in (B).

Figure 2. Early differential activation of DC subsets in peripheral lymphoid tissues. Mice were infected with WNV (100 PFU) by subcutaneous footpad inoculation, and popliteal LN and spleen collected at the indicated time points. $CD11c^+$ $CD26^+$ $XCR1^+$ $CD172a^-$ cDC1s, $CD11c^+$ $CD26^+$ $XCR1^-$ $CD172a^+$ cDC2s, and $B220^+$ $CD11c^{int}$ $SiglecH^+$ pDCs from the popLN (A and B) and spleen (C) were stained for activation markers MHC I and CD86 (n = 4). (A and C) Marker expression was shown by MFI, and (B) representative histograms are shown for popLN populations.

Figure 3. Early viral RNA detection and myeloid cell accumulation in CNS-draining lymph nodes and meninges. Mice were infected with WNV (100 PFU) by subcutaneous footpad inoculation, and tissues collected at the indicated time points. (A) Relative WNV RNA was quantified as described in Fig. 1B (n = 4). (B) Total cell numbers for $CD11c^{+}$ $CD26^{+}$ cDCs, $CD11c^{+}$ $CD11b^{hi}$ $Ly6C^{low}$ MHC II^{+} moDCs, $CD11c^{low}$ $CD11b^{hi}$ $Ly6C^{hi}$ monocytes, and $B220^{+}$ $CD11c^{int}$ $SiglecH^{+}$ pDCs were measured to assess shifts in cellular composition across the indicated tissues (n = 4).

Figure 4. Early cDC activation in CNS-draining lymph nodes and meninges. Mice were infected with WNV (100 PFU) by subcutaneous footpad inoculation, and tissues collected at the indicated time points. MHC I and CD86 expression were Relative WNV RNA was quantified as described in Fig. 1B (n = 4). (B) MHC I and CD86 marker expression was represented by MFI for $CD11c^{+}$ $CD26^{+}$ cDCs, $F4/80^{+}$ $CD11c^{low}$ $CD11b^{hi}$ $Ly6C^{hi}$ inflammatory monocyte/macrophage, and $F4/80^{+}$ $CD11c^{low}$ $CD11b^{hi}$ $Ly6C^{low}$ non-inflammatory monocyte/macrophage (n = 5). (1-B) and spleen (C) were stained for activation markers MHC I and CD86. (A) and (C) Marker expression represented by MFI, and (B) representative histograms are shown for popLN populations. Multiple t tests were performed to test significance (*ns* = not significant; $*p < 0.05$).

Figure 5. Accumulation of WNV-specific $CD8^{+}$ T cells in the meninges, brain, and peripheral and CNS-draining lymphoid tissues. Mice were infected with WNV (100 PFU) by subcutaneous footpad inoculation, and tissues collected at the indicated time

points. (A) Total number and frequency of NS4B Tet$^+$ CD8$^+$ T cells were quantified for the spleen across multiple time points (n = 4). (B) Total number and frequency of NS4B Tet$^+$ CD8$^+$ T cells were quantified for the CNS-draining LNs, meninges and brain across multiple time points (n = 4).

Figure 6. CD8$^+$ T cells in the CNS have altered surface marker expression compared to those in the periphery. (A) Experimental schematic. Naïve W4B cells were isolated from a CD45.1 W4B mouse and transferred into a naïve C57BL/6J mouse. One day post-transfer, recipient mice were infected. At 7 days p.i., tissues were collected for analysis via flow cytometry. (B) Gating strategy to identify transferred W4B cells. Viable CD45$^+$ CD3$^+$ CD8$^+$ cells were gated on congenic markers to identify the transferred (CD45.1) and non-transferred (CD45.2) populations. NS4B tetramer staining confirmed that the transferred cells were >99% WNV-specific. (C) Expression of CD44 and ICOS on W4B cells across tissues (n = 4). CD44 and ICOS MFI are shown as representative histograms. Non-WNV-specific NS4B Tet$^-$ CD8$^+$ T cells were used as a negative control (grey). (C-D) The legend for conditions depicted on bar graphs can be found at the bottom. (D) KLRG1 and PD-1 expression shown as percentages of total W4B cells (n = 4). Representative flow plots for the gating strategy are depicted with NS4B NS4B Tet$^-$ CD8$^+$ T cells used as a negative control (grey). Data are representative of two independent experiments. One-way ANOVA was performed to test significance (*ns* = not significant; **p* < 0.05; ***p* < 10^{-2}; ****p* < 10^{-3}; *****p* < 10^{-4}).

Figure 7. W4B Cells from the CNS have polyfunctional cytokine secretion. Adoptive transfers were performed as described in Fig. 6A. After tissue isolation, cells were stimulated *ex vivo* with NS4B peptide (1 μg/mL) for 5 h at 37°C. Cells were then permeabilized and stained for cytokines. Representative flow plots are shown for TNF-α and IFN-γ gating on $CD45.1^+$ $CD3^+$ $CD8^+$ cells (W4B cells). Unstimulated splenic W4B cells were used to define the negative population (grey). Populations were divided into quadrants (labeled 1-4) to identify double-negative cells (Q1), TNF-α single producers (Q2), IFN-γ single producers (Q3), and TNF-α/IFN-γ double producers (Q4). Bar graphs are shown for the percentage of cells in Q1-4 across tissues (n = 4). Data are representative of two independent experiments. One-way ANOVA was performed to test significance (*ns* = not significant; $*p < 0.05$; $**p < 10^{-2}$; $***p < 10^{-3}$; $****p < 10^{-4}$).

Figure 8. W4B cells isolated from the brain are transcriptionally distinct from splenic T cells. (A) Experimental schematic. Adoptive transfers were performed as described in Fig. 6A. At 7 days p.i., W4B cells were sorted from spleen and brain and total RNA was extracted for RNA-seq analysis. Naïve splenic W4B cells were sorted as a control (n = 4-5 per group). (B) Heat map showing mean gene expression values normalized and represented as log2-transformed fold change over mock spleen values. Expression fold change values correspond to the color gradient (right). The Venn diagram at the bottom highlights the total number of differentially expressed genes for W4B cells from the spleen (red) or brain (blue), as well as overlapping genes (yellow). (C) A scatter plot of log2-transformed expression fold change (FC) values is shown for comparison of up-regulated and down-regulated genes in W4B cells from infected

spleen (green) and brain (red). Cutoff values were as follows: ±2 fold change and $p < 0.001$. (D) Expression fold change values are shown for a panel of select genes grouped by functional category. Gene cluster descriptions can be found on the left. (E) Normalized read count values for select genes are shown for comparison between naïve spleen, 7 days p.i. (DPI) spleen, and 7 DPI brain. One-way ANOVA was performed to test significance (*ns* = not significant; $*p < 0.05$).

Figure 9. Brain W4B cells more effectively control WNV replication than Splenic W4B cells. (A) Experimental schematic. Cortical neurons were generated from embryonic day 13-15 fetal mice after culturing for 4 days in neuronal growth medium. Cortical neurons were infected with WNV (MOI of 0.01) and co-incubated for 24 h with W4B cells sorted from the spleen or brain of WNV-infected mice at 7 days p.i. Supernatants were collected and viral titers determined by FFA. (B) Viral titers of supernatants represented as focus-forming units (FFU) per mL in log10 scale. Relative reduction percentage normalizes the viral titer data to the untreated control. Data are representative of three independent experiments. One-way ANOVA was performed to test significance (*ns* = not significant; $*p < 0.05$; $**p < 10^{-2}$; $***p < 10^{-3}$; $****p < 10^{-4}$).

Figure 1

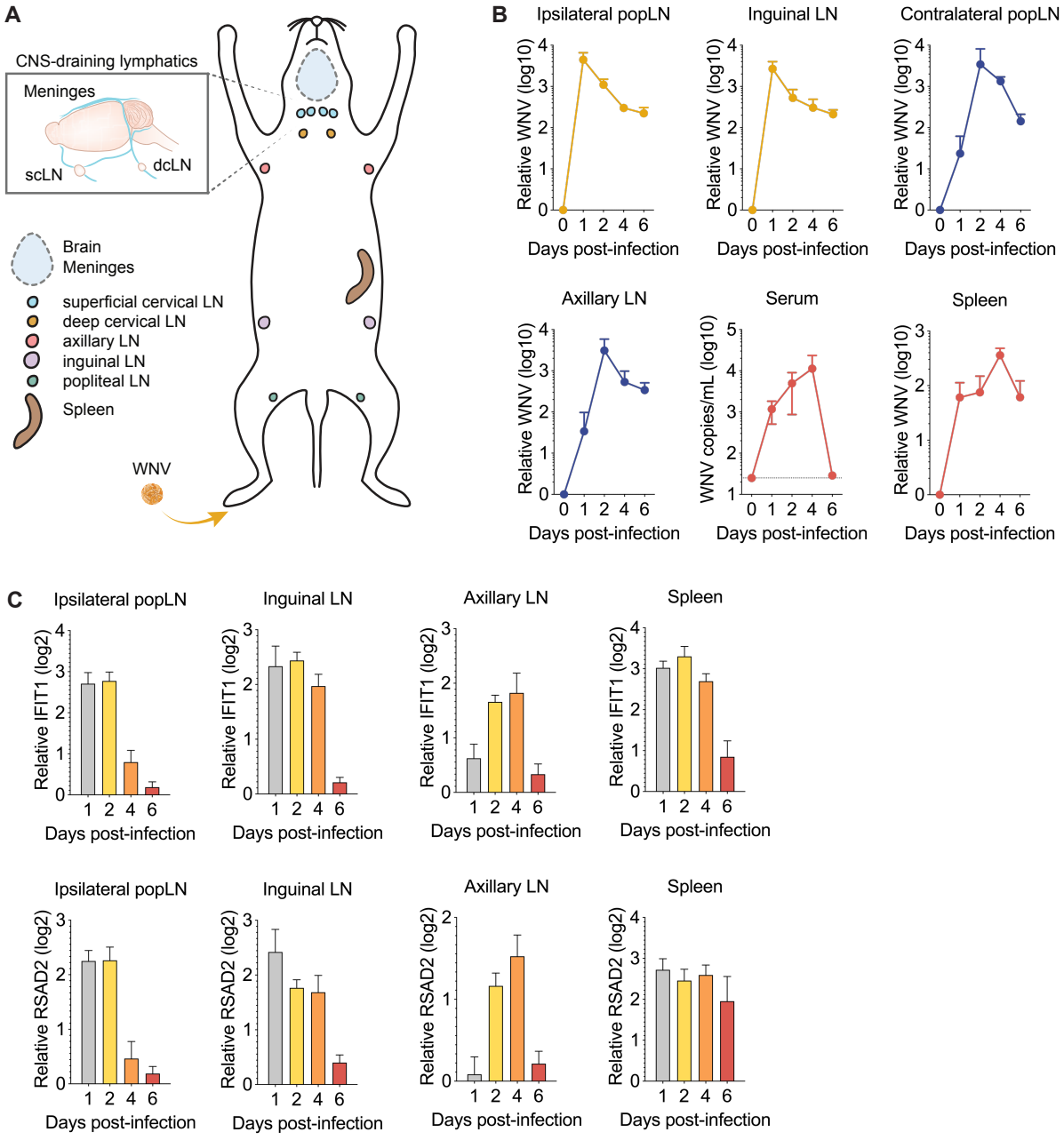
A
CNS-draining lymphatics
Meninges
scLN
dcLN
Brain
Meninges
superficial cervical LN
deep cervical LN
axillary LN
inguinal LN
popliteal LN
Spleen
WNV
B
Ipsilateral popLN
Inguinal LN
Contralateral popLN
Axillary LN
Serum
Spleen
Relative WNV (log10)
WNV copies/mL (log10)
Days post-infection
C
Ipsilateral popLN
Inguinal LN
Axillary LN
Spleen
Relative IFIT1 (log2)
Relative RSAD2 (log2)
Days post-infection

Figure 2

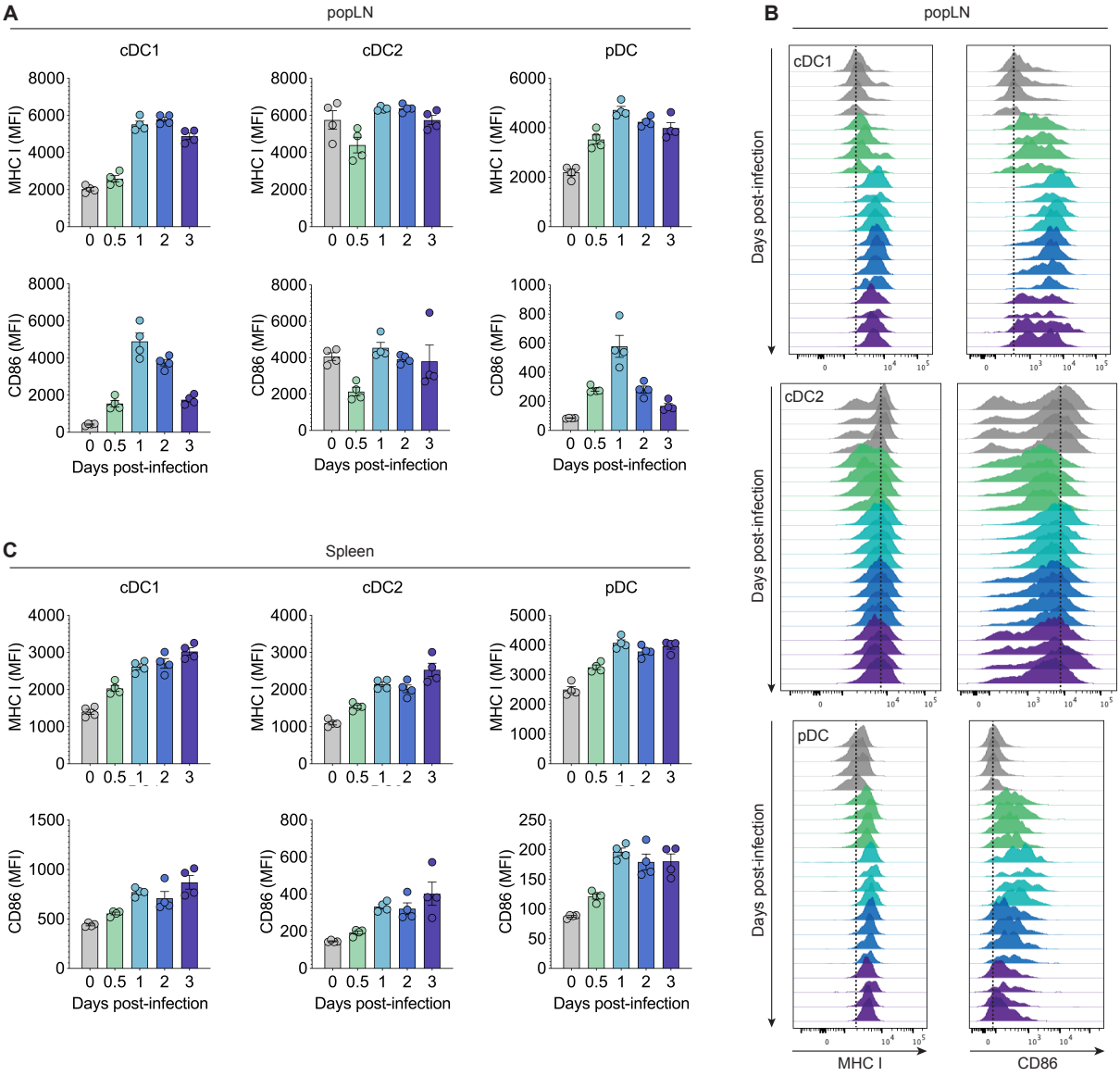
A
popLN
cDC1
cDC2
pDC
MHC I (MFI)
CD86 (MFI)
Days post-infection
B
popLN
cDC1
cDC2
pDC
Days post-infection
MHC I
CD86
C
Spleen
cDC1
cDC2
pDC
MHC I (MFI)
CD86 (MFI)
Days post-infection

Figure 3

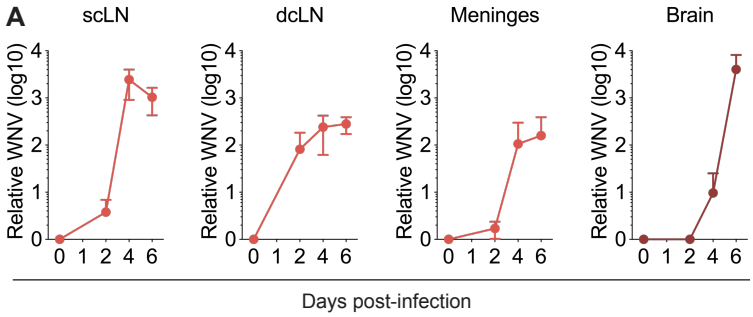
A
scLN
dcLN
Meninges
Brain
Relative WNV (log10)
0 1 2 3 4
0 1 2 4 6
Days post-infection

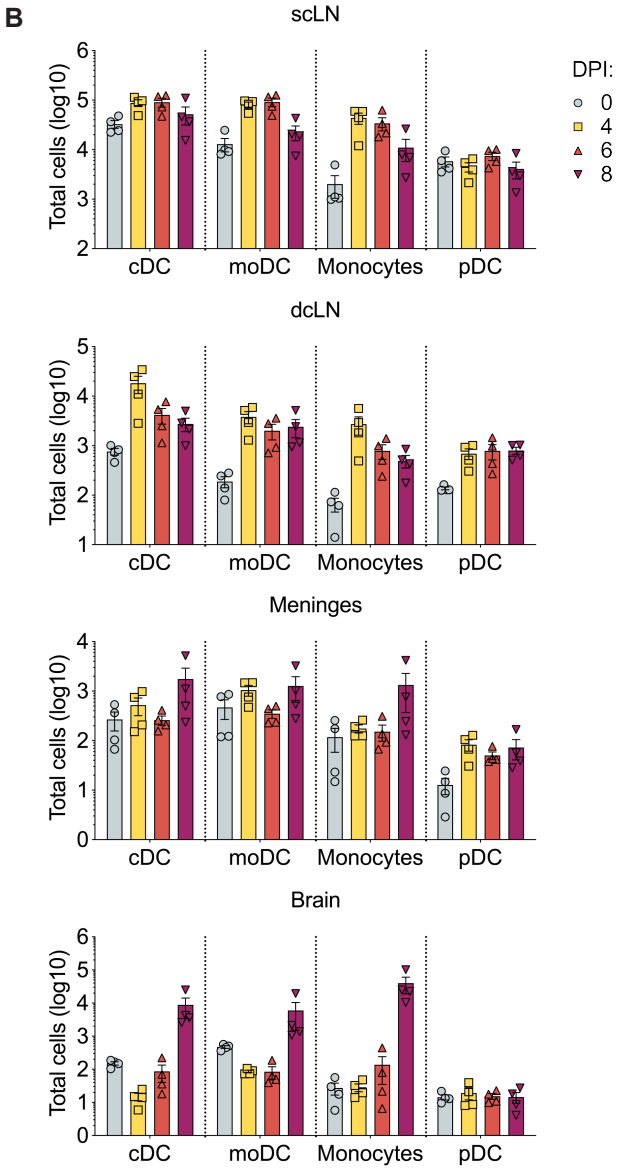
B
scLN
dcLN
Meninges
Brain
Total cells (log10)
cDC
moDC
Monocytes
pDC
DPI:
0
4
6
8

Figure 4

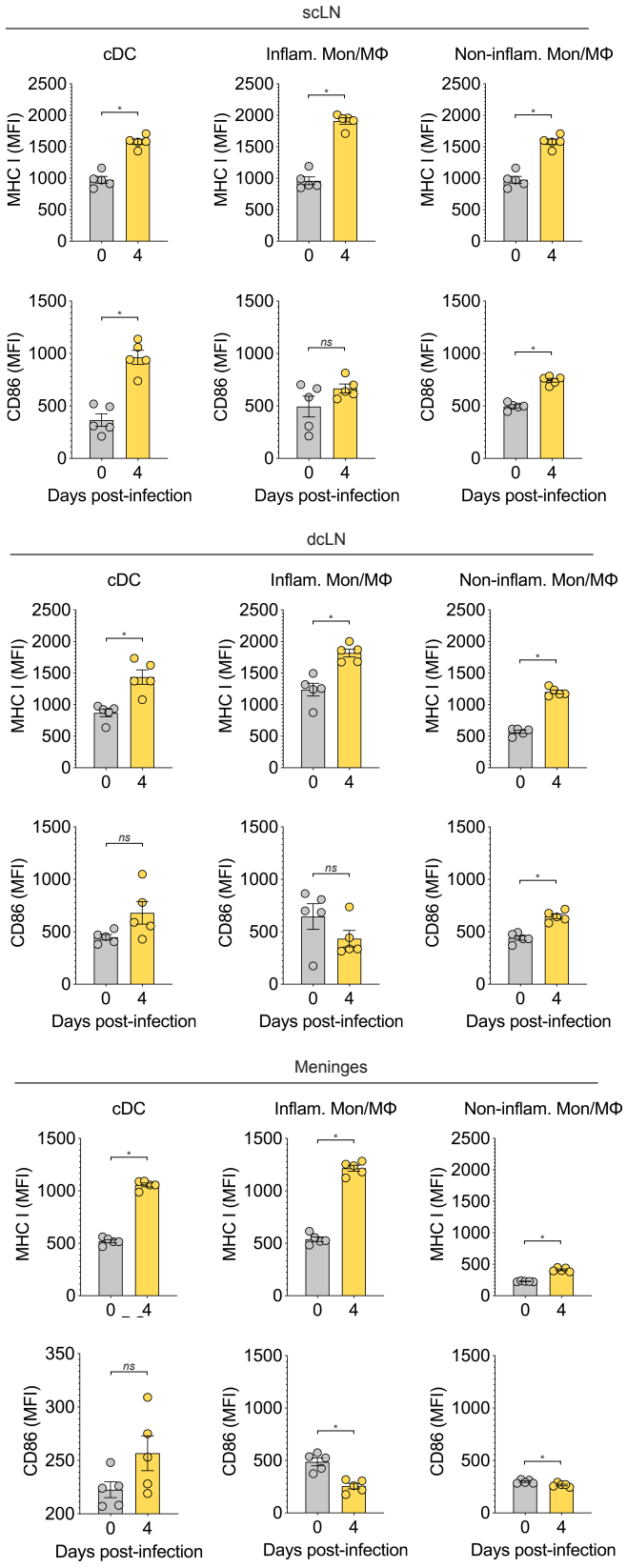
scLN
cDC
Inflam. Mon/MΦ
Non-inflam. Mon/MΦ
MHC I (MFI)
CD86 (MFI)
Days post-infection
dcLN
Meninges
ns

Figure 5

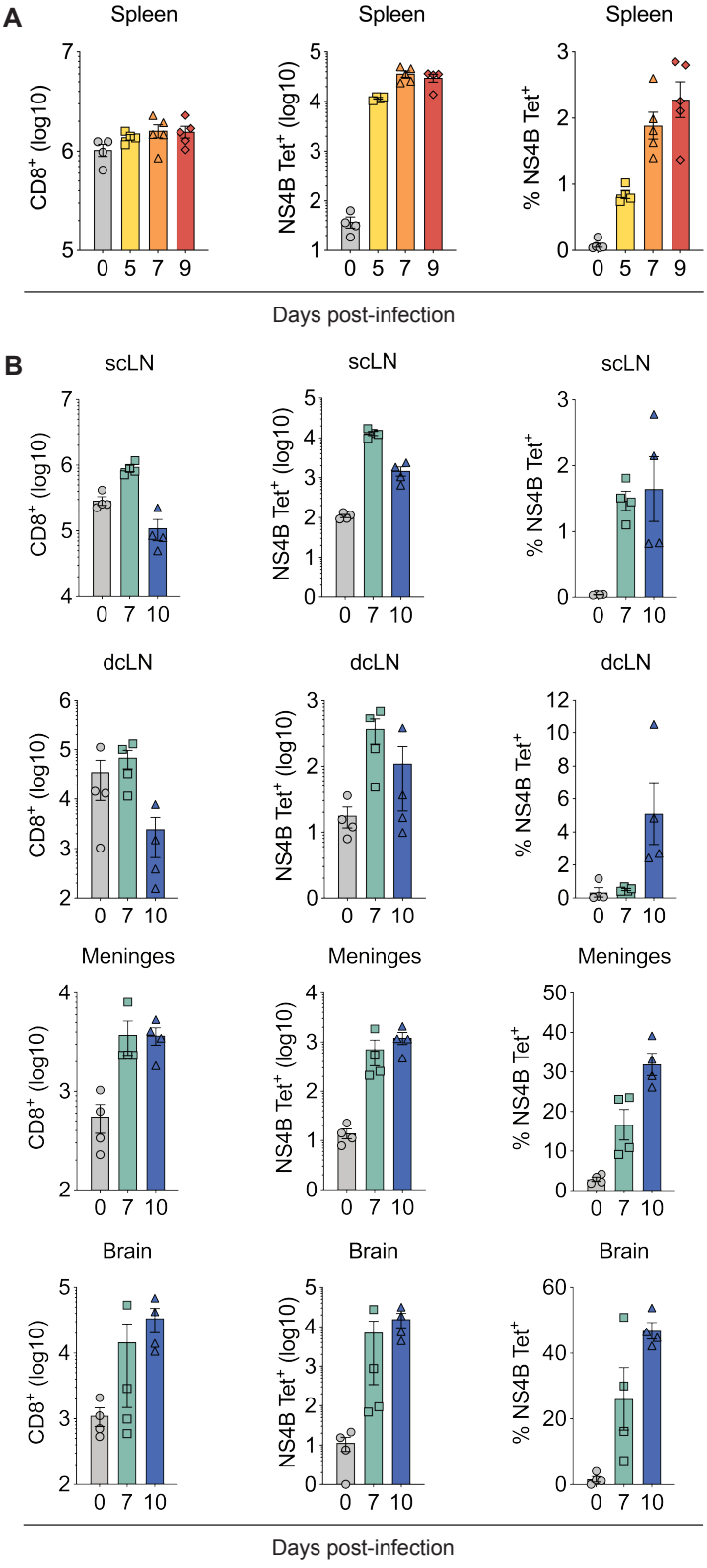
A
Spleen
Spleen
Spleen
CD8+ (log10)
NS4B Tet+ (log10)
% NS4B Tet+
0 5 7 9
Days post-infection
B
scLN
dcLN
Meninges
Brain
CD8+ (log10)
NS4B Tet+ (log10)
% NS4B Tet+
0 7 10
Days post-infection

Figure 6

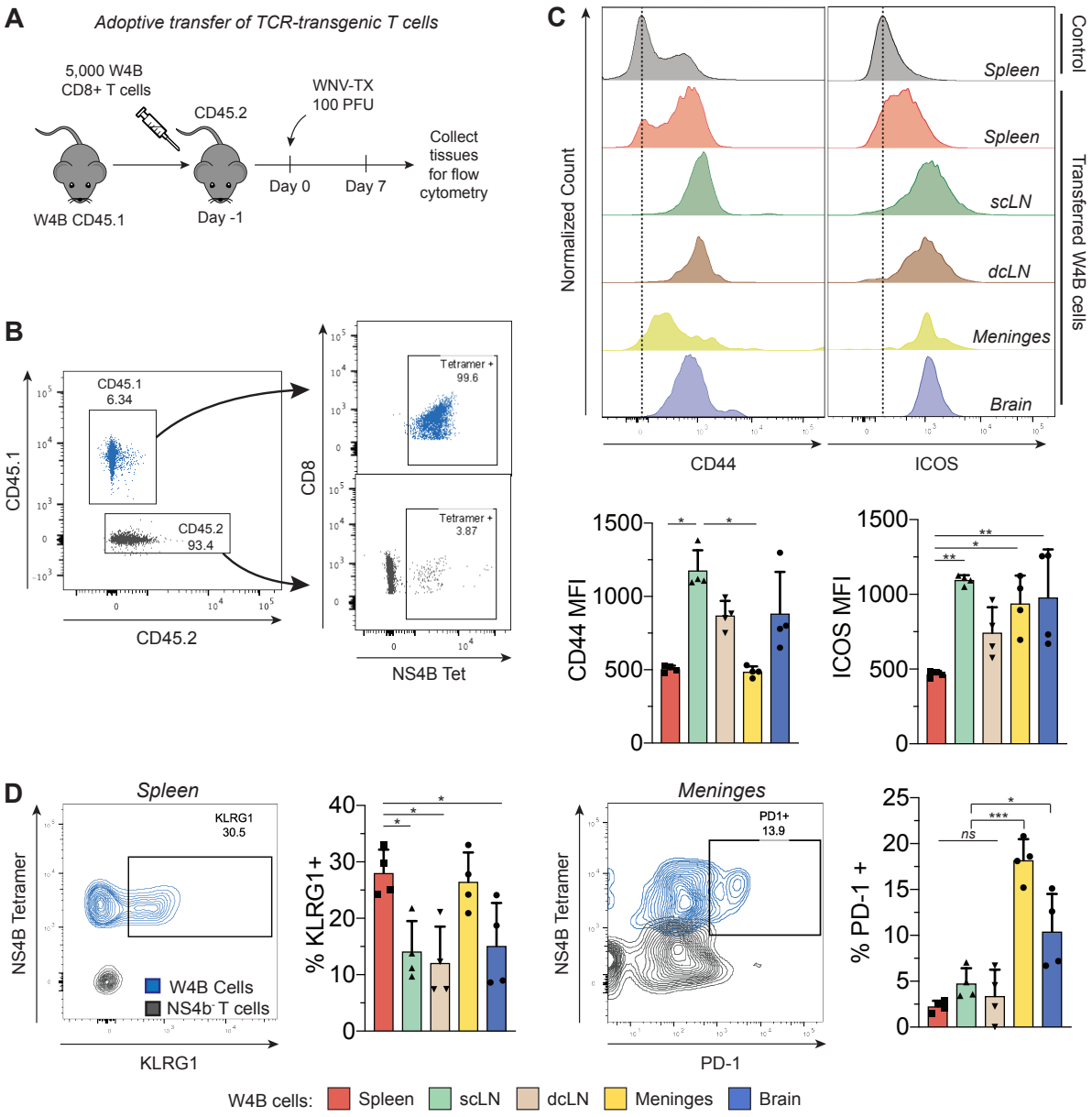
A
Adoptive transfer of TCR-transgenic T cells
5,000 W4B CD8+ T cells
CD45.2
WNV-TX 100 PFU
Collect tissues for flow cytometry
Day 0
Day 7
W4B CD45.1
Day -1
B
CD45.1 6.34
CD45.2 93.4
CD45.1
CD45.2
CD8
Tetramer + 99.6
Tetramer + 3.87
NS4B Tet
C
Control
Transferred W4B cells
Spleen
Spleen
scLN
dcLN
Meninges
Brain
Normalized Count
CD44
ICOS
CD44 MFI
ICOS MFI
D
Spleen
KLRG1 30.5
NS4B Tetramer
W4B Cells
NS4b- T cells
KLRG1
% KLRG1+
Meninges
PD1+ 13.9
PD-1
% PD-1 +
ns
W4B cells:
Spleen
scLN
dcLN
Meninges
Brain

Figure 7

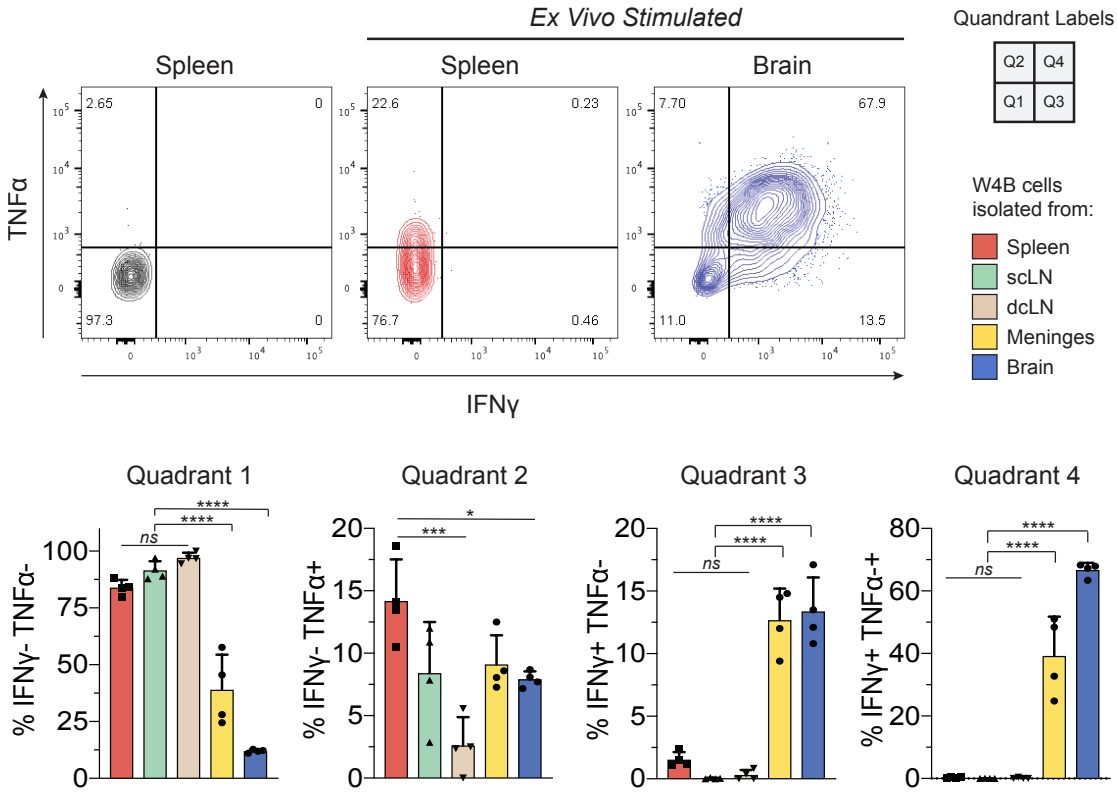
Ex Vivo Stimulated
Spleen
Spleen
Brain
TNFα
IFNγ
2.65
0
97.3
0
22.6
0.23
76.7
0.46
7.70
67.9
11.0
13.5
Quandrant Labels
Q2
Q4
Q1
Q3
W4B cells isolated from:
Spleen
scLN
dcLN
Meninges
Brain
Quadrant 1
Quadrant 2
Quadrant 3
Quadrant 4
% IFNγ- TNFα-
% IFNγ- TNFα+
% IFNγ+ TNFα-
% IFNγ+ TNFα-+
ns
****
***
*

Figure 8

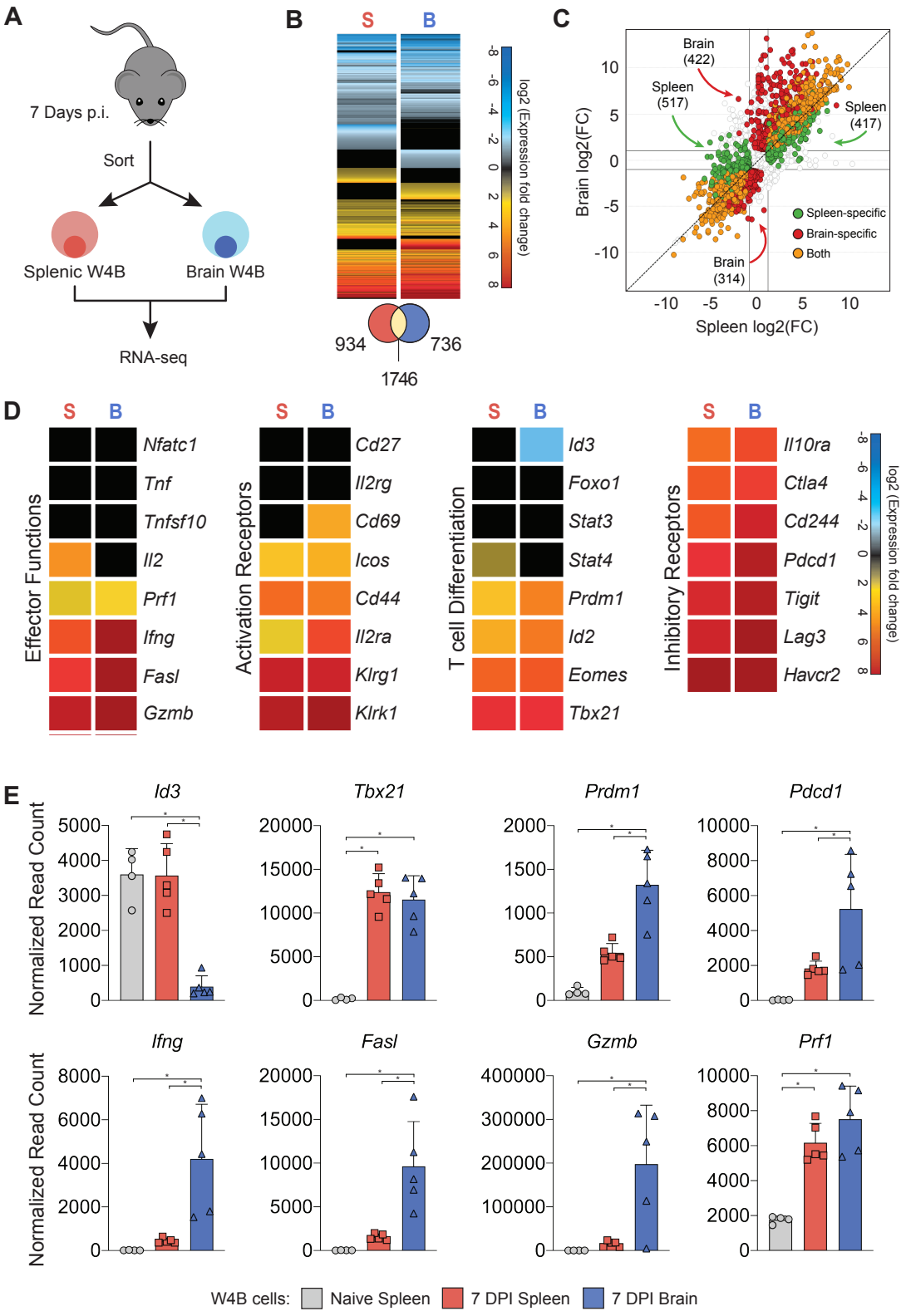
A
7 Days p.i.
Sort
Splenic W4B
Brain W4B
RNA-seq
B
S
B
log2 (Expression fold change)
934
736
1746
C
Brain (422)
Spleen (517)
Spleen (417)
Brain (314)
Spleen-specific
Brain-specific
Both
Brain log2(FC)
Spleen log2(FC)
D
Effector Functions
Nfatc1
Tnf
Tnfsf10
Il2
Prf1
Ifng
Fasl
Gzmb
Activation Receptors
Cd27
Il2rg
Cd69
Icos
Cd44
Il2ra
Klrg1
Klrk1
T cell Differentiation
Id3
Foxo1
Stat3
Stat4
Prdm1
Id2
Eomes
Tbx21
Inhibitory Receptors
Il10ra
Ctla4
Cd244
Pdcd1
Tigit
Lag3
Havcr2
E
Id3
Tbx21
Prdm1
Pdcd1
Ifng
Fasl
Gzmb
Prf1
Normalized Read Count
ns
W4B cells:
Naive Spleen
7 DPI Spleen
7 DPI Brain

Figure 9

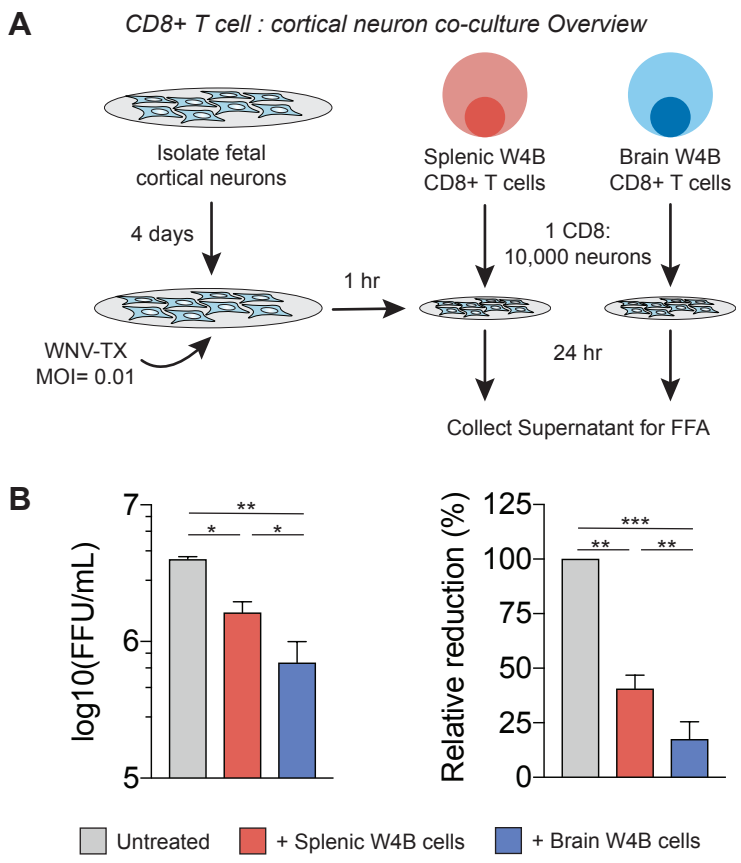
A
CD8+ T cell : cortical neuron co-culture Overview
Isolate fetal cortical neurons
4 days
WNV-TX MOI= 0.01
1 hr
Splenic W4B CD8+ T cells
Brain W4B CD8+ T cells
1 CD8: 10,000 neurons
24 hr
Collect Supernatant for FFA
B
log10(FFU/mL)
7
6
5
**
*
*
Relative reduction (%)
125
100
75
50
25
0
***
**
**
Untreated
+ Splenic W4B cells
+ Brain W4B cells

AUTHOR CONTRIBUTIONS

J.T.O. and A.V. contributed equally to this work. Both authors were involved in experimental design and execution, data analysis, figure generation, and manuscript preparation. D.E. provided valuable scientific discussion with regard to experimental design and assisted with tissue collection and RNA purification, as well as tissue collection, processing, and staining for flow cytometry to evaluate APC activation and immune cell accumulation. R.A. performed adoptive transfer experiments and tissue collection for bulk RNA-seq. M.S.S. and A.G. provided mentorship, expertise in virology and immunology, and guidance for experimental design and manuscript preparation.

DISCUSSION

Probing WNV infection at single-cell resolution

Conventional bulk transcriptional assays and knockout mouse models have largely informed our understanding of the host response to flavivirus infection. However, recent single-cell studies have highlighted the transcriptional variation in both viral RNA abundance and the IFN-I response across infected cells. Our findings using the novel approach of WNV-inclusive scRNA-seq revealed extensive transcriptional heterogeneity in the host response and viral RNA abundance across single cells. Our protocol, along with previously published work by Zanini and colleagues (89), demonstrates the feasibility of virus-inclusive scRNA-seq as a platform for parallel single-cell transcriptomic and viral RNA analysis with other non-polyadenylated RNA viruses. In our analysis, we observed high unimodal expression patterns for several ISGs (Irf7, Ddx58, Dhx58, Irf9, Stat1 and Stat2) despite few cells producing IFN-β transcript following WNV infection, supporting previously published findings on the importance of IFN-I dependent paracrine signaling and that only small fractions of cells produce IFN-β in response to viral infection (53, 88, 93-97).

Our work represents the first transcriptomic study of flavivirus infection to demonstrate correlation of ISGs and viral RNA within single cells. We observed both unimodal and bimodal expression signatures for previously validated WNV-targeting antiviral effector genes, all of which negatively correlated with viral RNA. The bimodality for a subset of ISGs which correlate with viral RNA abundance may stem from early viral antagonism or preexisting cell-intrinsic differences, such as the amount of critical signaling components, in primary infected cells. The low frequency of IFN-β producing

cells and aforementioned bimodality in ISG expression could be the result of variation at the level of chromatin organization (93-100). Recent development of commercially available single-cell ATAC (assay for transposase accessible chromatin) sequencing assays could provide further insight into how gene regulation via chromatin accessibility could contribute to heterogeneity in the host response across single cells. IFN-β producing cells might be better suited for IFN-I induction following viral infection due to cell-intrinsic differences in chromatin landscape or possibly could be more responsive to chromatin remodeling than non-producing cells.

In the future, WNV-inclusive scRNA-seq can be applied to *in vivo* studies, extending the resolution of transcriptional analyses to singe cells to better understand key features of cellular immunity. Conditional knockout (cKO) models utilizing the cre-*lox* system have been previously used to investigate the cell-intrinsic role of genes associated with the host response following WNV infection. Often these cKO models target critical signaling pathways to explore the contribution of cell-specific effects during pathogenesis. WNV-inclusive scRNA-seq of cKO cell populations and wild-type cell populations would provide valuable insight into the changes in transcriptional programming and capture any underlying heterogeneity across these cell populations. Furthermore, the capacity to correlate transcriptional trends with viral RNA abundance for cellular targets of WNV infection potentially provides an additional level of resolution, differentiating transcriptional signatures unique to infected and bystander cell populations. One potential hurdle to analyses of infected and bystander populations is that infection will not be synchronous in the same manner as *in vitro* assays. Therefore, such *in vivo* approaches might be best applied at early times post-infection or during

peak viral burden in respective tissues to capture the highest percentage of virally infected cells.

Exploring the role of meningeal immunity during WNV infection

Recent advances in the field of CNS immunity have shifted our understanding of CNS immune surveillance and inflammatory processes, and the meninges have been implicated as a central feature of the CNS-immune interface (147, 149, 164-167). Models of neurodegenerative diseases, autoimmunity, and neurotropic viral infection support a significant role for meningeal immunity in disease progression or resolution (147, 164, 167, 178, 180-182, 184). In both coronavirus infection and the EAE model of MS, antigen-experienced T cells require a reactivation signal within the meninges presumably from local APCs presenting cognate antigen (178, 183, 184). In the EAE model, stimulation of auto-reactive $CD4^+$ T cells results in CNS damage; however, for coronavirus infection, the reactivation signal is critical for prevention of fatal neuroinflammatory disease (178, 183, 184). This is akin to recent observations for neuroinvasive WNV infection. In these studies, the meninges were also speculated as a potential site of interactions between CNS-infiltrating WNV-specific $CD8^+$ T cells and CNS-localized APCs, which provide a critical reactivation signal for efficient viral clearance (146, 177). However, the involvement of meningeal immunity and how anatomic localization influences $CD8^+$ T cell programming during WNV infection remains underexplored.

Our work represents the first study to comprehensively evaluate phenotypic and transcriptional differences between WNV-specific $CD8^+$ T cells from the CNS and

peripheral compartments. We observed early detection and accumulation of viral RNA within the meninges and CNS-draining LNs. Furthermore, the viral kinetics in these compartments closely resembled the spleen. We speculate that WNV reaches the meningeal space via circulation during the early viremic stage where it is phagocytized by surveilling meningeal APCs and subsequently seeds the scLN and dcLN following drainage through meningeal lymphatics. This data is supported by cDC activation in these compartments, corresponding with viral RNA burden and notably occurring prior to early viral replication in the brain. Previously published work has demonstrated that mosquito saliva factors enhance WNV dissemination in peripheral lymphoid tissues and accelerate CNS invasion (31, 36, 37). Similar findings have also been observed for alphavirus infection (232). Furthermore, the immuno-modulatory effects of mosquito saliva factors have been demonstrated to not only lead to enhanced pathogenesis but also increased mortality in infected mice (233). Future studies could examine to what extent mosquito saliva factors similarly enhance early spread to CNS-draining lymphoid tissues and the meninges and contrast the host response across peripheral and CNS-draining lymphoid compartments.

Antigen and immune cell drainage to peripheral LNs is a crucial component of CNS immunity, although it remains an understudied aspect of neurotropic flavivirus infection. Here, we found that the temporal dynamics of WNV-specific $CD8^+$ T cell accumulation in CNS-draining LNs resembled that of the spleen. While spleen and brain WNV-specific $CD8^+$ T cells displayed disparate phenotypes, meningeal WNV-specific $CD8^+$ T cells and those from CNS-draining LNs exhibited unique intermediate phenotypes, suggesting that environmental cues in these distinct anatomic

compartments contribute to $CD8^+$ T cell re-programming during WNV infection. Previously published work has implicated CNS-localized APCs in reactivating CNS-infiltrating WNV-specific $CD8^+$ T cells, although the location and underlying mechanism of these interactions has yet to be fully elucidated. Our data supports that these interactions might be occurring in the meningeal space as the phenotype of meningeal WNV-specific $CD8^+$ T cells recapitulates that of brain WNV-specific $CD8^+$ T cells with respect to elevated PD-1 expression and IFN-γ and TNF-α production. However, it is important to note that meningeal $CD8^+$ T cells may have experienced environmental cues within the brain parenchyma, and therefore the contribution of heterogeneity in microenvironment exposure remains unclear. Extending these findings, brain WNV-specific $CD8^+$ T cells displayed a highly antiviral transcriptional signature and were more efficient at controlling WNV replication in cortical neurons than splenic WNV-specific $CD8^+$ T cells. The observed phenotypic divergence for $CD8^+$ T cells from these two distinct anatomic locations translated to a difference in functional capacity to mediate virologic control, suggesting that the CNS microenvironment influences $CD8^+$ T cell programming to promote efficient viral clearance from cortical neurons (Fig. 1). Additionally, a potential future study could examine the capacity of meningeal WNV-specific $CD8^+$ T cells to control WNV replication in cortical neurons as efficiently as brain WNV-specific $CD8^+$ T cells. This could further support the meninges as a potential site of APC reactivation of CNS-infiltrating $CD8^+$ T cells.

$CD8^+$ T cells utilize both cytolytic and noncytolytic measures to limit viral spread, including release of cytotoxic molecules, expression of death receptors, and secretion of antiviral cytokines such as TNF-α and IFN-γ (113, 136, 137, 139-141, 227, 234).

However, how CNS-infiltrating $CD8^+$ T cells coordinate viral clearance from infected neurons while limiting detrimental CNS damage and the long-term effects of chronic inflammatory processes in the CNS are relatively underexplored areas of neurotropic flavivirus pathogenesis and immunity. Given their enhanced PD-1 expression and TNF-α and IFN-γ production, future studies should investigate whether CNS-infiltrating WNV-specific $CD8^+$ T cells control WNV infection preferentially through cytolytic or noncytolytic mechanisms as compared to splenic WNV-specific $CD8^+$ T cells.

Antiviral $CD8^+$ T cells have been shown to persist in the CNS long after resolution of neurotropic viral infection, including recent work related to WNV and ZIKV (116, 134, 235-237). IFN-γ, an antiviral cytokine previously shown to be critical for WNV control, also dynamically regulates circuit plasticity, influencing synapse formation, learning and memory (134). Recent findings demonstrate that IFN-γ produced by persisting antiviral $CD8^+$ T cells promotes microglia-mediated elimination of presynaptic termini, resulting in spatial learning deficits after clearance of WNV from CNS (134). This seminal study prompts additional lines inquiry into the post-infectious CNS. Meningeal immunity could be central to CNS recovery following WNV clearance, and it remains unclear if or at what point the meninges returns to homeostasis following neurotropic flavivirus infection. Antiviral $CD8^+$ T cells retained within the parenchyma presumably require persistent or infrequent antigen presentation for continued IFN-γ production; however, the nature of these interactions remains open to future investigation. Intranasal infection of vesicular stomatitis virus (VSV) has been demonstrated to establish $CD103^+$ T_{RM} cells in the brain parenchyma, and viral antigen persisting up to six weeks after infection has been observed (236-238). Additionally,

recent studies indicate that the PD-1:PD-L1 signaling axis contributes to T_{RM} establishment in the brain parenchyma following infection with murine cytomegalovirus (MCMV) and murine polyoma virus (MuPyV) (221, 222). Future studies should investigate whether the elevated PD-1 expression observed for both meningeal and brain WNV-specific $CD8^+$ T cells remains through the resolution of WNV infection and corresponds with CD103 expression. If T_{RM} cells can be confidently identified, recall responses by memory cell populations from different tissue compartments could be evaluated to determine whether T_{RM} cells differentially control WNV infection of cortical neurons. Furthermore, whether viral clearance preferentially occurs in a cytolytic or noncytolytic manner could provide additional insight into the longevity $CD8^+$ T cell re-programming resulting from microenvironmental cues.

Lastly, viral perturbations of the CNS have been speculated to be a contributor to Alzheimer's disease (AD) pathogenesis, but a definitive link has yet to be established (239). Notably, a recent cohort study of Alzheimer's disease (AD) associated herpesvirus RNA abundance with multiple features of AD, including genetic risk networks, gene expression changes, clinical dementia ratings and neuropathology (240). Furthermore, associations between viral infection and MS have also been loosely implicated (241, 242). Much of the research in the field of MS and neurodegenerative diseases has centered on chronic viral infections due to the persistence of viral antigen. However, the mounting evidence that acute viral infections can lead to extended or persistent neuroinflammatory processes suggests that the impact of repeated viral perturbations of the CNS from both chronic and acute infection may cumulatively contribute to CNS pathology or diseases.

FIGURE LEGENDS

Figure 1. Microenvironmental cues within the CNS re-program WNV-specific CD8$^+$ T cells resulting in transcriptional, phenotypic, and functional differences. Working model of CD8$^+$ T cell programming during WNV infection. WNV-specific CD8$^+$ T cells are recruited to the CNS through CXCL10 released by neurons. Upon entry into the meninges and CNS, infiltrating WNV-specific CD8$^+$ T cells interact with CNS-localized APCs and undergo dramatic transcriptional and phenotypic changes, including enhanced antiviral cytokine production and upregulation of activation and inhibitory markers such as PD-1. CNS-reprogrammed WNV-specific CD8$^+$ T cells more efficiently control viral infection of neurons than peripheral WNV-specific CD8$^+$ T cells. The exact microenvironmental cues responsible for these changes have yet to be fully elucidated although published evidence support that interactions with some CNS-localized APC population are critical in re-programming infiltrating CD8$^+$ T cells.

Figure 1

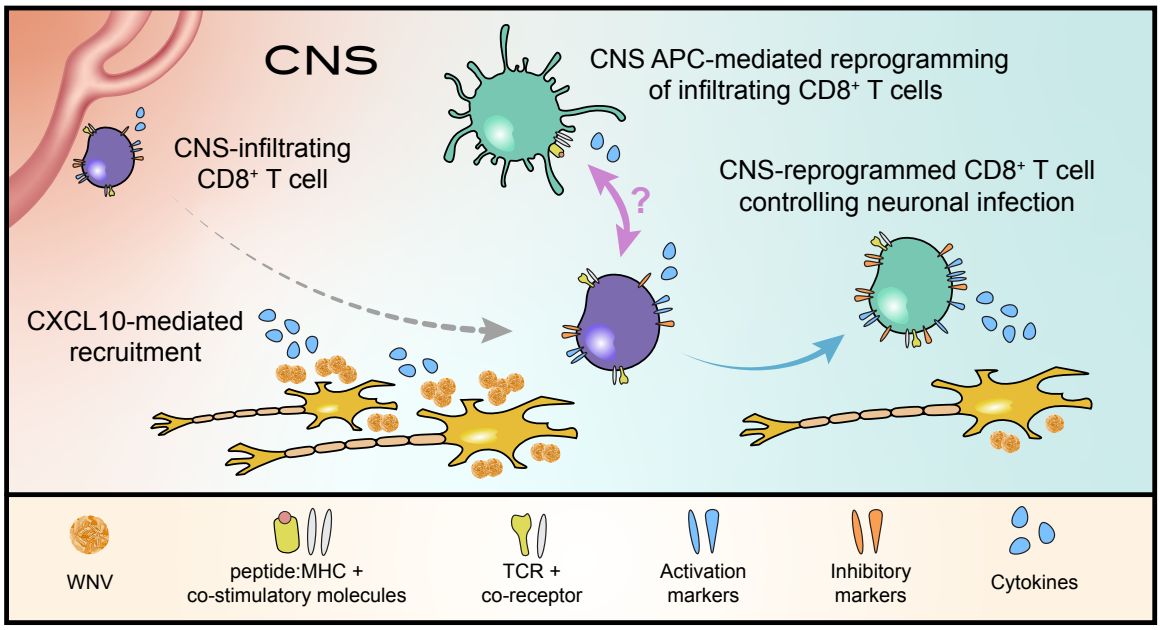
CNS
CNS APC-mediated reprogramming of infiltrating CD8⁺ T cells
CNS-infiltrating CD8⁺ T cell
?
CNS-reprogrammed CD8⁺ T cell controlling neuronal infection
CXCL10-mediated recruitment
WNV
peptide:MHC + co-stimulatory molecules
TCR + co-receptor
Activation markers
Inhibitory markers
Cytokines

BIBLIOGRAPHY

1. Chancey C, Grinev A, Volkova E, Rios M. The global ecology and epidemiology of West Nile virus. Biomed Res Int. 2015;2015:376230. doi: 10.1155/2015/376230. PubMed PMID: 25866777; PMCID: PMC4383390.

2. Krow-Lucal E, Lindsey NP, Lehman J, Fischer M, Staples JE. West Nile Virus and Other Nationally Notifiable Arboviral Diseases - United States, 2015. MMWR Morb Mortal Wkly Rep. 2017;66(2):51-5. doi: 10.15585/mmwr.mm6602a3. PubMed PMID: 28103209; PMCID: PMC5657660.

3. Suthar MS, Diamond MS, Gale M, Jr. West Nile virus infection and immunity. Nat Rev Microbiol. 2013;11(2):115-28. doi: 10.1038/nrmicro2950. PubMed PMID: 23321534.

4. Stanaway JD, Shepard DS, Undurraga EA, Halasa YA, Coffeng LE, Brady OJ, Hay SI, Bedi N, Bensenor IM, Castaneda-Orjuela CA, Chuang TW, Gibney KB, Memish ZA, Rafay A, Ukwaja KN, Yonemoto N, Murray CJL. The global burden of dengue: an analysis from the Global Burden of Disease Study 2013. Lancet Infect Dis. 2016;16(6):712-23. doi: 10.1016/S1473-3099(16)00026-8. PubMed PMID: 26874619; PMCID: PMC5012511.

5. Patel H, Sander B, Nelder MP. Long-term sequelae of West Nile virus-related illness: a systematic review. Lancet Infect Dis. 2015;15(8):951-9. doi: 10.1016/S1473-3099(15)00134-6. PubMed PMID: 26163373.

6. Sejvar JJ, Haddad MB, Tierney BC, Campbell GL, Marfin AA, Van Gerpen JA, Fleischauer A, Leis AA, Stokic DS, Petersen LR. Neurologic manifestations and outcome of West Nile virus infection. JAMA. 2003;290(4):511-5. doi: 10.1001/jama.290.4.511. PubMed PMID: 12876094.

7. Diamond MS, Pierson TC. Molecular Insight into Dengue Virus Pathogenesis and Its Implications for Disease Control. Cell. 2015;162(3):488-92. doi: 10.1016/j.cell.2015.07.005. PubMed PMID: 26232221; PMCID: PMC4522276.

8. Halstead SB. Dengue. Lancet. 2007;370(9599):1644-52. doi: 10.1016/S0140-6736(07)61687-0. PubMed PMID: 17993365.

9. Hadinegoro SR, Arredondo-Garcia JL, Capeding MR, Deseda C, Chotpitayasunondh T, Dietze R, Muhammad Ismail HI, Reynales H, Limkittikul K, Rivera-Medina DM, Tran HN, Bouckenooghe A, Chansinghakul D, Cortes M, Fanouillere K, Forrat R, Frago C, Gailhardou S, Jackson N, Noriega F, Plennevaux E, Wartel TA, Zambrano B, Saville M, Group C-TDVW. Efficacy and Long-Term Safety of a Dengue Vaccine in Regions of Endemic Disease. N Engl J Med. 2015;373(13):1195-206. doi: 10.1056/NEJMoa1506223. PubMed PMID: 26214039.

10. Hunsperger E, Peeling R, Gubler DJ, Ooi EE. Dengue pre-vaccination serology screening for the use of Dengvaxia(R). J Travel Med. 2019. doi: 10.1093/jtm/taz092. PubMed PMID: 31776549.

11. Douam F, Ploss A. Yellow Fever Virus: Knowledge Gaps Impeding the Fight Against an Old Foe. Trends Microbiol. 2018;26(11):913-28. doi: 10.1016/j.tim.2018.05.012. PubMed PMID: 29933925; PMCID: PMC6340642.

12. Garske T, Van Kerkhove MD, Yactayo S, Ronveaux O, Lewis RF, Staples JE, Perea W, Ferguson NM, Yellow Fever Expert C. Yellow Fever in Africa: estimating the burden of disease and impact of mass vaccination from outbreak and serological data. PLoS Med. 2014;11(5):e1001638. doi: 10.1371/journal.pmed.1001638. PubMed PMID: 24800812; PMCID: PMC4011853.

13. Monath TP, Vasconcelos PF. Yellow fever. J Clin Virol. 2015;64:160-73. doi: 10.1016/j.jcv.2014.08.030. PubMed PMID: 25453327.

14. Quaresma JA, Pagliari C, Medeiros DB, Duarte MI, Vasconcelos PF. Immunity and immune response, pathology and pathologic changes: progress and challenges in the immunopathology of yellow fever. Rev Med Virol. 2013;23(5):305-18. doi: 10.1002/rmv.1752. PubMed PMID: 23873723.

15. Shearer FM, Moyes CL, Pigott DM, Brady OJ, Marinho F, Deshpande A, Longbottom J, Browne AJ, Kraemer MUG, O'Reilly KM, Hombach J, Yactayo S, de Araujo VEM, da Nobrega AA, Mosser JF, Stanaway JD, Lim SS, Hay SI, Golding N, Reiner RC, Jr. Global yellow fever vaccination coverage from 1970 to 2016: an adjusted retrospective analysis. Lancet Infect Dis. 2017;17(11):1209-17. doi: 10.1016/S1473-3099(17)30419-X. PubMed PMID: 28822780; PMCID: PMC5666204.

16. Abbink P, Stephenson KE, Barouch DH. Zika virus vaccines. Nat Rev Microbiol. 2018;16(10):594-600. doi: 10.1038/s41579-018-0039-7. PubMed PMID: 29921914; PMCID: PMC6162149.

17. Beasley DW, Lewthwaite P, Solomon T. Current use and development of vaccines for Japanese encephalitis. Expert Opin Biol Ther. 2008;8(1):95-106. doi: 10.1517/14712598.8.1.95. PubMed PMID: 18081539.

18. Halstead SB, Thomas SJ. New Japanese encephalitis vaccines: alternatives to production in mouse brain. Expert Rev Vaccines. 2011;10(3):355-64. doi: 10.1586/erv.11.7. PubMed PMID: 21434803.

19. Kaiser JA, Barrett ADT. Twenty Years of Progress Toward West Nile Virus Vaccine Development. Viruses. 2019;11(9). doi: 10.3390/v11090823. PubMed PMID: 31491885; PMCID: PMC6784102.

20. Kramer LD, Styer LM, Ebel GD. A global perspective on the epidemiology of West Nile virus. Annu Rev Entomol. 2008;53:61-81. Epub 2007/07/25. doi: 10.1146/annurev.ento.53.103106.093258. PubMed PMID: 17645411.

21. Turell MJ, Dohm DJ, Sardelis MR, Oguinn ML, Andreadis TG, Blow JA. An update on the potential of north American mosquitoes (Diptera: Culicidae) to transmit West Nile Virus. J Med Entomol. 2005;42(1):57-62. Epub 2005/02/05. doi: 10.1093/jmedent/42.1.57. PubMed PMID: 15691009.

22. Vogels CB, Goertz GP, Pijlman GP, Koenraadt CJ. Vector competence of European mosquitoes for West Nile virus. Emerg Microbes Infect. 2017;6(11):e96. Epub 2017/11/09. doi: 10.1038/emi.2017.82. PubMed PMID: 29116220; PMCID: PMC5717085.

23. St Leger J, Wu G, Anderson M, Dalton L, Nilson E, Wang D. West Nile virus infection in killer whale, Texas, USA, 2007. Emerg Infect Dis. 2011;17(8):1531-3. Epub 2011/08/02. doi: 10.3201/eid1708.101979. PubMed PMID: 21801643; PMCID: PMC3381582.

24. Reisen WK, Barker CM, Carney R, Lothrop HD, Wheeler SS, Wilson JL, Madon MB, Takahashi R, Carroll B, Garcia S, Fang Y, Shafii M, Kahl N, Ashtari S, Kramer V, Glaser C, Jean C. Role of corvids in epidemiology of west Nile virus in southern California. J Med Entomol. 2006;43(2):356-67. Epub 2006/04/20. doi: 10.1603/0022-2585(2006)043[0356:rocieo]2.0.co;2. PubMed PMID: 16619622.

25. Eidson M, Schmit K, Hagiwara Y, Anand M, Backenson PB, Gotham I, Kramer L. Dead crow density and West Nile virus monitoring, New York. Emerg Infect Dis. 2005;11(9):1370-5. Epub 2005/10/19. doi: 10.3201/eid1109.040712. PubMed PMID: 16229764; PMCID: PMC3310601.

26. Root JJ, Oesterle PT, Nemeth NM, Klenk K, Gould DH, McLean RG, Clark L, Hall JS. Experimental infection of fox squirrels (Sciurus niger) with West Nile virus. Am J Trop Med Hyg. 2006;75(4):697-701. Epub 2006/10/14. PubMed PMID: 17038697.

27. Komar N, Langevin S, Hinten S, Nemeth N, Edwards E, Hettler D, Davis B, Bowen R, Bunning M. Experimental infection of North American birds with the New York 1999 strain of West Nile virus. Emerg Infect Dis. 2003;9(3):311-22. Epub 2003/03/20. doi: 10.3201/eid0903.020628. PubMed PMID: 12643825; PMCID: PMC2958552.

28. Girard YA, Popov V, Wen J, Han V, Higgs S. Ultrastructural study of West Nile virus pathogenesis in Culex pipiens quinquefasciatus (Diptera: Culicidae). J Med Entomol. 2005;42(3):429-44. Epub 2005/06/21. doi: 10.1093/jmedent/42.3.429. PubMed PMID: 15962797.

29. Houk EJ, Obie F, Hardy JL. Peritrophic membrane formation and the midgut barrier to arboviral infection in the mosquito, Culex tarsalis Coquillett (Insecta, Diptera). Acta Trop. 1979;36(1):39-45. Epub 1979/03/01. PubMed PMID: 35932.

30. Hardy JL, Houk EJ, Kramer LD, Reeves WC. Intrinsic factors affecting vector competence of mosquitoes for arboviruses. Annu Rev Entomol. 1983;28:229-62. Epub 1983/01/01. doi: 10.1146/annurev.en.28.010183.001305. PubMed PMID: 6131642.

31. Styer LM, Kent KA, Albright RG, Bennett CJ, Kramer LD, Bernard KA. Mosquitoes inoculate high doses of West Nile virus as they probe and feed on live hosts.

PLoS Pathog. 2007;3(9):1262-70. doi: 10.1371/journal.ppat.0030132. PubMed PMID: 17941708; PMCID: PMC1976553.

32. Hafer A, Whittlesey R, Brown DT, Hernandez R. Differential incorporation of cholesterol by Sindbis virus grown in mammalian or insect cells. J Virol. 2009;83(18):9113-21. Epub 2009/07/10. doi: 10.1128/JVI.00755-09. PubMed PMID: 19587056; PMCID: PMC2738221.

33. Hsieh P, Robbins PW. Regulation of asparagine-linked oligosaccharide processing. Oligosaccharide processing in Aedes albopictus mosquito cells. J Biol Chem. 1984;259(4):2375-82. Epub 1984/02/25. PubMed PMID: 6698972.

34. Davis CW, Nguyen HY, Hanna SL, Sanchez MD, Doms RW, Pierson TC. West Nile virus discriminates between DC-SIGN and DC-SIGNR for cellular attachment and infection. J Virol. 2006;80(3):1290-301. Epub 2006/01/18. doi: 10.1128/JVI.80.3.1290-1301.2006. PubMed PMID: 16415006; PMCID: PMC1346927.

35. Lim PY, Louie KL, Styer LM, Shi PY, Bernard KA. Viral pathogenesis in mice is similar for West Nile virus derived from mosquito and mammalian cells. Virology. 2010;400(1):93-103. Epub 2010/02/20. doi: 10.1016/j.virol.2010.01.029. PubMed PMID: 20167345; PMCID: PMC2835801.

36. Boylan BT, Moreira FR, Carlson TW, Bernard KA. Mosquito cell-derived West Nile virus replicon particles mimic arbovirus inoculum and have reduced spread in mice. PLoS Negl Trop Dis. 2017;11(2):e0005394. doi: 10.1371/journal.pntd.0005394. PubMed PMID: 28187142; PMCID: PMC5322982.

37. Styer LM, Lim PY, Louie KL, Albright RG, Kramer LD, Bernard KA. Mosquito saliva causes enhancement of West Nile virus infection in mice. J Virol.

2011;85(4):1517-27. doi: 10.1128/JVI.01112-10. PubMed PMID: 21147918; PMCID: PMC3028906.

38. Sejvar JJ. The long-term outcomes of human West Nile virus infection. Clin Infect Dis. 2007;44(12):1617-24. Epub 2007/05/23. doi: 10.1086/518281. PubMed PMID: 17516407.

39. Samuel MA, Diamond MS. Pathogenesis of West Nile Virus infection: a balance between virulence, innate and adaptive immunity, and viral evasion. J Virol. 2006;80(19):9349-60. doi: 10.1128/JVI.01122-06. PubMed PMID: 16973541; PMCID: PMC1617273.

40. Lazear HM, Pinto AK, Vogt MR, Gale M, Jr., Diamond MS. Beta interferon controls West Nile virus infection and pathogenesis in mice. J Virol. 2011;85(14):7186-94. doi: 10.1128/JVI.00396-11. PubMed PMID: 21543483; PMCID: PMC3126609.

41. Marin-Lopez A, Calvo-Pinilla E, Moreno S, Utrilla-Trigo S, Nogales A, Brun A, Fikrig E, Ortego J. Modeling Arboviral Infection in Mice Lacking the Interferon Alpha/Beta Receptor. Viruses. 2019;11(1). doi: 10.3390/v11010035. PubMed PMID: 30625992; PMCID: PMC6356211.

42. Samuel MA, Diamond MS. Alpha/beta interferon protects against lethal West Nile virus infection by restricting cellular tropism and enhancing neuronal survival. J Virol. 2005;79(21):13350-61. doi: 10.1128/JVI.79.21.13350-13361.2005. PubMed PMID: 16227257; PMCID: PMC1262587.

43. Giordano D, Draves KE, Young LB, Roe K, Bryan MA, Dresch C, Richner JM, Diamond MS, Gale M, Jr., Clark EA. Protection of mice deficient in mature B cells from West Nile virus infection by passive and active immunization. PLoS Pathog.

2017;13(11):e1006743. doi: 10.1371/journal.ppat.1006743. PubMed PMID: 29176765; PMCID: PMC5720816.

44. Shrestha B, Diamond MS. Role of CD8+ T cells in control of West Nile virus infection. J Virol. 2004;78(15):8312-21. doi: 10.1128/JVI.78.15.8312-8321.2004. PubMed PMID: 15254203; PMCID: PMC446114.

45. Faul EJ, Wanjalla CN, Suthar MS, Gale M, Wirblich C, Schnell MJ. Rabies virus infection induces type I interferon production in an IPS-1 dependent manner while dendritic cell activation relies on IFNAR signaling. PLoS Pathog. 2010;6(7):e1001016. doi: 10.1371/journal.ppat.1001016. PubMed PMID: 20661430; PMCID: PMC2908622.

46. Lazear HM, Lancaster A, Wilkins C, Suthar MS, Huang A, Vick SC, Clepper L, Thackray L, Brassil MM, Virgin HW, Nikolich-Zugich J, Moses AV, Gale M, Jr., Fruh K, Diamond MS. IRF-3, IRF-5, and IRF-7 coordinately regulate the type I IFN response in myeloid dendritic cells downstream of MAVS signaling. PLoS Pathog. 2013;9(1):e1003118. doi: 10.1371/journal.ppat.1003118. PubMed PMID: 23300459; PMCID: PMC3536698.

47. Pinto AK, Ramos HJ, Wu X, Aggarwal S, Shrestha B, Gorman M, Kim KY, Suthar MS, Atkinson JP, Gale M, Jr., Diamond MS. Deficient IFN signaling by myeloid cells leads to MAVS-dependent virus-induced sepsis. PLoS Pathog. 2014;10(4):e1004086. doi: 10.1371/journal.ppat.1004086. PubMed PMID: 24743949; PMCID: PMC3990718.

48. Suthar MS, Ma DY, Thomas S, Lund JM, Zhang N, Daffis S, Rudensky AY, Bevan MJ, Clark EA, Kaja MK, Diamond MS, Gale M, Jr. IPS-1 is essential for the control of West Nile virus infection and immunity. PLoS Pathog. 2010;6(2):e1000757. doi: 10.1371/journal.ppat.1000757. PubMed PMID: 20140199; PMCID: PMC2816698.

49. Krishnan MN, Ng A, Sukumaran B, Gilfoy FD, Uchil PD, Sultana H, Brass AL, Adametz R, Tsui M, Qian F, Montgomery RR, Lev S, Mason PW, Koski RA, Elledge SJ, Xavier RJ, Agaisse H, Fikrig E. RNA interference screen for human genes associated with West Nile virus infection. Nature. 2008;455(7210):242-5. doi: 10.1038/nature07207. PubMed PMID: 18690214; PMCID: PMC3136529.

50. Li J, Ding SC, Cho H, Chung BC, Gale M, Jr., Chanda SK, Diamond MS. A short hairpin RNA screen of interferon-stimulated genes identifies a novel negative regulator of the cellular antiviral response. MBio. 2013;4(3):e00385-13. doi: 10.1128/mBio.00385-13. PubMed PMID: 23781071; PMCID: PMC3684836.

51. Ma H, Dang Y, Wu Y, Jia G, Anaya E, Zhang J, Abraham S, Choi JG, Shi G, Qi L, Manjunath N, Wu H. A CRISPR-Based Screen Identifies Genes Essential for West-Nile-Virus-Induced Cell Death. Cell Rep. 2015;12(4):673-83. doi: 10.1016/j.celrep.2015.06.049. PubMed PMID: 26190106; PMCID: PMC4559080.

52. Marceau CD, Puschnik AS, Majzoub K, Ooi YS, Brewer SM, Fuchs G, Swaminathan K, Mata MA, Elias JE, Sarnow P, Carette JE. Genetic dissection of Flaviviridae host factors through genome-scale CRISPR screens. Nature. 2016;535(7610):159-63. doi: 10.1038/nature18631. PubMed PMID: 27383987; PMCID: PMC4964798.

53. Schoggins JW, Wilson SJ, Panis M, Murphy MY, Jones CT, Bieniasz P, Rice CM. A diverse range of gene products are effectors of the type I interferon antiviral response. Nature. 2011;472(7344):481-5. doi: 10.1038/nature09907. PubMed PMID: 21478870; PMCID: PMC3409588.

54. Zhang R, Miner JJ, Gorman MJ, Rausch K, Ramage H, White JP, Zuiani A, Zhang P, Fernandez E, Zhang Q, Dowd KA, Pierson TC, Cherry S, Diamond MS. A CRISPR screen defines a signal peptide processing pathway required by flaviviruses. Nature. 2016;535(7610):164-8. doi: 10.1038/nature18625. PubMed PMID: 27383988; PMCID: PMC4945490.

55. Lazear HM, Diamond MS. New insights into innate immune restriction of West Nile virus infection. Curr Opin Virol. 2015;11:1-6. doi: 10.1016/j.coviro.2014.12.001. PubMed PMID: 25554924; PMCID: PMC4456296.

56. Schneider WM, Chevillotte MD, Rice CM. Interferon-stimulated genes: a complex web of host defenses. Annu Rev Immunol. 2014;32:513-45. doi: 10.1146/annurev-immunol-032713-120231. PubMed PMID: 24555472; PMCID: PMC4313732.

57. Ray D, Shah A, Tilgner M, Guo Y, Zhao Y, Dong H, Deas TS, Zhou Y, Li H, Shi PY. West Nile virus 5'-cap structure is formed by sequential guanine N-7 and ribose 2'-O methylations by nonstructural protein 5. J Virol. 2006;80(17):8362-70. doi: 10.1128/JVI.00814-06. PubMed PMID: 16912287; PMCID: PMC1563844.

58. Sadler AJ, Williams BR. Interferon-inducible antiviral effectors. Nat Rev Immunol. 2008;8(7):559-68. doi: 10.1038/nri2314. PubMed PMID: 18575461; PMCID: PMC2522268.

59. Schoggins JW. Interferon-stimulated genes: roles in viral pathogenesis. Curr Opin Virol. 2014;6:40-6. doi: 10.1016/j.coviro.2014.03.006. PubMed PMID: 24713352; PMCID: PMC4077717.

60. Wu J, Chen ZJ. Innate immune sensing and signaling of cytosolic nucleic acids. Annu Rev Immunol. 2014;32:461-88. doi: 10.1146/annurev-immunol-032713-120156. PubMed PMID: 24655297.

61. Cheon H, Stark GR. Unphosphorylated STAT1 prolongs the expression of interferon-induced immune regulatory genes. Proc Natl Acad Sci U S A. 2009;106(23):9373-8. doi: 10.1073/pnas.0903487106. PubMed PMID: 19478064; PMCID: PMC2688000.

62. Larner AC, Chaudhuri A, Darnell JE, Jr. Transcriptional induction by interferon. New protein(s) determine the extent and length of the induction. J Biol Chem. 1986;261(1):453-9. PubMed PMID: 2934388.

63. Larner AC, Jonak G, Cheng YS, Korant B, Knight E, Darnell JE, Jr. Transcriptional induction of two genes in human cells by beta interferon. Proc Natl Acad Sci U S A. 1984;81(21):6733-7. doi: 10.1073/pnas.81.21.6733. PubMed PMID: 6436820; PMCID: PMC392005.

64. Isaacs A, Lindenmann J. Virus interference. I. The interferon. Proc R Soc Lond B Biol Sci. 1957;147(927):258-67. doi: 10.1098/rspb.1957.0048. PubMed PMID: 13465720.

65. Schindler C, Fu XY, Improta T, Aebersold R, Darnell JE, Jr. Proteins of transcription factor ISGF-3: one gene encodes the 91-and 84-kDa ISGF-3 proteins that are activated by interferon alpha. Proc Natl Acad Sci U S A. 1992;89(16):7836-9. doi: 10.1073/pnas.89.16.7836. PubMed PMID: 1502203; PMCID: PMC49806.

66. Levy DE, Kessler DS, Pine R, Reich N, Darnell JE, Jr. Interferon-induced nuclear factors that bind a shared promoter element correlate with positive and negative

transcriptional control. Genes Dev. 1988;2(4):383-93. doi: 10.1101/gad.2.4.383. PubMed PMID: 3371658.

67. Kawai T, Akira S. Toll-like receptors and their crosstalk with other innate receptors in infection and immunity. Immunity. 2011;34(5):637-50. doi: 10.1016/j.immuni.2011.05.006. PubMed PMID: 21616434.

68. Ni G, Ma Z, Damania B. cGAS and STING: At the intersection of DNA and RNA virus-sensing networks. PLoS Pathog. 2018;14(8):e1007148. doi: 10.1371/journal.ppat.1007148. PubMed PMID: 30114241; PMCID: PMC6095619.

69. Zhao J, Vijay R, Zhao J, Gale M, Jr., Diamond MS, Perlman S. MAVS Expressed by Hematopoietic Cells Is Critical for Control of West Nile Virus Infection and Pathogenesis. J Virol. 2016;90(16):7098-108. doi: 10.1128/JVI.00707-16. PubMed PMID: 27226371; PMCID: PMC4984631.

70. Ambrose RL, Mackenzie JM. West Nile virus differentially modulates the unfolded protein response to facilitate replication and immune evasion. J Virol. 2011;85(6):2723-32. doi: 10.1128/JVI.02050-10. PubMed PMID: 21191014; PMCID: PMC3067947.

71. Best SM. The Many Faces of the Flavivirus NS5 Protein in Antagonism of Type I Interferon Signaling. J Virol. 2017;91(3). doi: 10.1128/JVI.01970-16. PubMed PMID: 27881649; PMCID: PMC5244349.

72. Bowen JR, Quicke KM, Maddur MS, O'Neal JT, McDonald CE, Fedorova NB, Puri V, Shabman RS, Pulendran B, Suthar MS. Zika Virus Antagonizes Type I Interferon Responses during Infection of Human Dendritic Cells. PLoS Pathog.

2017;13(2):e1006164. doi: 10.1371/journal.ppat.1006164. PubMed PMID: 28152048; PMCID: PMC5289613.

73. Bowen JR, Zimmerman MG, Suthar MS. Taking the defensive: Immune control of Zika virus infection. Virus Res. 2017. doi: 10.1016/j.virusres.2017.08.018. PubMed PMID: 28867493; PMCID: PMC5832569.

74. Lubick KJ, Robertson SJ, McNally KL, Freedman BA, Rasmussen AL, Taylor RT, Walts AD, Tsuruda S, Sakai M, Ishizuka M, Boer EF, Foster EC, Chiramel AI, Addison CB, Green R, Kastner DL, Katze MG, Holland SM, Forlino A, Freeman AF, Boehm M, Yoshii K, Best SM. Flavivirus Antagonism of Type I Interferon Signaling Reveals Prolidase as a Regulator of IFNAR1 Surface Expression. Cell Host Microbe. 2015;18(1):61-74. doi: 10.1016/j.chom.2015.06.007. PubMed PMID: 26159719; PMCID: PMC4505794.

75. Mackenzie JM, Khromykh AA, Parton RG. Cholesterol manipulation by West Nile virus perturbs the cellular immune response. Cell Host Microbe. 2007;2(4):229-39. doi: 10.1016/j.chom.2007.09.003. PubMed PMID: 18005741.

76. Quicke KM, Diamond MS, Suthar MS. Negative regulators of the RIG-I-like receptor signaling pathway. Eur J Immunol. 2017;47(4):615-28. doi: 10.1002/eji.201646484. PubMed PMID: 28295214.

77. Quicke KM, Suthar MS. The innate immune playbook for restricting West Nile virus infection. Viruses. 2013;5(11):2643-58. doi: 10.3390/v5112643. PubMed PMID: 24178712; PMCID: PMC3856407.

78. Daffis S, Szretter KJ, Schriewer J, Li J, Youn S, Errett J, Lin TY, Schneller S, Zust R, Dong H, Thiel V, Sen GC, Fensterl V, Klimstra WB, Pierson TC, Buller RM,

Gale M, Jr., Shi PY, Diamond MS. 2'-O methylation of the viral mRNA cap evades host restriction by IFIT family members. Nature. 2010;468(7322):452-6. doi: 10.1038/nature09489. PubMed PMID: 21085181; PMCID: PMC3058805.

79. Neufeldt CJ, Cortese M, Acosta EG, Bartenschlager R. Rewiring cellular networks by members of the Flaviviridae family. Nat Rev Microbiol. 2018;16(3):125-42. doi: 10.1038/nrmicro.2017.170. PubMed PMID: 29430005.

80. Szretter KJ, Daniels BP, Cho H, Gainey MD, Yokoyama WM, Gale M, Jr., Virgin HW, Klein RS, Sen GC, Diamond MS. 2'-O methylation of the viral mRNA cap by West Nile virus evades ifit1-dependent and -independent mechanisms of host restriction in vivo. PLoS Pathog. 2012;8(5):e1002698. doi: 10.1371/journal.ppat.1002698. PubMed PMID: 22589727; PMCID: PMC3349756.

81. Zimmerman MG, Bowen JR, McDonald CE, Young E, Baric RS, Pulendran B, Suthar MS. STAT5: a Target of Antagonism by Neurotropic Flaviviruses. J Virol. 2019;93(23). doi: 10.1128/JVI.00665-19. PubMed PMID: 31534033; PMCID: PMC6854481.

82. Roosendaal J, Westaway EG, Khromykh A, Mackenzie JM. Regulated cleavages at the West Nile virus NS4A-2K-NS4B junctions play a major role in rearranging cytoplasmic membranes and Golgi trafficking of the NS4A protein. J Virol. 2006;80(9):4623-32. doi: 10.1128/JVI.80.9.4623-4632.2006. PubMed PMID: 16611922; PMCID: PMC1472005.

83. Grant A, Ponia SS, Tripathi S, Balasubramaniam V, Miorin L, Sourisseau M, Schwarz MC, Sanchez-Seco MP, Evans MJ, Best SM, Garcia-Sastre A. Zika Virus Targets Human STAT2 to Inhibit Type I Interferon Signaling. Cell Host Microbe.

2016;19(6):882-90. doi: 10.1016/j.chom.2016.05.009. PubMed PMID: 27212660; PMCID: PMC4900918.

84. Mazzon M, Jones M, Davidson A, Chain B, Jacobs M. Dengue virus NS5 inhibits interferon-alpha signaling by blocking signal transducer and activator of transcription 2 phosphorylation. J Infect Dis. 2009;200(8):1261-70. doi: 10.1086/605847. PubMed PMID: 19754307.

85. Ashour J, Laurent-Rolle M, Shi PY, Garcia-Sastre A. NS5 of dengue virus mediates STAT2 binding and degradation. J Virol. 2009;83(11):5408-18. doi: 10.1128/JVI.02188-08. PubMed PMID: 19279106; PMCID: PMC2681973.

86. Laurent-Rolle M, Morrison J, Rajsbaum R, Macleod JML, Pisanelli G, Pham A, Ayllon J, Miorin L, Martinez C, tenOever BR, Garcia-Sastre A. The interferon signaling antagonist function of yellow fever virus NS5 protein is activated by type I interferon. Cell Host Microbe. 2014;16(3):314-27. doi: 10.1016/j.chom.2014.07.015. PubMed PMID: 25211074; PMCID: PMC4176702.

87. Schulte MB, Andino R. Single-cell analysis uncovers extensive biological noise in poliovirus replication. J Virol. 2014;88(11):6205-12. doi: 10.1128/JVI.03539-13. PubMed PMID: 24648454; PMCID: PMC4093869.

88. Wimmers F, Subedi N, van Buuringen N, Heister D, Vivie J, Beeren-Reinieren I, Woestenenk R, Dolstra H, Piruska A, Jacobs JFM, van Oudenaarden A, Figdor CG, Huck WTS, de Vries IJM, Tel J. Single-cell analysis reveals that stochasticity and paracrine signaling control interferon-alpha production by plasmacytoid dendritic cells. Nat Commun. 2018;9(1):3317. doi: 10.1038/s41467-018-05784-3. PubMed PMID: 30127440; PMCID: PMC6102223.

89. Zanini F, Pu SY, Bekerman E, Einav S, Quake SR. Single-cell transcriptional dynamics of flavivirus infection. Elife. 2018;7. doi: 10.7554/eLife.32942. PubMed PMID: 29451494; PMCID: PMC5826272.

90. Russell AB, Elshina E, Kowalsky JR, Te Velthuis AJW, Bloom JD. Single-Cell Virus Sequencing of Influenza Infections That Trigger Innate Immunity. J Virol. 2019;93(14). doi: 10.1128/JVI.00500-19. PubMed PMID: 31068418; PMCID: PMC6600203.

91. Russell AB, Trapnell C, Bloom JD. Extreme heterogeneity of influenza virus infection in single cells. Elife. 2018;7. doi: 10.7554/eLife.32303. PubMed PMID: 29451492; PMCID: PMC5826275.

92. Avraham R, Haseley N, Brown D, Penaranda C, Jijon HB, Trombetta JJ, Satija R, Shalek AK, Xavier RJ, Regev A, Hung DT. Pathogen Cell-to-Cell Variability Drives Heterogeneity in Host Immune Responses. Cell. 2015;162(6):1309-21. doi: 10.1016/j.cell.2015.08.027. PubMed PMID: 26343579; PMCID: PMC4578813.

93. Hu J, Nudelman G, Shimoni Y, Kumar M, Ding Y, Lopez C, Hayot F, Wetmur JG, Sealfon SC. Role of cell-to-cell variability in activating a positive feedback antiviral response in human dendritic cells. PLoS One. 2011;6(2):e16614. doi: 10.1371/journal.pone.0016614. PubMed PMID: 21347441; PMCID: PMC3035661.

94. Patil S, Fribourg M, Ge Y, Batish M, Tyagi S, Hayot F, Sealfon SC. Single-cell analysis shows that paracrine signaling by first responder cells shapes the interferon-beta response to viral infection. Sci Signal. 2015;8(363):ra16. doi: 10.1126/scisignal.2005728. PubMed PMID: 25670204.

95. Rand U, Rinas M, Schwerk J, Nohren G, Linnes M, Kroger A, Flossdorf M, Kaly-Kullai K, Hauser H, Hofer T, Koster M. Multi-layered stochasticity and paracrine signal propagation shape the type-I interferon response. Mol Syst Biol. 2012;8:584. doi: 10.1038/msb.2012.17. PubMed PMID: 22617958; PMCID: PMC3377992.

96. Shalek AK, Satija R, Shuga J, Trombetta JJ, Gennert D, Lu D, Chen P, Gertner RS, Gaublomme JT, Yosef N, Schwartz S, Fowler B, Weaver S, Wang J, Wang X, Ding R, Raychowdhury R, Friedman N, Hacohen N, Park H, May AP, Regev A. Single-cell RNA-seq reveals dynamic paracrine control of cellular variation. Nature. 2014;510(7505):363-9. doi: 10.1038/nature13437. PubMed PMID: 24919153; PMCID: PMC4193940.

97. Zhao M, Zhang J, Phatnani H, Scheu S, Maniatis T. Stochastic expression of the interferon-beta gene. PLoS Biol. 2012;10(1):e1001249. doi: 10.1371/journal.pbio.1001249. PubMed PMID: 22291574; PMCID: PMC3265471.

98. Alvarez-Errico D, Vento-Tormo R, Sieweke M, Ballestar E. Epigenetic control of myeloid cell differentiation, identity and function. Nat Rev Immunol. 2015;15(1):7-17. doi: 10.1038/nri3777. PubMed PMID: 25534619.

99. Ford E, Thanos D. The transcriptional code of human IFN-beta gene expression. Biochim Biophys Acta. 2010;1799(3-4):328-36. doi: 10.1016/j.bbagrm.2010.01.010. PubMed PMID: 20116463.

100. Xue S, Liu C, Sun X, Li W, Zhang C, Zhou X, Lu Y, Xiao J, Li C, Xu X, Sun B, Xu G, Wang H. TET3 Inhibits Type I IFN Production Independent of DNA Demethylation. Cell Rep. 2016;16(4):1096-105. doi: 10.1016/j.celrep.2016.06.068. PubMed PMID: 27425624.

101. Hamlin RE, Rahman A, Pak TR, Maringer K, Mena I, Bernal-Rubio D, Potla U, Maestre AM, Fredericks AC, Amir ED, Kasarskis A, Ramos I, Merad M, Fernandez-Sesma A. High-dimensional CyTOF analysis of dengue virus-infected human DCs reveals distinct viral signatures. JCI Insight. 2017;2(13). doi: 10.1172/jci.insight.92424. PubMed PMID: 28679950; PMCID: PMC5499363.

102. Durrant DM, Robinette ML, Klein RS. IL-1R1 is required for dendritic cell-mediated T cell reactivation within the CNS during West Nile virus encephalitis. J Exp Med. 2013;210(3):503-16. doi: 10.1084/jem.20121897. PubMed PMID: 23460727; PMCID: PMC3600909.

103. Hildner K, Edelson BT, Purtha WE, Diamond M, Matsushita H, Kohyama M, Calderon B, Schraml BU, Unanue ER, Diamond MS, Schreiber RD, Murphy TL, Murphy KM. Batf3 deficiency reveals a critical role for CD8alpha+ dendritic cells in cytotoxic T cell immunity. Science. 2008;322(5904):1097-100. doi: 10.1126/science.1164206. PubMed PMID: 19008445; PMCID: PMC2756611.

104. Ganguly D, Haak S, Sisirak V, Reizis B. The role of dendritic cells in autoimmunity. Nat Rev Immunol. 2013;13(8):566-77. doi: 10.1038/nri3477. PubMed PMID: 23827956; PMCID: PMC4160805.

105. Gardner A, Ruffell B. Dendritic Cells and Cancer Immunity. Trends Immunol. 2016;37(12):855-65. doi: 10.1016/j.it.2016.09.006. PubMed PMID: 27793569; PMCID: PMC5135568.

106. Guilliams M, Ginhoux F, Jakubzick C, Naik SH, Onai N, Schraml BU, Segura E, Tussiwand R, Yona S. Dendritic cells, monocytes and macrophages: a unified

nomenclature based on ontogeny. Nat Rev Immunol. 2014;14(8):571-8. doi: 10.1038/nri3712. PubMed PMID: 25033907; PMCID: PMC4638219.

107. Murphy TL, Grajales-Reyes GE, Wu X, Tussiwand R, Briseno CG, Iwata A, Kretzer NM, Durai V, Murphy KM. Transcriptional Control of Dendritic Cell Development. Annu Rev Immunol. 2016;34:93-119. doi: 10.1146/annurev-immunol-032713-120204. PubMed PMID: 26735697; PMCID: PMC5135011.

108. Edelson BT, Kc W, Juang R, Kohyama M, Benoit LA, Klekotka PA, Moon C, Albring JC, Ise W, Michael DG, Bhattacharya D, Stappenbeck TS, Holtzman MJ, Sung SS, Murphy TL, Hildner K, Murphy KM. Peripheral CD103+ dendritic cells form a unified subset developmentally related to CD8alpha+ conventional dendritic cells. J Exp Med. 2010;207(4):823-36. doi: 10.1084/jem.20091627. PubMed PMID: 20351058; PMCID: PMC2856032.

109. Bachem A, Hartung E, Guttler S, Mora A, Zhou X, Hegemann A, Plantinga M, Mazzini E, Stoitzner P, Gurka S, Henn V, Mages HW, Kroczek RA. Expression of XCR1 Characterizes the Batf3-Dependent Lineage of Dendritic Cells Capable of Antigen Cross-Presentation. Front Immunol. 2012;3:214. doi: 10.3389/fimmu.2012.00214. PubMed PMID: 22826713; PMCID: PMC3399095.

110. Pinto AK, Daffis S, Brien JD, Gainey MD, Yokoyama WM, Sheehan KC, Murphy KM, Schreiber RD, Diamond MS. A temporal role of type I interferon signaling in CD8+ T cell maturation during acute West Nile virus infection. PLoS Pathog. 2011;7(12):e1002407. doi: 10.1371/journal.ppat.1002407. PubMed PMID: 22144897; PMCID: PMC3228803.

111. Kim S, Pinto AK, Myers NB, Hawkins O, Doll K, Kaabinejadian S, Netland J, Bevan MJ, Weidanz JA, Hildebrand WH, Diamond MS, Hansen TH. A novel T-cell receptor mimic defines dendritic cells that present an immunodominant West Nile virus epitope in mice. Eur J Immunol. 2014;44(7):1936-46. doi: 10.1002/eji.201444450. PubMed PMID: 24723377; PMCID: PMC4107030.

112. Zimmerman MG, Bowen JR, McDonald CE, Pulendran B, Suthar MS. West Nile Virus Infection Blocks Inflammatory Response and T Cell Costimulatory Capacity of Human Monocyte-Derived Dendritic Cells. J Virol. 2019;93(23). doi: 10.1128/JVI.00664-19. PubMed PMID: 31534040; PMCID: PMC6854506.

113. Halle S, Halle O, Forster R. Mechanisms and Dynamics of T Cell-Mediated Cytotoxicity In Vivo. Trends Immunol. 2017;38(6):432-43. doi: 10.1016/j.it.2017.04.002. PubMed PMID: 28499492.

114. Masopust D, Soerens AG. Tissue-Resident T Cells and Other Resident Leukocytes. Annu Rev Immunol. 2019;37:521-46. doi: 10.1146/annurev-immunol-042617-053214. PubMed PMID: 30726153.

115. Mueller SN, Gebhardt T, Carbone FR, Heath WR. Memory T cell subsets, migration patterns, and tissue residence. Annu Rev Immunol. 2013;31:137-61. doi: 10.1146/annurev-immunol-032712-095954. PubMed PMID: 23215646.

116. Schenkel JM, Masopust D. Tissue-resident memory T cells. Immunity. 2014;41(6):886-97. doi: 10.1016/j.immuni.2014.12.007. PubMed PMID: 25526304; PMCID: PMC4276131.

117. von Andrian UH, Mackay CR. T-cell function and migration. Two sides of the same coin. N Engl J Med. 2000;343(14):1020-34. doi: 10.1056/NEJM200010053431407. PubMed PMID: 11018170.

118. Grakoui A, Bromley SK, Sumen C, Davis MM, Shaw AS, Allen PM, Dustin ML. The immunological synapse: a molecular machine controlling T cell activation. Science. 1999;285(5425):221-7. doi: 10.1126/science.285.5425.221. PubMed PMID: 10398592.

119. Marchingo JM, Kan A, Sutherland RM, Duffy KR, Wellard CJ, Belz GT, Lew AM, Dowling MR, Heinzel S, Hodgkin PD. T cell signaling. Antigen affinity, costimulation, and cytokine inputs sum linearly to amplify T cell expansion. Science. 2014;346(6213):1123-7. doi: 10.1126/science.1260044. PubMed PMID: 25430770.

120. Kohlmeier JE, Cookenham T, Roberts AD, Miller SC, Woodland DL. Type I interferons regulate cytolytic activity of memory CD8(+) T cells in the lung airways during respiratory virus challenge. Immunity. 2010;33(1):96-105. doi: 10.1016/j.immuni.2010.06.016. PubMed PMID: 20637658; PMCID: PMC2908370.

121. Kaech SM, Tan JT, Wherry EJ, Konieczny BT, Surh CD, Ahmed R. Selective expression of the interleukin 7 receptor identifies effector CD8 T cells that give rise to long-lived memory cells. Nat Immunol. 2003;4(12):1191-8. doi: 10.1038/ni1009. PubMed PMID: 14625547.

122. Mackay LK, Rahimpour A, Ma JZ, Collins N, Stock AT, Hafon ML, Vega-Ramos J, Lauzurica P, Mueller SN, Stefanovic T, Tscharke DC, Heath WR, Inouye M, Carbone FR, Gebhardt T. The developmental pathway for CD103(+)CD8+ tissue-resident memory T cells of skin. Nat Immunol. 2013;14(12):1294-301. doi: 10.1038/ni.2744. PubMed PMID: 24162776.

123. Masopust D, Picker LJ. Hidden memories: frontline memory T cells and early pathogen interception. J Immunol. 2012;188(12):5811-7. doi: 10.4049/jimmunol.1102695. PubMed PMID: 22675215; PMCID: PMC3375618.

124. Rosato PC, Beura LK, Masopust D. Tissue resident memory T cells and viral immunity. Curr Opin Virol. 2017;22:44-50. doi: 10.1016/j.coviro.2016.11.011. PubMed PMID: 27987416; PMCID: PMC5346042.

125. Benechet AP, Menon M, Xu D, Samji T, Maher L, Murooka TT, Mempel TR, Sheridan BS, Lemoine FM, Khanna KM. T cell-intrinsic S1PR1 regulates endogenous effector T-cell egress dynamics from lymph nodes during infection. Proc Natl Acad Sci U S A. 2016;113(8):2182-7. doi: 10.1073/pnas.1516485113. PubMed PMID: 26862175; PMCID: PMC4776484.

126. Walsh DA, Borges da Silva H, Beura LK, Peng C, Hamilton SE, Masopust D, Jameson SC. The Functional Requirement for CD69 in Establishment of Resident Memory CD8(+) T Cells Varies with Tissue Location. J Immunol. 2019;203(4):946-55. doi: 10.4049/jimmunol.1900052. PubMed PMID: 31243092; PMCID: PMC6684481.

127. de la Roche M, Asano Y, Griffiths GM. Origins of the cytolytic synapse. Nat Rev Immunol. 2016;16(7):421-32. doi: 10.1038/nri.2016.54. PubMed PMID: 27265595.

128. Hashimoto-Tane A, Sakuma M, Ike H, Yokosuka T, Kimura Y, Ohara O, Saito T. Micro-adhesion rings surrounding TCR microclusters are essential for T cell activation. J Exp Med. 2016;213(8):1609-25. doi: 10.1084/jem.20151088. PubMed PMID: 27354546; PMCID: PMC4986522.

129. Pauls K, Schon M, Kubitza RC, Homey B, Wiesenborn A, Lehmann P, Ruzicka T, Parker CM, Schon MP. Role of integrin alphaE(CD103)beta7 for tissue-specific

epidermal localization of CD8+ T lymphocytes. J Invest Dermatol. 2001;117(3):569-75. doi: 10.1046/j.0022-202x.2001.01481.x. PubMed PMID: 11564161.

130. Woodland DL, Kohlmeier JE. Migration, maintenance and recall of memory T cells in peripheral tissues. Nat Rev Immunol. 2009;9(3):153-61. doi: 10.1038/nri2496. PubMed PMID: 19240755.

131. Erle DJ, Briskin MJ, Butcher EC, Garcia-Pardo A, Lazarovits AI, Tidswell M. Expression and function of the MAdCAM-1 receptor, integrin alpha 4 beta 7, on human leukocytes. J Immunol. 1994;153(2):517-28. PubMed PMID: 7517418.

132. McMaster SR, Wein AN, Dunbar PR, Hayward SL, Cartwright EK, Denning TL, Kohlmeier JE. Pulmonary antigen encounter regulates the establishment of tissue-resident CD8 memory T cells in the lung airways and parenchyma. Mucosal Immunol. 2018;11(4):1071-8. doi: 10.1038/s41385-018-0003-x. PubMed PMID: 29453412; PMCID: PMC6030505.

133. Menares E, Galvez-Cancino F, Caceres-Morgado P, Ghorani E, Lopez E, Diaz X, Saavedra-Almarza J, Figueroa DA, Roa E, Quezada SA, Lladser A. Tissue-resident memory CD8(+) T cells amplify anti-tumor immunity by triggering antigen spreading through dendritic cells. Nat Commun. 2019;10(1):4401. doi: 10.1038/s41467-019-12319-x. PubMed PMID: 31562311; PMCID: PMC6765014.

134. Garber C, Soung A, Vollmer LL, Kanmogne M, Last A, Brown J, Klein RS. T cells promote microglia-mediated synaptic elimination and cognitive dysfunction during recovery from neuropathogenic flaviviruses. Nat Neurosci. 2019;22(8):1276-88. doi: 10.1038/s41593-019-0427-y. PubMed PMID: 31235930; PMCID: PMC6822175.

135. Korn T, Kallies A. T cell responses in the central nervous system. Nat Rev Immunol. 2017;17(3):179-94. doi: 10.1038/nri.2016.144. PubMed PMID: 28138136.

136. Shrestha B, Diamond MS. Fas ligand interactions contribute to CD8+ T-cell-mediated control of West Nile virus infection in the central nervous system. J Virol. 2007;81(21):11749-57. doi: 10.1128/JVI.01136-07. PubMed PMID: 17804505; PMCID: PMC2168805.

137. Shrestha B, Pinto AK, Green S, Bosch I, Diamond MS. CD8+ T cells use TRAIL to restrict West Nile virus pathogenesis by controlling infection in neurons. J Virol. 2012;86(17):8937-48. doi: 10.1128/JVI.00673-12. PubMed PMID: 22740407; PMCID: PMC3416144.

138. Lanteri MC, Heitman JW, Owen RE, Busch T, Gefter N, Kiely N, Kamel HT, Tobler LH, Busch MP, Norris PJ. Comprehensive analysis of west nile virus-specific T cell responses in humans. J Infect Dis. 2008;197(9):1296-306. doi: 10.1086/586898. PubMed PMID: 18422442.

139. Shrestha B, Samuel MA, Diamond MS. CD8+ T cells require perforin to clear West Nile virus from infected neurons. J Virol. 2006;80(1):119-29. doi: 10.1128/JVI.80.1.119-129.2006. PubMed PMID: 16352536; PMCID: PMC1317548.

140. Shrestha B, Wang T, Samuel MA, Whitby K, Craft J, Fikrig E, Diamond MS. Gamma interferon plays a crucial early antiviral role in protection against West Nile virus infection. J Virol. 2006;80(11):5338-48. doi: 10.1128/JVI.00274-06. PubMed PMID: 16699014; PMCID: PMC1472130.

141. Shrestha B, Zhang B, Purtha WE, Klein RS, Diamond MS. Tumor necrosis factor alpha protects against lethal West Nile virus infection by promoting trafficking of

mononuclear leukocytes into the central nervous system. J Virol. 2008;82(18):8956-64. doi: 10.1128/JVI.01118-08. PubMed PMID: 18632856; PMCID: PMC2546880.

142. Seo YJ, Jothikumar P, Suthar MS, Zhu C, Grakoui A. Local Cellular and Cytokine Cues in the Spleen Regulate In Situ T Cell Receptor Affinity, Function, and Fate of CD8(+) T Cells. Immunity. 2016;45(5):988-98. doi: 10.1016/j.immuni.2016.10.024. PubMed PMID: 27851926; PMCID: PMC5131716.

143. Aguilar-Valenzuela R, Netland J, Seo YJ, Bevan MJ, Grakoui A, Suthar MS. Dynamics of Tissue-Specific CD8(+) T Cell Responses during West Nile Virus Infection. J Virol. 2018;92(10). doi: 10.1128/JVI.00014-18. PubMed PMID: 29514902; PMCID: PMC5923067.

144. Klein RS, Lin E, Zhang B, Luster AD, Tollett J, Samuel MA, Engle M, Diamond MS. Neuronal CXCL10 directs CD8+ T-cell recruitment and control of West Nile virus encephalitis. J Virol. 2005;79(17):11457-66. doi: 10.1128/JVI.79.17.11457-11466.2005. PubMed PMID: 16103196; PMCID: PMC1193600.

145. Zhang B, Chan YK, Lu B, Diamond MS, Klein RS. CXCR3 mediates region-specific antiviral T cell trafficking within the central nervous system during West Nile virus encephalitis. J Immunol. 2008;180(4):2641-9. doi: 10.4049/jimmunol.180.4.2641. PubMed PMID: 18250476.

146. Funk KE, Klein RS. CSF1R antagonism limits local restimulation of antiviral CD8(+) T cells during viral encephalitis. J Neuroinflammation. 2019;16(1):22. doi: 10.1186/s12974-019-1397-4. PubMed PMID: 30704498; PMCID: PMC6354430.

147. Herz J, Filiano AJ, Smith A, Yogev N, Kipnis J. Myeloid Cells in the Central Nervous System. Immunity. 2017;46(6):943-56. doi: 10.1016/j.immuni.2017.06.007. PubMed PMID: 28636961; PMCID: PMC5657250.

148. Herz J, Kipnis J. Bugs and Brain: How Infection Makes You Feel Blue. Immunity. 2016;44(4):718-20. doi: 10.1016/j.immuni.2016.03.010. PubMed PMID: 27096312.

149. Manglani M, McGavern DB. New advances in CNS immunity against viral infection. Curr Opin Virol. 2018;28:116-26. doi: 10.1016/j.coviro.2017.12.003. PubMed PMID: 29289900; PMCID: PMC5990251.

150. Klein RS, Garber C, Howard N. Infectious immunity in the central nervous system and brain function. Nat Immunol. 2017;18(2):132-41. doi: 10.1038/ni.3656. PubMed PMID: 28092376.

151. Klein RS, Hunter CA. Protective and Pathological Immunity during Central Nervous System Infections. Immunity. 2017;46(6):891-909. doi: 10.1016/j.immuni.2017.06.012. PubMed PMID: 28636958; PMCID: PMC5662000.

152. Dahm T, Rudolph H, Schwerk C, Schroten H, Tenenbaum T. Neuroinvasion and Inflammation in Viral Central Nervous System Infections. Mediators Inflamm. 2016;2016:8562805. doi: 10.1155/2016/8562805. PubMed PMID: 27313404; PMCID: PMC4897715.

153. Swanson PA, 2nd, McGavern DB. Viral diseases of the central nervous system. Curr Opin Virol. 2015;11:44-54. doi: 10.1016/j.coviro.2014.12.009. PubMed PMID: 25681709; PMCID: PMC4456224.

154. Azevedo RSS, de Sousa JR, Araujo MTF, Martins Filho AJ, de Alcantara BN, Araujo FMC, Queiroz MGL, Cruz ACR, Vasconcelos BHB, Chiang JO, Martins LC,

Casseb LMN, da Silva EV, Carvalho VL, Vasconcelos BCB, Rodrigues SG, Oliveira CS, Quaresma JAS, Vasconcelos PFC. In situ immune response and mechanisms of cell damage in central nervous system of fatal cases microcephaly by Zika virus. Sci Rep. 2018;8(1):1. doi: 10.1038/s41598-017-17765-5. PubMed PMID: 29311619; PMCID: PMC5758755.

155. Sousa AQ, Cavalcante DIM, Franco LM, Araujo FMC, Sousa ET, Valenca-Junior JT, Rolim DB, Melo MEL, Sindeaux PDT, Araujo MTF, Pearson RD, Wilson ME, Pompeu MML. Postmortem Findings for 7 Neonates with Congenital Zika Virus Infection. Emerg Infect Dis. 2017;23(7):1164-7. doi: 10.3201/eid2307.162019. PubMed PMID: 28459414; PMCID: PMC5512501.

156. Chimelli L, Melo ASO, Avvad-Portari E, Wiley CA, Camacho AHS, Lopes VS, Machado HN, Andrade CV, Dock DCA, Moreira ME, Tovar-Moll F, Oliveira-Szejnfeld PS, Carvalho ACG, Ugarte ON, Batista AGM, Amorim MMR, Melo FO, Ferreira TA, Marinho JRL, Azevedo GS, Leal J, da Costa RFM, Rehen S, Arruda MB, Brindeiro RM, Delvechio R, Aguiar RS, Tanuri A. The spectrum of neuropathological changes associated with congenital Zika virus infection. Acta Neuropathol. 2017;133(6):983-99. doi: 10.1007/s00401-017-1699-5. PubMed PMID: 28332092.

157. Watanabe R, Kakizaki M, Ikehara Y, Togayachi A. Formation of fibroblastic reticular network in the brain after infection with neurovirulent murine coronavirus. Neuropathology. 2016;36(6):513-26. doi: 10.1111/neup.12302. PubMed PMID: 27121485.

158. Lamers SL, Gray RR, Salemi M, Huysentruyt LC, McGrath MS. HIV-1 phylogenetic analysis shows HIV-1 transits through the meninges to brain and

peripheral tissues. Infect Genet Evol. 2011;11(1):31-7. doi: 10.1016/j.meegid.2010.10.016. PubMed PMID: 21055482; PMCID: PMC3005076.

159. Kim JV, Kang SS, Dustin ML, McGavern DB. Myelomonocytic cell recruitment causes fatal CNS vascular injury during acute viral meningitis. Nature. 2009;457(7226):191-5. doi: 10.1038/nature07591. PubMed PMID: 19011611; PMCID: PMC2702264.

160. Prinz M, Priller J. The role of peripheral immune cells in the CNS in steady state and disease. Nat Neurosci. 2017;20(2):136-44. doi: 10.1038/nn.4475. PubMed PMID: 28092660.

161. Gebhardt T, Palendira U, Tscharke DC, Bedoui S. Tissue-resident memory T cells in tissue homeostasis, persistent infection, and cancer surveillance. Immunol Rev. 2018;283(1):54-76. doi: 10.1111/imr.12650. PubMed PMID: 29664571.

162. Wu H, Liao W, Li Q, Long H, Yin H, Zhao M, Chan V, Lau CS, Lu Q. Pathogenic role of tissue-resident memory T cells in autoimmune diseases. Autoimmun Rev. 2018;17(9):906-11. doi: 10.1016/j.autrev.2018.03.014. PubMed PMID: 30005862.

163. Daniels BP, Holman DW, Cruz-Orengo L, Jujjavarapu H, Durrant DM, Klein RS. Viral pathogen-associated molecular patterns regulate blood-brain barrier integrity via competing innate cytokine signals. MBio. 2014;5(5):e01476-14. doi: 10.1128/mBio.01476-14. PubMed PMID: 25161189; PMCID: PMC4173776.

164. Louveau A, Herz J, Alme MN, Salvador AF, Dong MQ, Viar KE, Herod SG, Knopp J, Setliff JC, Lupi AL, Da Mesquita S, Frost EL, Gaultier A, Harris TH, Cao R, Hu S, Lukens JR, Smirnov I, Overall CC, Oliver G, Kipnis J. CNS lymphatic drainage and neuroinflammation are regulated by meningeal lymphatic vasculature. Nat Neurosci.

2018;21(10):1380-91. doi: 10.1038/s41593-018-0227-9. PubMed PMID: 30224810; PMCID: PMC6214619.

165. Louveau A, Smirnov I, Keyes TJ, Eccles JD, Rouhani SJ, Peske JD, Derecki NC, Castle D, Mandell JW, Lee KS, Harris TH, Kipnis J. Structural and functional features of central nervous system lymphatic vessels. Nature. 2015;523(7560):337-41. doi: 10.1038/nature14432. PubMed PMID: 26030524; PMCID: PMC4506234.

166. Mastorakos P, McGavern D. The anatomy and immunology of vasculature in the central nervous system. Sci Immunol. 2019;4(37). doi: 10.1126/sciimmunol.aav0492. PubMed PMID: 31300479; PMCID: PMC6816468.

167. Rua R, McGavern DB. Advances in Meningeal Immunity. Trends Mol Med. 2018;24(6):542-59. doi: 10.1016/j.molmed.2018.04.003. PubMed PMID: 29731353; PMCID: PMC6044730.

168. Korin B, Ben-Shaanan TL, Schiller M, Dubovik T, Azulay-Debby H, Boshnak NT, Koren T, Rolls A. High-dimensional, single-cell characterization of the brain's immune compartment. Nat Neurosci. 2017;20(9):1300-9. doi: 10.1038/nn.4610. PubMed PMID: 28758994.

169. Mrdjen D, Pavlovic A, Hartmann FJ, Schreiner B, Utz SG, Leung BP, Lelios I, Heppner FL, Kipnis J, Merkler D, Greter M, Becher B. High-Dimensional Single-Cell Mapping of Central Nervous System Immune Cells Reveals Distinct Myeloid Subsets in Health, Aging, and Disease. Immunity. 2018;48(2):380-95 e6. doi: 10.1016/j.immuni.2018.01.011. PubMed PMID: 29426702.

170. Norris GT, Kipnis J. Immune cells and CNS physiology: Microglia and beyond. J Exp Med. 2019;216(1):60-70. doi: 10.1084/jem.20180199. PubMed PMID: 30504438; PMCID: PMC6314530.

171. Aspelund A, Antila S, Proulx ST, Karlsen TV, Karaman S, Detmar M, Wiig H, Alitalo K. A dural lymphatic vascular system that drains brain interstitial fluid and macromolecules. J Exp Med. 2015;212(7):991-9. doi: 10.1084/jem.20142290. PubMed PMID: 26077718; PMCID: PMC4493418.

172. Hannocks MJ, Pizzo ME, Huppert J, Deshpande T, Abbott NJ, Thorne RG, Sorokin L. Molecular characterization of perivascular drainage pathways in the murine brain. J Cereb Blood Flow Metab. 2018;38(4):669-86. doi: 10.1177/0271678X17749689. PubMed PMID: 29283289; PMCID: PMC5888861.

173. Herz J, Louveau A, Da Mesquita S, Kipnis J. Morphological and Functional Analysis of CNS-Associated Lymphatics. Methods Mol Biol. 2018;1846:141-51. doi: 10.1007/978-1-4939-8712-2_9. PubMed PMID: 30242757.

174. Absinta M, Ha SK, Nair G, Sati P, Luciano NJ, Palisoc M, Louveau A, Zaghloul KA, Pittaluga S, Kipnis J, Reich DS. Human and nonhuman primate meninges harbor lymphatic vessels that can be visualized noninvasively by MRI. Elife. 2017;6. doi: 10.7554/eLife.29738. PubMed PMID: 28971799; PMCID: PMC5626482.

175. Anandasabapathy N, Victora GD, Meredith M, Feder R, Dong B, Kluger C, Yao K, Dustin ML, Nussenzweig MC, Steinman RM, Liu K. Flt3L controls the development of radiosensitive dendritic cells in the meninges and choroid plexus of the steady-state mouse brain. J Exp Med. 2011;208(8):1695-705. doi: 10.1084/jem.20102657. PubMed PMID: 21788405; PMCID: PMC3149213.

176. Serot JM, Foliguet B, Bene MC, Faure GC. Ultrastructural and immunohistological evidence for dendritic-like cells within human choroid plexus epithelium. Neuroreport. 1997;8(8):1995-8. PubMed PMID: 9223091.

177. Durrant DM, Daniels BP, Klein RS. IL-1R1 signaling regulates CXCL12-mediated T cell localization and fate within the central nervous system during West Nile Virus encephalitis. J Immunol. 2014;193(8):4095-106. doi: 10.4049/jimmunol.1401192. PubMed PMID: 25200953; PMCID: PMC4340598.

178. Rua R, Lee JY, Silva AB, Swafford IS, Maric D, Johnson KR, McGavern DB. Infection drives meningeal engraftment by inflammatory monocytes that impairs CNS immunity. Nat Immunol. 2019;20(4):407-19. doi: 10.1038/s41590-019-0344-y. PubMed PMID: 30886419; PMCID: PMC6481670.

179. Lauterbach H, Zuniga EI, Truong P, Oldstone MB, McGavern DB. Adoptive immunotherapy induces CNS dendritic cell recruitment and antigen presentation during clearance of a persistent viral infection. J Exp Med. 2006;203(8):1963-75. doi: 10.1084/jem.20060039. PubMed PMID: 16847068; PMCID: PMC2118382.

180. Da Mesquita S, Louveau A, Vaccari A, Smirnov I, Cornelison RC, Kingsmore KM, Contarino C, Onengut-Gumuscu S, Farber E, Raper D, Viar KE, Powell RD, Baker W, Dabhi N, Bai R, Cao R, Hu S, Rich SS, Munson JM, Lopes MB, Overall CC, Acton ST, Kipnis J. Functional aspects of meningeal lymphatics in ageing and Alzheimer's disease. Nature. 2018;560(7717):185-91. doi: 10.1038/s41586-018-0368-8. PubMed PMID: 30046111; PMCID: PMC6085146.

181. Matullo CM, O'Regan KJ, Hensley H, Curtis M, Rall GF. Lymphocytic choriomeningitis virus-induced mortality in mice is triggered by edema and brain

herniation. J Virol. 2010;84(1):312-20. doi: 10.1128/JVI.00727-09. PubMed PMID: 19828618; PMCID: PMC2798401.

182. Bartholomaus I, Kawakami N, Odoardi F, Schlager C, Miljkovic D, Ellwart JW, Klinkert WE, Flugel-Koch C, Issekutz TB, Wekerle H, Flugel A. Effector T cell interactions with meningeal vascular structures in nascent autoimmune CNS lesions. Nature. 2009;462(7269):94-8. doi: 10.1038/nature08478. PubMed PMID: 19829296.

183. Lopes Pinheiro MA, Kooij G, Mizee MR, Kamermans A, Enzmann G, Lyck R, Schwaninger M, Engelhardt B, de Vries HE. Immune cell trafficking across the barriers of the central nervous system in multiple sclerosis and stroke. Biochim Biophys Acta. 2016;1862(3):461-71. doi: 10.1016/j.bbadis.2015.10.018. PubMed PMID: 26527183.

184. Cupovic J, Onder L, Gil-Cruz C, Weiler E, Caviezel-Firner S, Perez-Shibayama C, Rulicke T, Bechmann I, Ludewig B. Central Nervous System Stromal Cells Control Local CD8(+) T Cell Responses during Virus-Induced Neuroinflammation. Immunity. 2016;44(3):622-33. doi: 10.1016/j.immuni.2015.12.022. PubMed PMID: 26921107.

185. Brien JD, Uhrlaub JL, Nikolich-Zugich J. West Nile virus-specific CD4 T cells exhibit direct antiviral cytokine secretion and cytotoxicity and are sufficient for antiviral protection. J Immunol. 2008;181(12):8568-75. PubMed PMID: 19050276; PMCID: PMC3504655.

186. Gorman MJ, Caine EA, Zaitsev K, Begley MC, Weger-Lucarelli J, Uccellini MB, Tripathi S, Morrison J, Yount BL, Dinnon KH, 3rd, Ruckert C, Young MC, Zhu Z, Robertson SJ, McNally KL, Ye J, Cao B, Mysorekar IU, Ebel GD, Baric RS, Best SM, Artyomov MN, Garcia-Sastre A, Diamond MS. An Immunocompetent Mouse Model of

Zika Virus Infection. Cell Host Microbe. 2018;23(5):672-85 e6. doi: 10.1016/j.chom.2018.04.003. PubMed PMID: 29746837; PMCID: PMC5953559.

187. Sen A, Rothenberg ME, Mukherjee G, Feng N, Kalisky T, Nair N, Johnstone IM, Clarke MF, Greenberg HB. Innate immune response to homologous rotavirus infection in the small intestinal villous epithelium at single-cell resolution. Proc Natl Acad Sci U S A. 2012;109(50):20667-72. doi: 10.1073/pnas.1212188109. PubMed PMID: 23188796; PMCID: PMC3528539.

188. Honda K, Takaoka A, Taniguchi T. Type I interferon [corrected] gene induction by the interferon regulatory factor family of transcription factors. Immunity. 2006;25(3):349-60. doi: 10.1016/j.immuni.2006.08.009. PubMed PMID: 16979567.

189. Morrison J, Laurent-Rolle M, Maestre AM, Rajsbaum R, Pisanelli G, Simon V, Mulder LC, Fernandez-Sesma A, Garcia-Sastre A. Dengue virus co-opts UBR4 to degrade STAT2 and antagonize type I interferon signaling. PLoS Pathog. 2013;9(3):e1003265. doi: 10.1371/journal.ppat.1003265. PubMed PMID: 23555265; PMCID: PMC3610674.

190. Kwon YJ, Heo J, Wong HE, Cruz DJ, Velumani S, da Silva CT, Mosimann AL, Duarte Dos Santos CN, Freitas-Junior LH, Fink K. Kinome siRNA screen identifies novel cell-type specific dengue host target genes. Antiviral Res. 2014;110:20-30. doi: 10.1016/j.antiviral.2014.07.006. PubMed PMID: 25046486.

191. Hoss-Homfeld A, Zwarthoff EC, Zawatzky R. Cell type specific expression and regulation of murine interferon alpha and beta genes. Virology. 1989;173(2):539-50. PubMed PMID: 2596029.

192. Nybakken GE, Oliphant T, Johnson S, Burke S, Diamond MS, Fremont DH. Structural basis of West Nile virus neutralization by a therapeutic antibody. Nature. 2005;437(7059):764-9. doi: 10.1038/nature03956. PubMed PMID: 16193056.

193. Picelli S, Faridani OR, Bjorklund AK, Winberg G, Sagasser S, Sandberg R. Full-length RNA-seq from single cells using Smart-seq2. Nat Protoc. 2014;9(1):171-81. doi: 10.1038/nprot.2014.006. PubMed PMID: 24385147.

194. Wu AR, Neff NF, Kalisky T, Dalerba P, Treutlein B, Rothenberg ME, Mburu FM, Mantalas GL, Sim S, Clarke MF, Quake SR. Quantitative assessment of single-cell RNA-sequencing methods. Nat Methods. 2014;11(1):41-6. doi: 10.1038/nmeth.2694. PubMed PMID: 24141493; PMCID: PMC4022966.

195. Marie I, Durbin JE, Levy DE. Differential viral induction of distinct interferon-alpha genes by positive feedback through interferon regulatory factor-7. EMBO J. 1998;17(22):6660-9. doi: 10.1093/emboj/17.22.6660. PubMed PMID: 9822609; PMCID: PMC1171011.

196. Sato M, Hata N, Asagiri M, Nakaya T, Taniguchi T, Tanaka N. Positive feedback regulation of type I IFN genes by the IFN-inducible transcription factor IRF-7. FEBS Lett. 1998;441(1):106-10. PubMed PMID: 9877175.

197. Sato M, Suemori H, Hata N, Asagiri M, Ogasawara K, Nakao K, Nakaya T, Katsuki M, Noguchi S, Tanaka N, Taniguchi T. Distinct and essential roles of transcription factors IRF-3 and IRF-7 in response to viruses for IFN-alpha/beta gene induction. Immunity. 2000;13(4):539-48. PubMed PMID: 11070172.

198. Brass AL, Huang IC, Benita Y, John SP, Krishnan MN, Feeley EM, Ryan BJ, Weyer JL, van der Weyden L, Fikrig E, Adams DJ, Xavier RJ, Farzan M, Elledge SJ.

The IFITM proteins mediate cellular resistance to influenza A H1N1 virus, West Nile virus, and dengue virus. Cell. 2009;139(7):1243-54. doi: 10.1016/j.cell.2009.12.017. PubMed PMID: 20064371; PMCID: PMC2824905.

199. Gorman MJ, Poddar S, Farzan M, Diamond MS. The Interferon-Stimulated Gene Ifitm3 Restricts West Nile Virus Infection and Pathogenesis. J Virol. 2016;90(18):8212-25. doi: 10.1128/JVI.00581-16. PubMed PMID: 27384652; PMCID: PMC5008082.

200. Kajaste-Rudnitski A, Mashimo T, Frenkiel MP, Guenet JL, Lucas M, Despres P. The 2',5'-oligoadenylate synthetase 1b is a potent inhibitor of West Nile virus replication inside infected cells. J Biol Chem. 2006;281(8):4624-37. doi: 10.1074/jbc.M508649200. PubMed PMID: 16371364.

201. Liu XY, Chen W, Wei B, Shan YF, Wang C. IFN-induced TPR protein IFIT3 potentiates antiviral signaling by bridging MAVS and TBK1. J Immunol. 2011;187(5):2559-68. doi: 10.4049/jimmunol.1100963. PubMed PMID: 21813773.

202. Perelygin AA, Scherbik SV, Zhulin IB, Stockman BM, Li Y, Brinton MA. Positional cloning of the murine flavivirus resistance gene. Proc Natl Acad Sci U S A. 2002;99(14):9322-7. doi: 10.1073/pnas.142287799. PubMed PMID: 12080145; PMCID: PMC123139.

203. Szretter KJ, Brien JD, Thackray LB, Virgin HW, Cresswell P, Diamond MS. The interferon-inducible gene viperin restricts West Nile virus pathogenesis. J Virol. 2011;85(22):11557-66. doi: 10.1128/JVI.05519-11. PubMed PMID: 21880757; PMCID: PMC3209274.

204. Verhelst J, Parthoens E, Schepens B, Fiers W, Saelens X. Interferon-inducible protein Mx1 inhibits influenza virus by interfering with functional viral ribonucleoprotein

complex assembly. J Virol. 2012;86(24):13445-55. doi: 10.1128/JVI.01682-12. PubMed PMID: 23015724; PMCID: PMC3503048.

205. Li Y, Banerjee S, Wang Y, Goldstein SA, Dong B, Gaughan C, Silverman RH, Weiss SR. Activation of RNase L is dependent on OAS3 expression during infection with diverse human viruses. Proc Natl Acad Sci U S A. 2016;113(8):2241-6. doi: 10.1073/pnas.1519657113. PubMed PMID: 26858407; PMCID: PMC4776461.

206. Huang da W, Sherman BT, Lempicki RA. Systematic and integrative analysis of large gene lists using DAVID bioinformatics resources. Nat Protoc. 2009;4(1):44-57. doi: 10.1038/nprot.2008.211. PubMed PMID: 19131956.

207. Huang da W, Sherman BT, Lempicki RA. Bioinformatics enrichment tools: paths toward the comprehensive functional analysis of large gene lists. Nucleic Acids Res. 2009;37(1):1-13. doi: 10.1093/nar/gkn923. PubMed PMID: 19033363; PMCID: PMC2615629.

208. Macosko EZ, Basu A, Satija R, Nemesh J, Shekhar K, Goldman M, Tirosh I, Bialas AR, Kamitaki N, Martersteck EM, Trombetta JJ, Weitz DA, Sanes JR, Shalek AK, Regev A, McCarroll SA. Highly Parallel Genome-wide Expression Profiling of Individual Cells Using Nanoliter Droplets. Cell. 2015;161(5):1202-14. doi: 10.1016/j.cell.2015.05.002. PubMed PMID: 26000488; PMCID: PMC4481139.

209. Baranek T, Manh TP, Alexandre Y, Maqbool MA, Cabeza JZ, Tomasello E, Crozat K, Bessou G, Zucchini N, Robbins SH, Vivier E, Kalinke U, Ferrier P, Dalod M. Differential responses of immune cells to type I interferon contribute to host resistance to viral infection. Cell Host Microbe. 2012;12(4):571-84. doi: 10.1016/j.chom.2012.09.002. PubMed PMID: 23084923.

210. Inc. I. Effects of Index Misassignment on Multiplexing and Downstream Analysis. 2017.

211. Lanciotti RS, Kerst AJ, Nasci RS, Godsey MS, Mitchell CJ, Savage HM, Komar N, Panella NA, Allen BC, Volpe KE, Davis BS, Roehrig JT. Rapid detection of west nile virus from human clinical specimens, field-collected mosquitoes, and avian samples by a TaqMan reverse transcriptase-PCR assay. J Clin Microbiol. 2000;38(11):4066-71. PubMed PMID: 11060069; PMCID: PMC87542.

212. Love MI, Huber W, Anders S. Moderated estimation of fold change and dispersion for RNA-seq data with DESeq2. Genome Biol. 2014;15(12):550. doi: 10.1186/s13059-014-0550-8. PubMed PMID: 25516281; PMCID: PMC4302049.

213. Upadhyay AA, Kauffman RC, Wolabaugh AN, Cho A, Patel NB, Reiss SM, Havenar-Daughton C, Dawoud RA, Tharp GK, Sanz I, Pulendran B, Crotty S, Lee FE, Wrammert J, Bosinger SE. BALDR: a computational pipeline for paired heavy and light chain immunoglobulin reconstruction in single-cell RNA-seq data. Genome Med. 2018;10(1):20. doi: 10.1186/s13073-018-0528-3. PubMed PMID: 29558968; PMCID: PMC5859752.

214. Andrews S. FastQC: a quality control tool for high throughput sequence data. 2010.

215. Harrow J, Frankish A, Gonzalez JM, Tapanari E, Diekhans M, Kokocinski F, Aken BL, Barrell D, Zadissa A, Searle S, Barnes I, Bignell A, Boychenko V, Hunt T, Kay M, Mukherjee G, Rajan J, Despacio-Reyes G, Saunders G, Steward C, Harte R, Lin M, Howald C, Tanzer A, Derrien T, Chrast J, Walters N, Balasubramanian S, Pei B, Tress M, Rodriguez JM, Ezkurdia I, van Baren J, Brent M, Haussler D, Kellis M, Valencia A,

Reymond A, Gerstein M, Guigo R, Hubbard TJ. GENCODE: the reference human genome annotation for The ENCODE Project. Genome Res. 2012;22(9):1760-74. doi: 10.1101/gr.135350.111. PubMed PMID: 22955987; PMCID: PMC3431492.

216. Pickett BE, Sadat EL, Zhang Y, Noronha JM, Squires RB, Hunt V, Liu M, Kumar S, Zaremba S, Gu Z, Zhou L, Larson CN, Dietrich J, Klem EB, Scheuermann RH. ViPR: an open bioinformatics database and analysis resource for virology research. Nucleic Acids Res. 2012;40(Database issue):D593-8. doi: 10.1093/nar/gkr859. PubMed PMID: 22006842; PMCID: PMC3245011.

217. Dobin A, Davis CA, Schlesinger F, Drenkow J, Zaleski C, Jha S, Batut P, Chaisson M, Gingeras TR. STAR: ultrafast universal RNA-seq aligner. Bioinformatics. 2013;29(1):15-21. doi: 10.1093/bioinformatics/bts635. PubMed PMID: 23104886; PMCID: PMC3530905.

218. Lun AR, D. Single Cell Experiment: S4 Classes for Single Cell Data. Bioconductor2018.

219. McCarthy DJ, Campbell KR, Lun AT, Wills QF. Scater: pre-processing, quality control, normalization and visualization of single-cell RNA-seq data in R. Bioinformatics. 2017;33(8):1179-86. doi: 10.1093/bioinformatics/btw777. PubMed PMID: 28088763; PMCID: PMC5408845.

220. Scialdone A, Natarajan KN, Saraiva LR, Proserpio V, Teichmann SA, Stegle O, Marioni JC, Buettner F. Computational assignment of cell-cycle stage from single-cell transcriptome data. Methods. 2015;85:54-61. doi: 10.1016/j.ymeth.2015.06.021. PubMed PMID: 26142758.

221. Shwetank, Abdelsamed HA, Frost EL, Schmitz HM, Mockus TE, Youngblood BA, Lukacher AE. Maintenance of PD-1 on brain-resident memory CD8 T cells is antigen independent. Immunol Cell Biol. 2017;95(10):953-9. doi: 10.1038/icb.2017.62. PubMed PMID: 28829048; PMCID: PMC5698165.

222. Prasad S, Hu S, Sheng WS, Chauhan P, Singh A, Lokensgard JR. The PD-1: PD-L1 pathway promotes development of brain-resident memory T cells following acute viral encephalitis. J Neuroinflammation. 2017;14(1):82. doi: 10.1186/s12974-017-0860-3. PubMed PMID: 28407741; PMCID: PMC5390367.

223. Wherry EJ, Kurachi M. Molecular and cellular insights into T cell exhaustion. Nat Rev Immunol. 2015;15(8):486-99. doi: 10.1038/nri3862. PubMed PMID: 26205583; PMCID: PMC4889009.

224. Malek TR. The biology of interleukin-2. Annu Rev Immunol. 2008;26:453-79. doi: 10.1146/annurev.immunol.26.021607.090357. PubMed PMID: 18062768.

225. Wherry EJ, Ha SJ, Kaech SM, Haining WN, Sarkar S, Kalia V, Subramaniam S, Blattman JN, Barber DL, Ahmed R. Molecular signature of CD8+ T cell exhaustion during chronic viral infection. Immunity. 2007;27(4):670-84. doi: 10.1016/j.immuni.2007.09.006. PubMed PMID: 17950003.

226. Xin A, Masson F, Liao Y, Preston S, Guan T, Gloury R, Olshansky M, Lin JX, Li P, Speed TP, Smyth GK, Ernst M, Leonard WJ, Pellegrini M, Kaech SM, Nutt SL, Shi W, Belz GT, Kallies A. A molecular threshold for effector CD8(+) T cell differentiation controlled by transcription factors Blimp-1 and T-bet. Nat Immunol. 2016;17(4):422-32. doi: 10.1038/ni.3410. PubMed PMID: 26950239; PMCID: PMC5779087.

227. Burdeinick-Kerr R, Griffin DE. Gamma interferon-dependent, noncytolytic clearance of sindbis virus infection from neurons in vitro. J Virol. 2005;79(9):5374-85. doi: 10.1128/JVI.79.9.5374-5385.2005. PubMed PMID: 15827152; PMCID: PMC1082728.

228. Lanteri MC, O'Brien KM, Purtha WE, Cameron MJ, Lund JM, Owen RE, Heitman JW, Custer B, Hirschkorn DF, Tobler LH, Kiely N, Prince HE, Ndhlovu LC, Nixon DF, Kamel HT, Kelvin DJ, Busch MP, Rudensky AY, Diamond MS, Norris PJ. Tregs control the development of symptomatic West Nile virus infection in humans and mice. J Clin Invest. 2009;119(11):3266-77. doi: 10.1172/JCI39387. PubMed PMID: 19855131; PMCID: PMC2769173.

229. O'Neal JT, Upadhyay AA, Wolabaugh A, Patel NB, Bosinger SE, Suthar MS. West Nile Virus-Inclusive Single-Cell RNA Sequencing Reveals Heterogeneity in the Type I Interferon Response within Single Cells. J Virol. 2019;93(6). doi: 10.1128/JVI.01778-18. PubMed PMID: 30626670; PMCID: PMC6401468.

230. Lau KS, Cortez-Retamozo V, Philips SR, Pittet MJ, Lauffenburger DA, Haigis KM. Multi-scale in vivo systems analysis reveals the influence of immune cells on TNF-alpha-induced apoptosis in the intestinal epithelium. PLoS Biol. 2012;10(9):e1001393. doi: 10.1371/journal.pbio.1001393. PubMed PMID: 23055830; PMCID: PMC3463506.

231. Travis MA, Reizis B, Melton AC, Masteller E, Tang Q, Proctor JM, Wang Y, Bernstein X, Huang X, Reichardt LF, Bluestone JA, Sheppard D. Loss of integrin alpha(v)beta8 on dendritic cells causes autoimmunity and colitis in mice. Nature. 2007;449(7160):361-5. doi: 10.1038/nature06110. PubMed PMID: 17694047; PMCID: PMC2670239.

232. Fong SW, Kini RM, Ng LFP. Mosquito Saliva Reshapes Alphavirus Infection and Immunopathogenesis. J Virol. 2018;92(12). doi: 10.1128/JVI.01004-17. PubMed PMID: 29593049; PMCID: PMC5974479.

233. Reagan KL, Machain-Williams C, Wang T, Blair CD. Immunization of mice with recombinant mosquito salivary protein D7 enhances mortality from subsequent West Nile virus infection via mosquito bite. PLoS Negl Trop Dis. 2012;6(12):e1935. doi: 10.1371/journal.pntd.0001935. PubMed PMID: 23236530; PMCID: PMC3516580.

234. Herz J, Johnson KR, McGavern DB. Therapeutic antiviral T cells noncytopathically clear persistently infected microglia after conversion into antigen-presenting cells. J Exp Med. 2015;212(8):1153-69. doi: 10.1084/jem.20142047. PubMed PMID: 26122661; PMCID: PMC4516789.

235. Steinbach K, Vincenti I, Kreutzfeldt M, Page N, Muschaweckh A, Wagner I, Drexler I, Pinschewer D, Korn T, Merkler D. Brain-resident memory T cells represent an autonomous cytotoxic barrier to viral infection. J Exp Med. 2016;213(8):1571-87. doi: 10.1084/jem.20151916. PubMed PMID: 27377586; PMCID: PMC4986533.

236. Wakim LM, Woodward-Davis A, Bevan MJ. Memory T cells persisting within the brain after local infection show functional adaptations to their tissue of residence. Proc Natl Acad Sci U S A. 2010;107(42):17872-9. doi: 10.1073/pnas.1010201107. PubMed PMID: 20923878; PMCID: PMC2964240.

237. Wakim LM, Woodward-Davis A, Liu R, Hu Y, Villadangos J, Smyth G, Bevan MJ. The molecular signature of tissue resident memory CD8 T cells isolated from the brain. J Immunol. 2012;189(7):3462-71. doi: 10.4049/jimmunol.1201305. PubMed PMID: 22922816; PMCID: PMC3884813.

238. Turner DL, Cauley LS, Khanna KM, Lefrancois L. Persistent antigen presentation after acute vesicular stomatitis virus infection. J Virol. 2007;81(4):2039-46. doi: 10.1128/JVI.02167-06. PubMed PMID: 17151119; PMCID: PMC1797569.

239. Itzhaki RF, Lathe R, Balin BJ, Ball MJ, Bearer EL, Braak H, Bullido MJ, Carter C, Clerici M, Cosby SL, Del Tredici K, Field H, Fulop T, Grassi C, Griffin WS, Haas J, Hudson AP, Kamer AR, Kell DB, Licastro F, Letenneur L, Lovheim H, Mancuso R, Miklossy J, Otth C, Palamara AT, Perry G, Preston C, Pretorius E, Strandberg T, Tabet N, Taylor-Robinson SD, Whittum-Hudson JA. Microbes and Alzheimer's Disease. J Alzheimers Dis. 2016;51(4):979-84. doi: 10.3233/JAD-160152. PubMed PMID: 26967229; PMCID: PMC5457904.

240. Readhead B, Haure-Mirande JV, Funk CC, Richards MA, Shannon P, Haroutunian V, Sano M, Liang WS, Beckmann ND, Price ND, Reiman EM, Schadt EE, Ehrlich ME, Gandy S, Dudley JT. Multiscale Analysis of Independent Alzheimer's Cohorts Finds Disruption of Molecular, Genetic, and Clinical Networks by Human Herpesvirus. Neuron. 2018;99(1):64-82 e7. doi: 10.1016/j.neuron.2018.05.023. PubMed PMID: 29937276; PMCID: PMC6551233.

241. Mechelli R, Manzari C, Policano C, Annese A, Picardi E, Umeton R, Fornasiero A, D'Erchia AM, Buscarinu MC, Agliardi C, Annibali V, Serafini B, Rosicarelli B, Romano S, Angelini DF, Ricigliano VA, Buttari F, Battistini L, Centonze D, Guerini FR, D'Alfonso S, Pesole G, Salvetti M, Ristori G. Epstein-Barr virus genetic variants are associated with multiple sclerosis. Neurology. 2015;84(13):1362-8. doi: 10.1212/WNL.0000000000001420. PubMed PMID: 25740864; PMCID: PMC4388746.

242. Virtanen JO, Jacobson S. Viruses and multiple sclerosis. CNS Neurol Disord Drug Targets. 2012;11(5):528-44. doi: 10.2174/187152712801661220. PubMed PMID: 22583435; PMCID: PMC4758194.